ABSTRACT

DURHAM, CHRISTINA LOUISE. Spatial Dynamics in an Estuarine System: Modeling Biophysical Components and Interactions to Advance Blue Crab Fishery Management. (Under the direction of David B. Eggleston.)

Estuaries are dynamic ecosystems with abiotic environments that exhibit extreme space-time variability. Cyclic variation is somewhat predictable, but hurricanes and large-scale atmospheric disturbances can rapidly and drastically alter anticipated conditions. These disturbances can induce rapid biological responses across large spatial scales and frequently shift distribution patterns of mobile species. Physical conditions recover relatively quickly from climactically driven perturbations, and most physically-induced animal migrations are also temporary and reversible. Nevertheless, in the case of a commercially valuable fish species, even short-term alterations can change their vulnerability (i.e., catchability) to fishery-independent surveys, which provide valuable data used in population assessment.

We examined the effects of salinity and other physical forcing mechanisms on the spatial distribution of ecologically and economically important blue crabs (*Callinectes sapidus*) in Pamlico Sound, NC. Pamlico Sound is the second largest estuary in the U.S. and is prone to hurricane activity. The blue crab fishery, North Carolina's most important, is managed using indices of spawning stock biomass (SSB) and catch-per-unit effort generated from a fishery-independent trawl survey that does not sample shallow (< 2 m deep) regions. If environmental conditions affect the proportion of the population located within the survey region at a given time, then these indices are susceptible to bias resulting from variations in crab catchability. When the majority of the population is distributed in the Pamlico Sound survey area, a relatively high catchability would inflate estimates of relative population size.

Likewise, when the population is less aggregated in mainstem Pamlico Sound and distributed further up in shallow water tributaries, relative population size would be underestimated by a relatively low catchability. Our objectives, to investigate the potential existence of aggregations and their environmental causes and to develop ways to account for environmental variability to obtain unbiased estimates of relative population abundance, were accomplished in two parts using three different statistical models.

First, we modeled salinity observations collected in Pamlico Sound over the past 20 years as a function of recent and long-term freshwater influx from four rivers, distance to nearby inlets, and hurricane incidence. Maps of salinity predictions generated by this model illustrated changes in spatial salinity patterns during 40 survey time periods that encompassed a variety of climatic conditions.

Salinity predictions were used to characterize the relationship between salinity and the presence and spatial distribution of blue crab SSB to predict historic distribution patterns. Observed survey SSB was modeled as function of space-time variable environmental factors that likely affect crab catchability in order to estimate time period-specific SSB means that were adjusted for these environmental effects. The time series of estimated means comprise an environmentally-adjusted SSB index that is more suitable for tracking relative population size over time than the index currently used to manage the fishery. This adjustment validated conclusions drawn from previous analyses and field observations that blue crab SSB has decreased over the past 20 years, most notably since 1999.

A second model, including factors that did not change over time but likely affected crab spatial distribution, allowed us to predict SSB at a given space-time location.

Predictions revealed consistent SSB spatial distribution patterns over successive monthly time periods and under variable environmental conditions. This information could help managers station no-take marine reserves to better conserve the blue crab spawning stock.

In addition to yielding results that will better inform blue crab fishery managers, this research significantly increases the knowledge base regarding the effects of abiotic forcing events on mobile estuarine species. Furthermore, these methods provide a rigorous and robust analytical template to create future adjustment indices to manage mobile species that change their spatial distribution in response to environmental variables.

Spatial Dynamics in an Estuarine System: Modeling Biophysical Components and Interactions to Advance Blue Crab Fishery Management

by
Christina L. Durham

A thesis submitted to the Graduate Faculty of
North Carolina State University
in partial fulfillment of the
requirements for the Degree of
Master of Science

Marine, Earth and Atmospheric Sciences

Raleigh, North Carolina

2009

APPROVED BY:

David B. Eggleston Committee Chair	Joseph E. Hightower
Daniel Kamykowski	Amy Nail Reader / Statistical Consultant

DEDICATION

This work is dedicated to my graduate school support network:

Geoff Bell, Kevin Gross, Justin Keesee, and Sunny Snider

Who believed with me in the good times, for me in the bad times, and in me at all times.

I couldn't have gotten through without you.

And to lappy: Thanks for never crashing too badly.

BIOGRAPHY

Christina Louise Durham was born on November 22, 1980, the day after her mother discovered who shot J.R. She lived her entire childhood on the water: half on Long Island's south shore and half on the Eastern Shore of Virginia (a.k.a. "the land that time forgot"). While she remembers clamming and crabbing with her dad as a child, Christina's first exposure to the study of marine life came her junior year at Northampton High School, where she would later graduate valedictorian. It was then that dreams of being a Pulitzer-Prize winning journalist / principal dancer with the Joffrey ballet ended, and she set her sights on a career in marine science.

She enrolled in the Marine Science Program at the University of South Carolina in the fall of 1999 to expand her knowledge of the marine environment. Her studies over the next four years were as diverse as her summer fellowships and technician positions. She played in the mud with clams, tied blue crab to leashes, and helped acquire a new ferry pier ladder at the Virginia Institute of Marine Science. She watched barnacles grow (faster than it sounds) and bathed manatees at the Florida Institute of Technology and learned at her alma mater how to change the oil in an ICP-MS while reading German. Her undergraduate pièce de résistance involved building a mud snail feeding arena to examine the effects of soluble pollutants on chemoreception, an apparatus that doubled in function as an inter-tidal WWE Cage Match venue. After four years of non-stop science, she graduated magna cum laude, Phi Beta Kappa, and exhausted.

A brief career in pharmaceutical mass-tort corporate litigation reminded her why she loved marine science and renewed her research enthusiasm. She moved to Astoria, OR to work as a biological aid to the Marine Shellfish Program at the Oregon Department of Fish and Wildlife and became interested in fisheries management after many hours spent on boat landings, clam-filled beaches, and sardine seiners. That interest led her to apply to graduate school in the hopes of attaining the skills and knowledge necessary to build a career forwarding marine fisheries sustainability.

Rejecting UNC-CH for the second time in her collegiate career, Christina began graduate studies one branch down her marine ecology family tree with David Eggleston at North Carolina State University, thinking that she would again be waist deep in salt water before the year was out. It soon became apparent that the only thing she would be waist deep in for the next seven semesters was SAS coding files. Luckily, she was able to convince Dr. Eggleston to let her stand up from her computer long enough to travel to the cultural Mecca that is Pascagoula, MS to assist in the collection of the fisheries trawl survey data that she spends hours analyzing. While there, she met her dashing boyfriend Justin.

Thankful for the wonderful friends she met in graduate school and for all that is Raleigh, she will spend the next year in Washington D.C. hoping to convince some of the men and women on Capitol Hill to allocate more time and resources to fisheries research and conservation measures.

ACKNOWLEDGEMENTS

This project would not have been possible without two very important people. I am grateful to Dave Eggleston for his guidance and encouragement. His insight has certainly made me a better scientist, and I will always appreciate his caring demeanor: you were the advisor that I needed. I am forever indebted to Amy Nail, who went above and beyond the call of duty to mentor me throughout this process. Thanks to her countless time and effort, I know more about statistics than I thought was ever possible. All that I have accomplished during my NC State tenure is a direct result of their unwavering support. I thank the remainder of my committee, Drs. Joe Hightower and Dan Kamykowski, as well as Dr. Montse Fuentes, for their perspective, insight, patience, and assistance. These four things were critical to the (eventual) completion of this research.

No woman is an island, and neither is any Eggleston lab member. I wholeheartedly thank all past and present lab mates, especially Geoff Bell, Erika Millstein, Ray Mroch, Gayle Playa, Brandon Puckett, and Ryan Rindone for their constant and selfless assistance with research and life issues large and small. The same level of gratitude is extended to Anita McCulloch, who I will always consider part of my lab family.

I got by with a **lot** of help from my friends. To the ladies near, Becky Bartel, Kayde Brownlee, Christin Marten, Jess Picha, Laura Shewmon, Sunny Snider, Lauren Westmoreland, and far, Judy Matulich-Hall, Julie McKeel, Lynne Story, Laura Woodworth, you are the women who inspired me to succeed. I thank the men, Jim Fleming, Will Fields,

Kevin Gross, and Jason Morton for learning to deal with an emotional female. And to Justin Keesee, there are no words.

Finally, I would like to thank the entire NOAA/NMFS Pascagoula Lab and the crew of the NOAA R/V Oregon II for both entertainment and logistical support, and both the Environmental Defense Fund and the Blue Crab Advanced Research Consortium (BCARC) for funding this research.

TABLE OF CONTENTS

LIST OF TABLES

CHAPTER 1

CHAPTER 2

LIST OF FIGURES

CHAPTER 1

CHAPTER 2

LIST OF APPENDICIES

CHAPTER 1:

Developing process-based statistical models of bottom salinity in Pamlico Sound, NC

ABSTRACT

Estuarine salinity varies over both space and time, and this variation routinely alters both biotic and abiotic system components. Anticipating this variability is challenging; salinity at a specific location is the result of interactions among physical forcing mechanisms that control the amount of fresh and salt water present at that site. Here we develop and evaluate two space-time statistical models of bottom salinity in Pamlico Sound, NC, and we provide a methodological template for modeling salinity in other estuaries. Both models consist of a process-based component and a random component, where the process component is a function of recent and long-term fresh water influx from four rivers, distance to nearby inlets, and hurricane incidence. For one of the models we also use a different intercept for each point in time to account for any time-varying quantity that might affect but has not been adequately represented by the other terms in the model. In both models, the random error component has a different spatial correlation structure for each time period. We build these models using observational data collected by the North Carolina Division of Marine Fisheries over a 2.5 week time period each June and September from 1987 to 2006. The final process-only model explains 89% of the variability in salinity in a withheld dataset, and generates time-period-specific spatial predictions with an overall root mean squared error of 2.0 units of salinity. Similarly, the process plus time model explains 87% of the withheld-dataset variability and has an overall root mean squared error (RMSE) of 2.1. We map process-only predictions to visually examine changes in estuarine salinity distribution patterns across 20 years of variable climatic conditions and to identify any consistent patterns that would aid in

future salinity forecasting. With careful selection of system-specific explanatory variables, the outlined procedure and supplemental code can be used by anyone to model and predict estuarine salinity or any other normally-distributed quantity over space and time.

1. INTRODUCTION

1.1. Background

Estuarine salinity is a direct response to dynamic meteorological, hydrological, and chemical processes, and it exhibits large space/time variability (Cloern and Nichols 1985). Salinity affects the physiological functioning of all resident organisms (Kinne 1964); abrupt or persistent changes in typical salinity patterns can alter species composition, distribution, and abundance, which can in turn affect habitat quality, fisheries catches, and ecosystem resilience (Tabb and Jones 1962; Anderson et al. 1973; Russell 1977; Knott and Martour 1992; Sklar 1998; Mallin and Corbett 2002, 2006; Burkholder et al. 2004; Paerl et al. 2001, 2006; Rome 2005; Balthis 2006).

Pamlico Sound (PS), North Carolina is the largest lagoonal estuary in the U.S. The range of salinities across PS at any given time is typically greater than 15, as measured using the Practical Salinity Scale (Schwartz and Chestnut 1973, Giese et al. 1979, Pietrafesa et al. 1986, Buzzelli et al. 2003, Reyns 2004, this study). Salinities in a single area can vary by more than 5 units daily (Buzzelli et al. 2003), semi-monthly (Reyns 2004), seasonally (Giese et al. 1979, Molina 2002), interannually (Pietrafesa et al. 1986, Stanley and Nixon 1992), and episodically. Record floods experienced after the landfall of three sequential hurricanes (Dennis, Floyd, and Irene) in fall 1999 depressed observed bottom salinities in PS by more than 50 percent (Paerl et al. 2001). This reduction caused a mass migration of blue crab (*Callinectes sapidus*) out of upriver tributaries to escape freshening conditions and resulted in a more concentrated population that was increasingly susceptible to fishing pressure (Eggleston et al. 2004). Similar down-estuary displacements of juvenile Atlantic croaker

(*Micropogonias undulates*) have been noted after large rainfall events, with fish moving from primary nursery areas protected from trawling to secondary non-nursery areas vulnerable to fishing pressure (Searcy et al. 2007). Given that global climate change is predicted to increase the frequency of extreme weather events (e.g. floods, droughts, hurricanes; Webster et al. 2005), the need to accurately predict the spatiotemporal dynamics of salinity is unprecedented.

The main goal of this work was to predict estuarine bottom salinity at any location in space and time under a variety of freshwater influx conditions using PS as an example system. PS is a shallow estuary with wind-driven currents and low tidal forcing that is frequently subject to both droughts and floods, the latter of which is often due to hurricanes. Bottom (as opposed to surface) salinity was chosen as the variable of interest because it characterizes habitats of demersal species that are important both as members of benthic food webs and as targets of valuable commercial and recreational fisheries. (Hereafter, the term 'salinity' will always refer to bottom salinity unless otherwise noted.) In future work, we will use these predictions to characterize the relationship between salinity and the presence and spatial distribution of commercially-viable fish populations to predict distribution patterns under various salinity regimes.

1.2. Previous work

Models of estuarine salinity in the literature are based on either (i) differential equations or (ii) statistical principles. Both constructs characterize a dependent variable of interest in space and time using relationships with state variables; they differ in the way that these relationships are modeled. The first models the dependent variable directly using

differential equations that are derived from physical laws and solved through a series of approximations and assumptions. The second uses a sample of direct observations of the dependent variable to probabilistically model the population of observations of the dependent variable as a function of multiple covariates; the equation of the relationship between them is the one whose function minimizes uncertainty given the data. In the context of this work, there are two key differences between the constructs: data requirements and spatial resolution. Although statistical models can require more observational data than differential equation models, they can also generate predictions over a finer spatial resolution. Predictions from differential equation models are grid-cell averages, whose spatial resolution ranges from square kilometers to thousands of square kilometers. Statistical model predictions can be for specific coordinates in space.

Most models of PS salinity are differential-equation-based models. A number of investigators (Lin et al. 2007, 2008a; Xia et al. 2007) have modified the Environmental Fluid Dynamics Code (EFDC; Hamrick 1996) to customize it to PS by incorporating freshwater influx (FWI) from major tributary rivers as well as tide and wind effects on circulation patterns. These authors used visual inspection to compare maps of PS surface and bottom salinity predictions from their models to monthly average salinity contour maps generated from historical observations (Schwartz and Chesnut 1973) and found the two to be similar, but none of them compared their predictions to observations directly to quantify uncertainty.

Xu et al. (2008) predicted surface and bottom salinity and temperature in Pamlico River Estuary (PRE), a tributary of PS, using the model in Xia et al. (2007) modified to account for differential river flow and wind patterns resulting from environmental forcing

events. Salinity predictions generated at 30 second intervals over a spatial grid with varying cell size (range: 200-800 m^2) compared well to observations from eight long-term PRE monitoring stations (R^2 between predictions and observations at the surface: 0.85; at depth: 0.79). Although these authors incorporated environmental variation in a model that produced salinity predictions suitable to assess long-term space-time trends, the PRE is a fraction (18%) of the total aerial extent of PS. To predict salinity across the entire sound, the model would need significant spatial domain expansion and re-parameterization, and such extensions are not currently planned (J. Lin, pers. comm. on behalf of Xu et al. 2008.).

Few statistical models have been constructed to describe space-time distributions of water quality features in PS (but see Reed et al. 2008), but many exist for use in both proximal and distant estuarine systems. Table 1 lists a few references along with both the parameter being modeled in each study as well as the system of interest. Notably, Rathbun's (1998) multiple linear regression model with spatially-correlated errors predicted salinity and dissolved oxygen (DO) within Charleston Harbor, SC over a two week time period in 1988 as a function of spatial coordinates and distance to the estuary mouth. The applications of this model are restricted, however, because Rathbun did not model the processes that affect salinity. This model can thus only predict salinity and DO under similar climatic conditions to those present when samples were collected. In addition, Rathbun only reported standard errors of the kriging predictor. He made no comparison of model-generated predictions to salinity observations that were not included in model fitting to investigate prediction error of the overall method.

After reviewing the literature, it was clear that no existing model accomplished our goal. We chose to construct two space-time statistical models of salinity: one with only process-based explanatory variables and another that considered time as an additional explanatory variable. The "process-based" variables are based on short- and long-term freshwater influx data, hurricane landfall data, distance between the site of interest and each of four tributary rivers, and distance between the site and each of three inlets. To the best of our knowledge, these are the only process-based models constructed for lagoon-type estuaries like PS that produce a salinity prediction at a specific point in space and time. In addition, the methods used here could be modified to construct process-based space-time statistical models for salinity in other estuarine systems if data were available.

2. METHODS

Models were built in several steps. Through literature reviews and discussions with colleagues, we identified physical forcing mechanisms believed to affect PS salinity over space and time. We searched for data that could be used directly or indirectly to represent these mechanisms, and then developed meaningful explanatory variables from this data in Sections 2.1 through 2.9. The choices we made reflected our modeling context and thus might differ in an alternate modeling context. When we use the phrase "modeling context," we refer to the modeling objectives, the geographical features of the region being modeled, and the spatial and temporal coverage and resolution of the data. We describe the variable selection process in Sections 2.10 through 2.12, first using ordinary least squares (OLS) linear regression to select the mean trend and then modeling the spatial correlation in the

deviations from this mean trend. The two models, "process" (containing process-based variables only) and "time" (with process variables and a variable corresponding to time period), were compared in terms of their ability to predict salinity in a withheld dataset of observations. We used the better model to create maps of salinity predictions for 40 2.5-week time periods from 1987-2006 to make generalizations about salinity patterns under different, highly variable FWI conditions.

2.1. Data sources

2.1.1. Salinity observations in Pamlico Sound

The Pamlico Sound Trawl Survey Program 195 (or 'the survey' within this work) has been monitoring stocks of dominant estuarine species in PS since 1987. The North Carolina Division of Marine Fisheries (NCDMF) conducts survey sampling in June and September to assess species abundance in relatively deep water (>2 m) habitats using a weighted stratified random sampling design based on area. PS is divided into seven areal strata that are further subdivided into one square minute (or one square nautical mile) grid cells. A total of 54 core sampling station locations, one per grid cell, are designated within the seven strata, with more stations assigned to larger strata. Thirty stations are located in main-stem PS, and eight stations each are located in the Neuse, Pamlico, and Pungo rivers. Coordinates of specific trawling sites at each station location are randomly generated to occur within the grid cell. Measurements of surface and bottom temperature, salinity, and dissolved oxygen are collected using a YSI-85 multi-function meter at the beginning of each trawl and recorded along with depth and spatial reference coordinates. Figure 1 depicts depth contours across the survey's overall spatial domain *S*, or the area of PS > 2 m deep.

During data pre-processing, salinity observations at individual sites were discarded if they fell outside of a plausible salinity range for PS (0-35) or if their spatial coordinates erroneously placed them outside of PS entirely (i.e. over land or in the Atlantic Ocean). Site coordinates, as well as all other latitude and longitude coordinates used in the remainder of this analysis, were converted from decimal degrees to northings (y-direction) and eastings (x-direction) in nautical miles (nmi) from a reference point located southwest of *S* at 34.6°N, -77.1°W to ensure that they were positive in both the x- and y-directions.

This work uses June and September survey data from 1987-2006, which will henceforth be called the temporal domain (*T*). Forty time periods, or specific month/year combinations in which survey samples were collected, exist in the temporal domain (*P*=40). Time period is indexed using the subscript *t*, where *t*=1, ..., *P*. A single time period is approximately 2.5 weeks long: the amount of time it takes NCDMF to sample the 54 core stations within *S*. Occasionally not all 54 core stations are sampled, so n_t refers to the number of sites in time period *t*. Site refers to a specific spatial location nested within a particular time period, sites are indexed using the subscript *i* where *i* =1, ..., n_t. The dataset includes *N* =2100 total observations of salinity, where $N = \sum_{t=1}^{T} n_t$. Sal_{it} refers to salinity at site *i* in time period *t*.

2.1.2. Freshwater influx (FWI)

Since the watersheds of the Neuse, Pamlico, Roanoke, and Chowan rivers encompass 80% of the total land drainage area into PS (Bales 2003), FWI from these four tributaries was assumed to account for the majority of riverine freshwater delivered to the estuary. FWI

observations are average daily river discharge rates collected by one US Geological Survey (USGS) gauge station per tributary (from S-N): (i) Neuse River station in Kinston, NC (Station #02089500) gauging Neuse River inflow, (ii) Tar-Pamlico River station in Tarboro, NC (Station #02083500) gauging Pamlico River inflow, (iii) Roanoke River station in Roanoke Rapids, NC (Station # 02080500) gauging Roanoke River inflow, and (iv) Ahoskie Creek station in Ahoskie, NC (Station # 02053500) gauging Chowan River inflow. These particular stations were chosen because they were the closest gauge stations to PS on their respective rivers that recorded data throughout *T*. Discharge rates were downloaded from the USGS Water Resources website for the state of North Carolina (USGS 2009b) in ft^3/sec and were converted to m^3/sec.

2.2. Explanatory variable creation and evaluation

Six key factors are known to affect estuarine salinity (Pritchard 1954, 1967); three (FWI from rivers, evaporation, and direct precipitation) describe the amount of freshwater at a given location, one (saltwater input from the ocean) describes the amount of saltwater at a given location, and the remaining two (winds and tides) describe the mixing processes that unite the two water masses. Spatial coordinates of sample sites have been used as explanatory variables in other statistical salinity models (Little et al. 1997, Rathbun 1998) and here they might serve as surrogates for causal factors not included. Land-falling hurricanes have also had significant impact on observed PS salinities (Ramus et al. 2003, Paerl et al. 2005). In the following sections, we address each of these eight factors in more detail.

2.3. Freshwater from rivers: calculating relative freshwater influx index (FWII)

After obtaining daily average river discharge rates from the four gauge stations for every day during T (7,305 days total), we created short- and long-term indices to describe the influence of freshwater over the previous week (7 days) and the previous two months (61 days) from a given river on a given sal_{it} as a function of the distance that separates site i from the source of the FWI. We expect that salinity in PS is affected by both a long-term average FWI to the system, as well as a short-term average FWI, the latter representing changes in freshwater delivery rates resulting from extreme FWI events immediately prior to survey sampling. To describe long-term conditions, we calculated separate $2mo\_FWI_{rt}$ metrics for each river r (r =1,…,4) in time period t by averaging daily discharge rates in the 61 days prior to m_t, the first day of the survey in t. This length of time was chosen to correspond to the average freshwater residence time of the rivers (Bales and Robbins 1995, Lilly 1998, Paerl et al. 2001) and to provide a temporal lag between the upriver gauging of freshwater and the delivery of that water to S. Ramus et al. (2003) calculated a seven-day residence time for the Neuse and Pamlico Rivers after Hurricanes Dennis and Floyd deposited 1 m of rainfall in eastern NC four days before the September 1999 survey. We thus created short-term FWI metrics, or $1wk\_FWI_{rt}$, by averaging daily discharge rates in the 7 days prior to m_t. [As a side note, river residence times may not be appropriate to use in every system to calculate a temporal duration of freshwater influx that affects observed salinity. No rule exists requiring their usage; they were simply selected as plausible ranges based on the information above.]

To include these metrics in the model, a unique measure of the influence of $1wk\_FWI_{rt}$ and $2mo\_FWI_{rt}$, was required for each space-time location. Since freshwater from

river *r* in time period *t* should have more of an effect on sal_{it} the closer site *i* was to the river itself, we calculated both a one-week and two-month freshwater influx index (FWII) by dividing each FWI_{rt} by $dist_{rit}$, or the distance between the gauge station on river *r* and a given *it* sample location as follows:

(1) $$1wk\_FWII_{rit} = \frac{1wk\_FWI_{rt}}{dist_{rit}}$$

$$2mo\_FWII_{rit} = \frac{2mo\_FWI_{rt}}{dist_{rit}}$$

As was the case with calculating the appropriate time duration for short- and long-term FWI, there were no rules to govern the calculation of $dist_{rit}$. The coordinates of each river gauge station were used to calculate distance (as opposed to using the coordinates of the mouth of each river) because the gauge station was the specific location of FWI data. $Dist_{rit}$ was calculated using Euclidian distance (i.e. distance as the crow flies) after considering Little et al. (1997) whose work compared the relative accuracy of predictions of numerous water quality parameters generated from two different multiple linear regression models that contained the explanatory variable "distance to inlet mouth." Predictions from models that used water-path distance (i.e. distance along the path of a river) to calculate this variable were found in most cases to be no more accurate than those produced by models that used Euclidean distance. Neither Little et al. (1997) nor Rathbun (1998) drew a clear conclusion regarding the best method to use in all situations to calculate estuarine distances, and because calculating water-path distances between 2100 space-time locations and each of four river

gauge stations would be cumbersome, Euclidean distance was used in this study to calculate distances between two points.

The 320 FWI_{rt} values (*1wk_* and $2mo\_FWI_{rt}$ for each of four rivers across 40 time periods) generated 16,800 different values of $FWII_{rit}$ indices, or eight $FWII_{rit}$ explanatory variables (one for each river and time duration) per *it* location. We additionally considered as explanatory variables all possible pair-wise interactions between the eight *1wk_* and $2mo\_FWII_{rit}$ from different rivers (24 interactions in all), as we expected that the effect of $FWII_{rit}$ on salinity from river *r* could change based on the $FWII_{rit}$ from another river during the same time period.

2.4. Evaporation and direct precipitation

Annual mean PS evaporation is less than annual mean direct precipitation, indicating a net gain of freshwater (Giese et al. 1979). This analysis ignored evaporative processes, assuming that direct precipitation more than accounted for the amount of freshwater removed. Direct precipitation was also ignored due to a lack of spatial resolution in the data. Because direct precipitation constitutes only 8% of the total mean freshwater volume delivered to PS, with FWI from tributary rivers accounting for the other 92% (Giese et al. 1979), we felt that riverine FWI adequately approximated the total freshwater delivery to the system.

2.5. Saltwater from the ocean

Mean Atlantic Ocean salinity in the vicinity of PS is typically around 35 (Molina 2002). Although inner continental-shelf salinity exhibits some spatial variability (Pietrafesa et al. 1994), we followed the modeling efforts of Xie and Pietrafesa (1999) and assumed

constant open ocean salinity. This assumption makes the volume of saltwater at site *i* in time period *t* a function only of $dist_{sit,}$ or the Euclidian distance between site *i* and *s*, the geographic center of one of PS's major inlets (from N-S: Oregon, Hatteras, and Ocracoke) where *s*=1,2,3. We later decided that saltwater entering from the inlet closest to site *i* might approximate the total amount of saltwater reaching that site and thus perhaps explain the same proportion of variability in salinity as the group of three $dist_{sit}$ variables. Using one explanatory variable instead of three would create a more parsimonious model, so distance to the nearest inlet, or $closest\_inlet\_dist_{it}$, was considered separately; equal to the smallest of the three $dist_{sit}$.

2.6. Wind speed and direction

A prevailing wind field that is north/northeastward from March to August and south/southwestward from September to February is the primary driver of currents in PS (Pietrafesa and Janowitz 1986, Xie and Eggleston 1999, Eggleston et al. in press). While wind speed and direction could play a role in determining a particular sal_{it} on time-scales of hours to days (Reed et al. 2008, Reynolds-Fleming et al. 2008); on timeframes of 2-3 weeks, the moving average of wind speed in PS is relatively invariant except when hurricanes are present in the system (Eggleston et al. in press; G. Janowitz, pers. comm.). To examine the effects of seasonal wind patterns on the spatial distribution of salinity, we created the categorical indicator variable $month_{it}$, corresponding to the month in which site *i* in time period *t* was sampled. A different variable represents the effect of land-falling hurricanes on salinity (see Section 2.9).

2.7. Tides

Though the physical mixing of water from surface to depth during tidal cycling should influence estuarine salinity, tidal signal in PS is almost entirely lost at distances greater than 10 km from the inlets (Pietrafesa et al. 1986, Molina 2002). Therefore, the influence of tidal motions on salinity was included only by way of the distance-to-inlet variables.

2.8. Spatial coordinates (northing and easting)

Estuarine salinity varies over space, so it was logical to consider spatial coordinates as explanatory variables. Although spatial coordinates do not clarify the process by which salinity varies over space and time, as they could explain variability in salinity not accounted for by other model variables. In scatterplots, salinity appeared quadratic in easting and cubic in northing. The quadratic function of easting can be explained by tracing a path along the 35º 16' N parallel (**A** on Fig. 1): salinity should initially increase when traveling east across PS, reach a maximum at the saltwater plume near Ocracoke and Hatteras Inlets, and decrease again on the other side of the plume in the waters on the western shore of Hatteras Island near Buxton, NC. The cubic function of northing is best described near the mouth of Croatan Sound at a longitude of 75º 42' W (**B** on Fig. 1), where salinity should increase traveling south from Albemarle Sound and reach a local maximum near Oregon Inlet, decrease continuing past the saltwater inlet plume, and increase again as the Hatteras Inlet saltwater plume is reached. For this reason, $easting_{it}$, $easting_{it}^2$, $northing_{it}$, $northing_{it}^2$, $northing_{it}^3$, and the interactions $northing_{it}*easting_{it}$, $northing_{it}^2*easting_{it}$, *and* $northing_{it}*easting_{it}^2$ were all

considered as explanatory variables. All coordinates were centered before they were squared or cubed by subtracting the mean over all observations.

2.9. Hurricane landfalls

Hurricanes can rapidly introduce large volumes of freshwater to estuaries via riverine influx, push large volumes of saltwater in through inlets, and alter circulation patterns through abrupt changes in wind speed and direction. Off the coast of North Carolina, they have also been known to open new inlets to PS, which can additionally alter current flow and increase saltwater intrusion (Paerl et al. 2005). $1wk\_FWII_{rit}$ should capture the majority of the variability in PS salinity attributed to hurricane-produced FWI, but the presence of a hurricane immediately prior to the survey should affect other physical mixing processes that could, in turn, affect salinity. Three additional explanatory variables account for non-FWI related variability in salinity due to hurricane landfalls. These variables are unique to a given time period *t* but not a given site *i* within *t*.

- $inverse\_days\_survey_t$ = continuous variable that represents the inverse number of days between m_t and the most recent hurricane landfall in NC. If no hurricanes made landfall in the 61 days prior to m_t, this variable=0.
- $category_t$ = category of the most recent hurricane landfall in NC rated on the Stafford-Simpson scale (1,…,5). If no hurricanes made landfall in the 61 days prior to m_t, this variable=0.
- no_storms_t = total number of hurricanes making landfall in NC in the 61 days prior to m_t.

2.10. Variable selection

We identified a total of 49 potential explanatory variables: $easting_{it}$, $easting_{it}^2$, $northing_{it}$, $northing_{it}^2$, $northing_{it}^3$ and interactions (9 variables); $1wk\_FWII_{rit}$ and $2mo\_FWII_{rit}$

(8) and pair-wise interactions (24); $closest\_inlet\_dist_{it}$; $dist_{sit}$ (3); $month_{it}$; and three hurricane variables ($inverse\_days\_survey_t$, $category_t$, and no_storms_t). We chose to use an ordinary least squares (OLS) linear regression approach with an adjusted R^2 variable selection criterion to select the optimal combination of these variables (i.e., the one that explained the most variability in the response using the fewest number of variables) by creating multiple candidate models. Adjusted R^2, a modified version of R^2 that introduces a penalty for the number of model explanatory variables by dividing each sum of squares by its associated degrees of freedom (df), was used because candidate models contained different numbers of explanatory variables. While R^2 increases as more explanatory variables are added to a model, adjusted R^2 only increases if the added variable decreases the model's error sum of squares enough to offset the loss in error df.

Because $closest\_inlet\_dist_{it}$ and the set of three $dist_{sit}$ variables contained redundant information, we decided that it was inappropriate for the model to include both. To choose between them, we regressed sal_{it} on the set of three $dist_{sit}$ and $closest\_inlet\_dist_{it}$ separately and obtained adjusted R^2's of 0.38 and 0.34, respectively. To determine whether the modest gain in percent variability explained by the three $dist_{sit}$ would still hold when variables that also described the physical location of location *it* were included, we added three different combinations of candidate easting and northing variables to each model. Table 2 reports the values of adjusted R^2 for the eight linear regression models. Once models included easting, northing, and their interactions, the model with the set of three $dist_{sit}$ variables explained no more variability in salinity than did the model with $closest\_inlet\_dist_{it}$ (adjusted R^2=0.43 for each). $Closest\_inlet\_dist_{it}$ was thus used in the remainder of analyses.

To decide what additional variable combinations to include in the model, we used an iterative procedure similar to forward selection. Sal_{it} was regressed against five independent explanatory variables ($closest\_inlet\_dist_{it}$, $month_{it}$, $inverse\_days\_survey_t$, $category_t$, and no_storms_t) and two sets of FWII metrics (the $1wk\_FWII_{rit}$ set and the $2mo\_FWII_{rit}$ set) separately. The four FWII metrics from each time duration were always included as a group because collinearity among these metrics produces inflated standard errors that make it difficult to use p-values to determine which are needed in the model. Table 3 ranks the eight regression models in order of decreasing adjusted R^2. The $2mo\_FWII_{rit}$ set had the largest adjusted R^2 (0.38); it became the base of the mean trend process model. The mean trend model was then built up from this foundation: variables or sets of variables whose individual models had the next largest adjusted R^2 were sequentially added to the base and the adjusted R^2 of the resultant model was compared to that of the base model without the addition. If the new model showed no improvement over the previous (i.e. adjusted R^2 did not increase after the variable addition), the newly added variable was removed; otherwise, it was retained. We continued to add variables in the order in which they are listed in Table 3 until no additional variables remained; at which point the base mean trend process model contained 10 total explanatory variables (the $2mo\_FWII_{rit}$ set, $closest\_inlet\_dist_{it}$, the $1wk\_FWII_{rit}$ set, and $inverse\_days\_survey_t$) and had an adjusted R^2 of 0.57.

Next, we evaluated the addition of the pair-wise interactions between $1wk\_FWII_{rit}$ and $2mo\_FWII_{rit}$ to the model. These 24 interactions were also considered a set based on the aforementioned rationale, and their inclusion was evaluated using the same selection procedure. Even though the addition of the interactions decreased error df by 24, adjusted R^2

of the model with interactions (0.66) was larger than that of the model with no interactions (0.57), so the set was retained.

Spatial coordinate variables were evaluated in groups according to their polynomial order as a final step, with squared and cubic terms added before interactions. Table 4 lists the results of this stepwise addition process to the existing base mean trend model. We considered these variables last, because we only wanted to include them if they explained additional variability in the response after other, more process-based variables were examined. Upon examination, we determined that including all variables except $northing_{it}^2 * easting_{it}^2$ continued to increase adjusted R^2. The final mean trend process model (below) included 42 explanatory variables and had a final adjusted R^2 of 0.73.

Variables included in final mean trend process model:
$2mo\_FWII_{rit}$, $closest\_inlet\_dist_{it}$, $1wk\_FWII_{rit}$, $inverse\_days\_survey_{t,}$ ($2mo\_FWII_{rit} * 2mo\_FWII_{rit}$), ($1wk\_FWII_{rit} * 1wk\_FWII_{rit}$), ($2mo\_FWII_{rit} * 1wk\_FWII_{rit}$), $easting_{it}$, $northing_{it}$, $easting_{it}^2$, $northing_{it}^2$, $northing_{it} * easting_{it}$, $northing_{it}^3$, $northing_{it} * easting_{it}^2$, and $northing_{it}^2 * easting_{it}$

During model construction, we noted in scatter plots between sal_{it} and $2mo\_FWII_{rit}$ that there appeared to be several groups of observations with different slopes (Fig. 2). Upon closer examination, it was determined that each group corresponded to the $2mo\_FWII_{rit}$ values within a set of time periods. To incorporate this apparent time-period effect on salinity, we created a second mean trend model by repeating the analysis process described above that included time period as a factor and the interactions between time period and the $2mo\_FWII_{rit}$ as continuous explanatory variables. We discuss the utility of each model, which we name, respectively, process and time, in Section 4.2.

The initial linear regression model of sal_{it} vs. *time_period* had an adjusted R^2 of 0.41, making it the base of the new mean trend model (refer to Table 3 for comparison). Before evaluating interactions, the mean trend time model ultimately contained 48 explanatory variables (the set of 39 *time_period* variables, the $2mo\_FWII_{rit}$ set, $closest\_inlet\_dist_{it}$, and the $1wk\_FWII_{rit}$ set) and had an adjusted R^2 of 0.78. When the set of interactions between *time_period* and $2mo\_FWII_{rit}$ was added, the model was not of full rank (i.e., not all columns in the design matrix were linearly independent) and thus not uniquely estimable. Because we were originally motivated to create this alternate model to evaluate these interactions, we removed the $1wk\_FWII_{rit}$ set to include the $time\_period*2mo\_FWII_{rit}$ interaction set. This new model ($sal_{it} = time\_period + 2mo\_FWII_{rit} + closest\_inlet\_dist_{it} + time\_period*2mo\_FWII_{rit}$) was of full rank, and it became the new base, as its adjusted R^2 (0.89) was larger than that of the previous mean trend time model that included $1wk\_FWII_{rit}$ (0.78). After investigating spatial coordinate variables, the final mean trend time model (below) had an adjusted R^2 of 0.91 using 204 variables:

Variables included in final mean trend time model:
time_period, $2mo\_FWII_{rit}$, $closest\_inlet\_dist_{it}$, ($time\_period*2mo\_FWII_{rit}$), $easting_{it}$, $northing_{it}$, $easting_{it}^2$, and $northing_{it}^2$

2.11. Statistical theory

In matrix notation, the regression models we have fit up to this point are of the following form:

$$sal_t = X\beta + \varepsilon_t \qquad \varepsilon_t \sim N(0, \sigma^2 I) \tag{2}$$

$\boldsymbol{Sal_t}$ is an n_t x 1 vector of all salinities observed in time period t. $\boldsymbol{X}$ is an n_t x p matrix where p is the total number of explanatory variables in the model plus the intercept. Each column in $\boldsymbol{X}$ corresponds to a single explanatory variable in the model (with all 1's in the first column for the intercept) while each row corresponds to a particular *it* location. $\boldsymbol{\beta}$ is a p x 1 vector of unknown regression coefficients to be estimated for each explanatory variable. ($\boldsymbol{X\beta}$ is the mean trend portion of this model). The deviations between salinity observed at every site i in time period t and the mean salinity in t are included in $\boldsymbol{\varepsilon_t}$, an n_t x 1 column vector of errors. We assume that these errors are distributed normally with mean 0, represented by the n_t x 1 vector of zeros, and variance σ^2. Multiplying σ^2 by the identity matrix ($\boldsymbol{I}$) of size n_t, indicates that errors are independent and identically distributed (iid).

Spatial data, however, is often found to exhibit correlation over space, and the presence of this correlation would violate the previous assumption of independent errors. To incorporate this spatial structure into the model, the error distribution in Equation 2 is modified:

$$(3) \qquad sal_t = X\beta + \varepsilon_t \qquad\qquad \varepsilon_t \sim N(0, \Sigma_t)$$

Notice in Equation 3 that the mean trend portion of the model remains the same; the difference lies in the modeling of the error distribution. Here, the expected value of each element in $\boldsymbol{\varepsilon_t}$ is still zero, but the variance is instead described by the n_t dimensional square matrix $\boldsymbol{\Sigma_t}$. The i^{th} diagonal element of $\boldsymbol{\Sigma_t}$ is the variance of ε_{it}, which we assume equals σ^2 for all i. The element in the i^{th} row and the j^{th} column of $\boldsymbol{\Sigma_t}$ is the covariance between ε_{it} and ε_{jt}

(where $j = 1,\ldots, (i\text{-}1)$). These covariances (*Cov*) are a function of d_{ij}, the distance that separates locations i and j, and they can be calculated using the general formula

$$(4) \qquad Cov\{\varepsilon_{it}, \varepsilon_{jt}\} = f(d_{ij}) * \sigma^2$$

Covariance is a measure of similarity, and it typically decreases with increasing d_{ij}. Depending on the rate and pattern of decay, spatial covariance can be modeled by one of a number of theoretical functional forms, most of which are characterized by three parameters. Figure 3 illustrates a sample covariogram (dots) of observed data from June 1994 overlaid by the modeled Exponential covariance function (smooth curve). The sill is the overall or maximum variance of the process and is equal to $\sigma^2 + \sigma^2_n$. The nugget (σ^2_n) is a measure of the discontinuity at the origin; it represents measurement error or variability at a scale smaller than the minimum distance separating two sites in the dataset. The range (ρ) is the distance at which the covariance decays to zero; the practical range (θ) observed here is the distance at which the covariance has reached 5% of σ^2, which is considered to effectively equal zero. Certain functional forms (Exponential, Gaussian) use θ while others (Spherical) use ρ.

Modeling spatial correlation when it is present is important because it leverages previously unused information contained in residual error structure to generate more accurate predictions of the response at unsampled locations. Models that ignore existing spatial correlation produce estimates of regression coefficients that are unbiased, but the standard errors, confidence intervals, and p-values for these estimates are not trustworthy (Kitanidis 1997). This unreliable information could alter the interpretation of model results.

2.12. Modeling spatially correlated error

Throughout this section, we describe the modeling of the spatial correlation among deviations from the mean trend at sites within a single time period using the process model as the example. Although observations are collected over time, we assume that no temporal correlation exists between time periods because the separation between June and September is probably greater than the time period within which temporal correlation is present.

We examined covariograms created from mean-trend process-model residuals for each time period (40 covariograms in all) to look for possible spatial patterns in error distribution as an exploratory exercise, and noted that residuals in every time period appeared to exhibit some form of spatial structure (Fig. 3). To determine the functional form that best described this structure, we re-fit the mean trend process model separately for each time period a total of eleven times (40 time periods x 11 = 440 total evaluations) using restricted maximum likelihood estimation (REML). The first ten evaluations each included one of ten covariance functions (Exponential, Gaussian, Spherical, Linear, and Power, each with and without a nugget). The eleventh contained no spatial covariance function and was the final mean trend model run for one time period at a time. We chose REML over maximum likelihood (ML) because it generates less bias when estimating variance and covariance parameters (Patterson and Thompson 1971).

We used the Bayesian information criterion (BIC) to select the best-fitting model given the data (i.e. the one with the smallest BIC) in each time period. BIC is appropriate for comparing likelihood models with different numbers of explanatory variables because it penalizes model complexity (i.e. the number of parameters in model; Schwarz 1978). From

this exercise, we confirmed the presence of spatial correlation in residuals by observing that individual time period evaluations of the mean trend process model that incorporated spatial covariance functions had lower BICs than those where error was modeled as iid in the majority (39) of time periods. (The mean trend time model performed similarly with majority equaling 33 time periods).

To correctly account for spatial covariance, we needed to determine the most appropriate parameterization for $\boldsymbol{\Sigma}$ based on our modeling context. Because of software limitations (SAS Proc Mixed), we needed to specify a single functional form in all time periods. Exploratory work indicated that each time period had unique estimates for the range and the sill depending on the proportion of variability in salinity unexplained by the mean trend. We therefore wanted a model with different range and sill estimates for each time period group. This translates mathematically to a N by N block diagonal covariance matrix (5), where off-diagonal elements are zero matrices and diagonal elements ($\boldsymbol{E}_1, \boldsymbol{E}_2, \ldots \boldsymbol{E}_T$) are n_t x n_t matrices with element ij of $\boldsymbol{E}_T$ given by the equation in Table 5 that corresponds to the particular covariance function used.

$$\Sigma = \begin{bmatrix} \mathrm{E}_1 & 0 & 0 & 0 \\ 0 & \mathrm{E}_2 & 0 & 0 \\ 0 & 0 & \ddots & \vdots \\ 0 & 0 & \ldots & \mathrm{E}_T \end{bmatrix} \tag{5}$$

Cross-validation was used to select the best spatial covariance function by comparing the predictive accuracy of the mean trend process model with iid errors to predictions generated by the process model with each of six spatial covariance functions (Exponential,

Gaussian, and Spherical both with and without nuggets). Because the Power and Linear functions were infrequently selected as best fitting in exploratory analyses, they were excluded from consideration here. To cross-validate, each of the candidate models was fit to a base dataset that contained a randomly-chosen 90% of the total number of observations (N_B=1890). The nugget estimate was the same for all time periods again because of software constraints. However, this seemed a reasonable assumption because measurements were collected following the same protocol for the entirety of the survey, which should make measurement error in the method constant over time. Regression coefficient estimates were used to predict salinity in a test dataset containing the remaining 10% of the observations that were withheld from model fitting procedures (N_E=210). The test dataset did not contain the same number of observations from each time period, but it did contain at least three observations per time period.

Four different selection criteria were used to evaluate model fit. We first computed the root mean squared error (RMSE) of the test dataset predictions for each model run. RMSE in units of the response variable and is a measure of standard error for unbiased estimators. It is calculated using the formula

$$RMSE = \sqrt{\frac{\sum_{i,t=1} (y_{it} - \hat{y}_{it})^2}{N_E}} \quad (6)$$

where y_{it} corresponds to the actual observed salinity at station location *it* and $\hat{y}_{it}$ is the salinity predicted by the model at location *it*. A lower RMSE indicates more accurate model

predictions. We should note that if the model predicted salinity at a location to be less than zero, we manually set the prediction equal to zero before calculating RMSE. It is not possible to have a negative salinity value, although Proc Mixed occasionally predicted them because we were not able to specify a truncated normal distribution. We also examined the values of the slope, intercept, and coefficient of determination (R^2) of the regression of observed salinity on predicted salinity in the test dataset. If the model predictions were perfect, the regression would have a slope equal to one, an intercept equal to zero, and an R^2 equal to 1. In Table 6, we compared candidate models and selected the model whose predictions best satisfied these four criteria (minimum RMSE, slope close to one, intercept close to zero, and R^2 as close to one as possible). Table 6 additionally reports three base dataset model fit statistics: –2 log likelihood, Akaike's information criterion (AIC), and BIC. The model selected in this step was the end model.

From Table 6, it is clear that salinity predictions were better (based on the above criteria) when either model, process or time, included any spatial covariance function. Of the time models, including an Exponential spatial covariance function with a nugget produced predictions with the lowest RMSE (2.1), the slope closest to one (0.92), and the intercept closest to zero (1.55). When examining process models, four models (Exponential and Spherical both with and without a nugget) performed equally well, and better, in terms of the selection criteria, than all of the time models. Of the four best process models, the model with an Exponential covariance function with a nugget had the lowest AIC (7580.0) and BIC (7711.7) and for this reason it was chosen as the best model to predict salinity in PS; it explained 89% of the variability in salinity in the test dataset and generated predictions with

RMSE of 2.0. We now fit this model using the full dataset, interpolated salinity at evenly spaced 1 nmi (1.85 km) increments across the spatial domain, and created retrospective maps of salinity predictions and their corresponding standard errors for each time period.

3. RESULTS: EVALUATING FRESHWATER INFLUX SCENARIOS

Overall, predicted salinities ranged from –4.9 to 29.3, which is similar to the range of overall observed salinities (0.1 to 30.7). Forty-two salinity predictions, less than 0.1% of the total number of predictions, were negative and set to zero. Within each time period, prediction standard errors were typically lowest in the neighborhood of observations. The range of standard errors, however, varied among time periods. The overall standard error range was 0.22 to 6.25, but more than 90% of prediction locations had standard errors less than 2.5.

To look for systematic patterns of salinity under similar FWI, we examined 16 possible freshwater influx scenarios (Table 7) spanning drought conditions to average freshwater influx conditions to flood conditions. Each scenario consisted of different combinations of classes of FWI for both one-week and two-months prior to the survey. *1wk_* and $2mo\_FWI_{rt}$ was considered 'low' if it was below the 25th percentile of observed FWI across all time periods for that river, 'moderate' if it was between 25th and 75th percentile of observed FWI, 'high' if it was between the 75th and 95th percentile, and 'flood' if it was above the 95th percentile. Overall one-week and two-month FWI for the entire time period was considered low or high if at least two rivers in that time period exhibited low or high inflow, moderate if at least three rivers in that time period exhibited moderate inflow, and

flood if at least one river exhibited extremely high inflow. Table 7 shows that the majority of these scenarios are represented by time periods within the observed dataset. The first and second columns give the 16 combinations of two-month and one-month flow class, the third tells which time periods exemplify this scenario. Time periods were also ranked 1-40 by mean predicted salinity (1=lowest mean salinity; 40=highest); those rankings are listed in column four. We selected three scenarios to detail in the remainder of this section: one to describe an average case (moderate to moderate FWI) and one to describe each extreme case (low to low FWI and flood to flood FWI) in order to demonstrate the possible range of variability in salinity patterns. Time period maps illustrating these selected scenarios are reproduced here; the remainder will be available online during late summer 2009.

3.1. Moderate to moderate FWI

June 2005 provides an example of salinity distributions resulting from moderate FWI to PS in both the two months and one week prior to the survey. Within the left pane of Figure 4, we note that predicted salinity in this time period was less than 9.6 in both the Neuse and Pamlico Rivers. The transition of the color ramp from cool to warm colors illustrates that predicted salinity increased moving east across PS, reaching a maximum just south of Oregon Inlet. The eight legend color categories are based on percentiles (%) of the distribution of observed salinity across all time periods: minimum value to 5%; 5-10%; 10-25%; 25-50%; 50-75%; 75-90%; 90-95%; and 95% to maximum value. Comparing this map to the map of observed salinities in the top right pane, the same east-west salinity gradient exists in the observations. The area of highest predicted salinity corresponds to a lone purple

observation just south of the inlet. We know that observed salinity at that site was greater than 25.7 because both maps share the same legend (actual salinity observed: 26.5).

Comparing the map of prediction standard errors in the lower right pane of Figure 4 to the other two maps, we make the same observation here that we will in all subsequent time periods: standard errors are lowest for predictions near observations and increase with increasing distance from observations. This transition is indicated through a color gradient shift from cool colors surrounding sites where salinity was observed (low SE) to warm (higher SE) colors farther away from sample sites. The same eight percentile groups are used to classify colors on the SE map legend, here based on the distribution of prediction standard errors across all time periods, where standard errors are in the same units as salinity.

In this time period as in all others, salinity predictions are only generated for locations within the spatial domain, which does not extend either to Albemarle Sound or to the heads of the Neuse and Pamlico Rivers.

3.2. Low to low FWI

To examine the effects of both prolonged and abbreviated low FWI on PS salinity patterns, we compared maps of June 1999 (Fig. 5A) and June 2002 (Fig. 5B). These time periods occurred at the beginning and end, respectively, of North Carolina's 1998-2002 drought (Weaver 2005). As in the previous scenario, patterns in the predictions mirror those seen in the observations. Comparing these maps to our map of predicted salinity under moderate FWI, we observe in all three a similar west-east salinity gradient with higher salinities along the sound's eastern coast than on the western shore near the Outer Banks. Overall predicted salinity is higher in both June 1999 and 2002, where the majority of

salinity predictions were greater than 20, than in June 2005, where predicted salinities are mainly between 9 and 18. This is undoubtedly due to decreased FWI observed in June 1999 and 2002 relative to June 2005. For June 2002, as was the case for June 2005, mixing near the inlets is evident in both the observations and predictions, though this time we see the mixing at the southern inlets as well. Mixing near the inlets is not evident for June 1999, possibly due to differences in current circulation.

Observed and predicted salinities were much higher in mainstem PS in June 2002 than in June 1999, despite the fact that both had similar values for *1wk_* and *2mo_FWI* variables from three of the four tributary rivers (*1wk_* and *2mo_FWI* from the Roanoke River in June 1999 was twice what it was in June 2002). Different historical system states likely produced this result. As noted, June 1999 was more than a year into a four-year drought: weekly average stream flow conditions for the 30 weeks prior to m_t were each between the 6^{th} and 20^{th} percentile of average FWI measured for that week over the last 30 years (USGS 2009a). By June 2002, NC had been experiencing drought conditions for four years (186 weeks). Thus salinity was probably higher in June 2002 than in June 1999 due to a cumulative FWI deficit that became more pronounced over time.

It is interesting to note that June 2002, the time period with both the larger range of observed salinity and the higher predicted overall salinity of the two, had overall lower predicted standard errors. In June 2002, the majority of standard errors are less than 1.01, while for June 1999; they fall between 1.01 and 1.81 at almost all prediction locations. These results demonstrate the fact that the magnitude of the prediction standard error at space-time location *it* is a function of both the certainty and variability of the deviations from the mean

trend. Predictions are associated with greater certainty when they are closer to observations, but at the same time, mean trend portion of the model explains more variability in salinity in some time periods than in others, resulting in overall less variability in residual errors in that time period and thus a lower σ^2_t. When σ^2_t is lower, standard errors at individual prediction locations are also lower.

3.3. Flood to flood FWI—with and without hurricanes

To examine the effects of extremely high freshwater inflow on PS salinity patterns, we compared maps created for September 1999 and June 2003 (Fig. 6A and B, respectively). FWI was extremely high in September 1999 as a result of the 500-year floods produced by Hurricanes Dennis (25 d. pre-survey) and Floyd (11 d. pre-survey), while in June 2003, extremely high FWI was due to an eight-month series of above-average precipitation totals prior to the survey (a.k.a. the end of the 1998-2002 drought). Again, model predictions mirrored observations, and prediction standard errors were larger in one time period (September 1999) than in the other (June 2003). Compared to each other, salinity was much lower in June 2003, with more than 99% of predicted salinities less than 14.5, than in September 1999, where over two-thirds of predicted salinities were greater than 14.5. Compared to our example of moderate FWI, predicted salinity in PS is lower in June 2003, most likely due to its increased *1wk_* and $2mo\_FWI_{rt}$. Predicted salinity in September 1999, however, was higher than it was in June 2005, despite the increased influx of freshwater. In June 2003, salinities were similar across the main-stem of PS, while in September 1999, mixing near Hatteras Inlet was evident.

Differences in overall magnitude of predicted salinity between these two time periods can potentially be explained by differences in historical system state. Severe flooding conditions resulted from hurricane rainfall in 1999; however, that rainfall was deposited onto a watershed that had been in a state of severe drought for the previous 44 weeks (see Section 3.2, above). Flooding, albeit less severe, was also noted in June 2003, but these floods resulted from consistent, above-average precipitation and stream flow that began 25 weeks prior to m_t. By June 2003, the PS system likely contained more freshwater overall than it did in September 1999, resulting in lower salinities even in the absence of a large FWI pulse.

Differences in spatial salinity patterns observed in this FWI class could also have resulted from the presence or absence of hurricanes in the system. Predicted salinity varied greatly between these two time periods in the vicinity of Ocracoke and Hatteras Inlets: in September 1999, predicted salinity ranged from 18.5 to 24.7 in this region, while in June 2003, only two prediction locations had salinities greater than 14.5. This area of saltier water in September 1999 likely resulted from the forcing of Atlantic Ocean water through the inlets by the west/northwestward hurricane-force winds that accompanied Dennis and Floyd. Seasonal winds in June 2003 were north/northeastward with an average speed of 10 mph, which would have resulted in a smaller influx volume of salt water (see Xie and Eggleston 1999).

4. DISCUSSION

Although the direct effects of climate change on coastal environments (e.g. sea-level rise) are visually apparent, many indirect effects can also impact the structure (e.g., plant and

animal composition) and function (e.g., plant and animal production, nutrient cycling) of estuarine and wetland ecosystems across the Southeastern US. Because water exchange between lagoonal estuaries and the open ocean is particularly restricted, there is greater potential in systems like PS for changes in precipitation patterns (increased or decreased rainfall) and storm frequencies to result in major alterations to the ecosystem. Changes in precipitation will affect the amount and timing of river and stream flow, which will in turn impact nutrient delivery and cycling and estuarine flushing rates. Increased storm activity may open new inlets, which would undoubtedly alter current flow in the system, increase tidal action, and allow a greater influx volume of seawater that carries with it both different chemical signals and mobile species. Salinity is therefore a practical estuarine characteristic to use to study the impacts of these changes, as both effects include enhanced water exchange that will impact overall estuarine salinity content (Brinson et al., 1985, 1995; Corbett et al., 2007).

Our process-based statistical model explained 89% of observed variability in salinity in Pamlico Sound over 20 years of variable climatic conditions between 1987-2006. Among our candidate variable set, most of the variability in salinity was explained by variables created to approximate the amount of fresh or salt water at a particular *it* location; however, one hurricane predictor variable, $inverse\_days\_survey_t$, was present in the final model. Its parameter estimate was positive, reflecting that strong hurricane winds push more saltwater into PS through inlets than would enter under typical seasonal wind conditions (e.g., Xie and Eggleston 1999). When hurricanes make landfall immediately before m_t, little time is available for riverine FWI to reach sites in eastern PS to counteract this hurricane-driven

saltwater influx. The ability to predict salinity changes in response to hurricane presence is particularly important in PS given that (i) 12% of all tropical cyclonic events recorded in the Atlantic Ocean have passed through North Carolina, (ii) NC is second to Florida in terms of recorded number of land-falling hurricanes (State Climate Office of North Carolina 2009a), (iii) the frequency of Atlantic hurricanes has increased over the last 10 years, and (iv) this increase is expected to persist over the next 10 to 40 years (Paerl et al. 2001, Goldenberg et al. 2001). Our model is the only one known to incorporate hurricane variables into a predictive model of salinity for an estuarine system.

4.1. Model selection and spatial correlation

Our modeling goal was to accurately predict salinity at unsampled locations in PS, thus, the process model with an Exponential spatial covariance function with a nugget was the best for our modeling context because it optimized test dataset criteria. It is important to let individual modeling context dictate which model selection criteria are used. For example, time-based models as a whole exhibited smaller BICs than did process models (Table 6). If we were exclusively using BIC as our selection criterion, we would have selected the time model with spherical spatial covariance functions without a nugget as our best model, but this was not the criterion that satisfied our goals.

If our objective had been solely to predict salinity in hypothetical FWI scenarios, it might have been helpful to withhold an entire time period of observations in our test dataset in addition to a number of observations from each time period. This approach would have allowed a more thorough examination of model accuracy by generating test dataset predictions using a different combination of values for explanatory variables than was used

to fit the model. If an entire time period is withheld, care should be taken to ensure that the value of each explanatory variable in the withheld time period was not the most extreme value for that variable in the observed dataset. This guarantees that predictions are interpolations and not extrapolations, as predictions of the latter type are often less meaningful and subject to greater uncertainty.

Models that included spatial correlation produced predictions that, according to test dataset criteria, were better than models that did not (Table 6), but the mean trend alone explained a large portion of the variability in salinity in both process and time models. In many geostatistical analyses, data are only spatially de-trended (i.e. Leecaster 2003, Ping et al. 2004, Guan et al. 2005, Jensen and Miller 2005, Lloyd 2006, Paretzke et al. 2006, Gundogdu and Guney 2007 and others). Using additional explanatory variables in a mean trend model, however, can explain bigger proportions of both the spatial structure over both large and small distances and could result in deviations from the mean that no longer exhibit spatial patterns (M. Fuentes, pers. comm.). In our process model, 18 time periods had range parameter estimates that were not significantly different from zero (α=0.05). Observations in each of these time periods were thus spatially independent, likely because two-thirds of the variability in salinity was already explained by the mean trend.

The two-step process used here (i.e. selecting variables for the mean trend and then modeling spatial covariance) is not ideal in all situations. Overall variable selection results may have differed slightly if explanatory variables had been selected concurrent to modeling spatial covariance. This does not, however, invalidate the variable selection procedure used in this work. We wanted to create a model that explained as much variability in salinity as

was possible using interpretable explanatory variables because we were primarily interested in the process that affects salinity at a given space-time location, and we only wanted to incorporate spatial covariance if it improved the fit of this pre-existing model. Adjusted R^2 favors more complex models than either AIC or BIC, so we used it to select the mean trend, reasoning that it should include all variables that in any way help to explain portions of response variability. While (*i*) specific variables in the mean trend might have been slightly different using an alternate model construction process and (*ii*) we admit that if performing this analysis again we might have used different variable selection procedures, we are still satisfied with the end result, as the final model predicted salinity in a withheld data set with a considerable degree of accuracy.

4.2. Process model vs. time model applications

We chose the process model over the time model to generate salinity predictions to satisfy our objectives, but a different set of objectives might result in a different decision. Each model type has different applications based on the explanatory variables included, and they should ultimately be used to address different questions.

Because the majority of the process model's candidate predictor variables are processes known to affect salinity, positing causal relationships is more appropriate here than with other predictive models that contain many variables that are not process-based. Even though our model is based on data collected from two different months, $month_{it}$ was not included as a predictor variable in our final model; we thus have the ability to predict and map salinity distributions in any past, present or future PS time period. This omission allows for a variety of practical applications. For example, physical oceanographers can use process

model predictions to ground-truth PS hydrodynamic models that also predict salinity (e.g. Xie and Pietrafesa, 1999, Xia et al. 2007, Lin et al. 2007; 2008). Marine ecologists interested in the effects of salinity on the distribution and abundance of estuarine organisms, and the response of mobile organisms to changes in salinity, can use process model predictions to guide sampling design, and to predict ecological responses to future conditions. Finally, our process model could be used by NCDMF scientists to evaluate trawl site placement in future surveys, both P195 and others, especially if they are interested in further examining the effect of salinity on species distribution. Before now, salinity could not be predicted in advance of the P195 survey. Using the output from this model, sites could be systematically relocated within strata prior to sampling to evaluate fisheries abundance across the entire salinity gradient within a given month and year time period. Ensuring that all salinities of interest are represented in the survey allows for a more rigorous test of the relationship between an organism's distribution and its physical environment.

We originally constructed our time model after observing multiple time-period-specific relationships between salinity and $2mo\_FWII_{rit}$ (Fig. 2); hypothesizing that a model that included time period as a predictor variable would produce the most accurate retrospective predictions of salinity according to our criteria. This was not the case, but it is important for others who might use this type of model to realize that the inclusion of the *time_period* variable instantly limited the possible applications of the model. A time-based model can only be used to retrospectively predict salinity in previously sampled time periods and it would only be useful here for those who wanted to examine PS salinity patterns during June or September 1987-2006. For instance, if a researcher wanted to examine the effect of

salinity on Atlantic croaker distribution after Hurricane Fran in 1996, and samples were collected only in the weeks after the hurricane and at no other time, they could use the September 1996 salinity map and predictions generated from our time model to inform their analysis. Unlike the process model, the time model is unable to predict future salinity distributions; one could only generalize what salinity distributions might look like if hypothetical future Year X had values of predictor variables, namely *1wk_* and $2mo\_FWI_{rt}$, similar to those in one of the time periods present within the data series.

4.3. Model improvement

To improve upon our model in the future, a more exhaustive attempt could be made to incorporate wind speed and direction, since this forcing mechanism drives the majority of water movement and mixing within PS (Pietrafesa and Janowitz 1986). Although the spatial resolution of our wind data is limited (two wind gauges exist within *S* that have collected data throughout *T*), it has recently been demonstrated that wind speed and direction are spatially coherent along the main axes of PS (Eggleston et al., in press). This finding suggests that it is possible to decompose vector wind speed data from a single weather station to calculate an effective wind speed metric for each survey site based on the distance and compass orientation of location *it* relative to the weather station. Such an effort would require a thorough exploratory analysis to identify the temporal duration over which wind speed was thought to affect PS salinity to determine the number of days before m_t to use to calculate an average wind speed per time period.

PS's freshwater residence time is approximately 11 months (Molina 2002), so creating a variable to represent the total amount of freshwater present in the sound prior to m_t

using a time duration longer than 61 days might explain more variability in salinity. This variable would differ from our FWI metrics because it would correspond to a volume of water as opposed to a rate of influx. Because it could potentially account for differences in salinity patterns seen in time periods with similar one week and two month FWI conditions, such a variable warrants future investigation.

The *1wk_* and $2mo\_FWII_{rt}$ variables might have explained larger proportions of variability in salinity if they had been constructed using different FWI sources and/or different distance calculation methods. For example, FWII metrics might have better reflected freshwater conditions within the survey's spatial domain if it had been possible to obtain freshwater inflow data at locations on each river that were closer to observed sample locations. We chose to use the furthest downstream gauge station on each river that also recorded data over the entirety of the temporal domain. Likewise, using water-path distance as opposed to Euclidean distance might have better represented the effect of the FWI from each river on salinity at a given *it* sample location. The argument supporting the use of water-path distances when modeling water quality parameters in stream and estuarine systems is logical, however, results from studies that directly compared these two distance methods are inconclusive. Gardner et al. (2003) noted more accurate predictions of stream temperatures when models incorporated water-path distance, but only when this distance was further modified and weighted by stream order. Peterson et al. (2006) predicted various nutrient concentrations in 17 Maryland rivers and concluded that water-path distances worked well when predicting concentrations of certain nutrients but not others and that Euclidean distance appeared to be the most suitable distance measure overall. Because

neither these two studies nor those discussed in Section 2.3 (Little et al. 1997, Rathbun 1998) demonstrated marked predictive improvement using water-path distance in all cases, we could not justify spending the time needed to hand-calculate 4,800 water-path distances in this analysis. However, since this issue lacks definitive resolution, it would be interesting in future work to compare differences in Pamlico Sound salinity predictions using both distance methods. Such an examination would be possible if water-path distances could be calculated using an automated procedure similar to the one used in Jensen et al. (2006).

4.4. Applications of the model-building process to other estuaries

This study developed and evaluated space-time predictive models of salinity for Pamlico Sound, NC and generated the methods necessary to replicate this modeling effort in other systems to create similar salinity predictive models. To apply this methodology to another system, one needs to consider the effects of important forcing mechanisms (described in Sections 2.2 through 2.9) that dictate the value of salinity observed at a given site in space and time. Once process-relationships are defined, all that remains is data acquisition and design of appropriate predictor variables to include before model fitting and evaluation can begin. For example, like PS, the northern Gulf of Mexico (GoM) off the coast of Louisiana is another area highly prone to hurricanes and sea level rise that could benefit greatly from a predictive salinity model. A number of modifications should be made to our PS salinity predictor variables to reflect the forcing mechanisms that govern bottom salinity in the GoM. One such modification involves the directionality of the outflow of the Mississippi and Atchafalaya rivers, which combined discharge approximately 90% of the freshwater that enters the GoM continental shelf (Cochrane and Kelly 1986). Sixty percent

of Mississippi River freshwater inflow flows west to initially form the strong Louisiana Coastal Current (LCC); the remaining 40% flows east. Almost all of the Atchafalaya River inflow is entrained in the LCC and flows west from its point-source entry (Dinnel and Wiseman 1986). The same general formula can be applied to calculate short and long term $FWII_{rit}$ (equation 1). To incorporate directionality into these FWII metrics, indicator variables ($direct_{rit}$) could be created that correspond to the orientation of sample location *it* from point-source locations of either Mississippi or Atchafalaya River inflow onto the continental shelf. $Direct_{rit}$ for the Mississippi River should, for example, equal 0.6 for stations west of the Balize delta and 0.4 for stations east of the delta. Similarly, $direct_{rit}$ for the Atchafalaya River should equal zero for stations east of Atchafalaya Bay, and one for all western stations. Incorporating the interaction between these indicator variables and their respective $FWII_{rit}$ variables into a GoM salinity model will more appropriately characterize the dynamics of the system and thereby possibly create a better predictive salinity model.

5. CONCLUSIONS

We created a model to hindcast and forecast salinity in a lagoonal estuary, with the latter becoming increasingly important in the face of global climate change. This model can generate predictions of bottom salinity for Pamlico Sound, NC, that are more spatially-resolute than any previous bottom salinity predictions encountered in the literature for this system. We used model predictions to generate maps of salinity distributions in PS for 40 time periods over the last 20 years will that allow other researchers to observe changes in isohaline locations under variable freshwater influx conditions. Our salinity predictions can

be used to inform future analyses including, but not limited to: (1) the examination of historical distribution patterns of estuarine species relative to salinity variability, (2) the evaluation of existing sampling designs for field trawl survey programs, and (3) the prediction of salinity changes under various global climate change scenarios.

6. REFERENCES

Anderson, A. M., W. J. Davis, M. P. Lynch, and J. R. Schubel. 1973. *Effects of Hurricane Agnes on the Environment and Organisms of Chesapeake Bay*. The Chesapeake Bay Research Council, Johns Hopkins University, Baltimore, MD.

Bales, J. D. 2003. Effects of hurricane Floyd inland flooding, September–October 1999, on tributaries to Pamlico Sound, North Carolina. *Estuaries and Coasts* **26**:1319-1328.

Bales, J. D., and J. C. Robbins. 1995. Simulation of hydrodynamics and solute transport in the Pamlico River estuary, North Carolina. *US Geological Survey, Raleigh, NC (USGS Open-file Rep. No. 94-454)*.

Balthis, W., J. Hyland, and D. Bearden. 2006. Ecosystem Responses to Extreme Natural Events: Impacts of Three Sequential Hurricanes in Fall 1999 on Sediment Quality and Condition of Benthic Fauna in the Neuse River Estuary, North Carolina. *Environmental Monitoring and Assessment* **119**:367-389.

Brinson, M. M., H. D. Bradshaw, and M. N. Jones. 1985. Transitions in forested wetlands along gradients of salinity and hydroperiod. *Journal of the Elisha Mitchell Scientific Society* **101**:76–94.

Brinson, M., R. Christian, and L. Blum. 1995. Multiple states in the sea-level induced transition from terrestrial forest to estuary. *Estuaries and Coasts* **18**:648-659.

Burkholder, J., D. Eggleston, H. Glasgow, C. Brownie, R. Reed, G. Janowitz, M. Posey, G. Melia, C. Kinder, R. Corbett, D. Toms, T. Alphin, N. Deamer, and J. Springer. 2004. Comparative impacts of two major hurricane seasons on the Neuse River and western Pamlico Sound ecosystems. *Proceedings of the National Academy of Sciences* **101**:9291-9296.

Buzzelli, C., J. Ramus, and H. Paerl. 2003. Ferry-based monitoring of surface water quality in North Carolina estuaries. *Estuaries and Coasts* **26**:975-984.

Chehata, M., D. Jasinski, M. C. Monteith, and W. B. Samuels. 2007. Mapping Three-Dimensional Water-Quality Data in the Chesapeake Bay Using Geostatistics 1. *JAWRA Journal of the American Water Resources Association* **43**:813-828.

Cloern, J. E., and F. H. Nichols. 1985. Time scales and mechanisms of estuarine variability, a synthesis from studies of San Francisco Bay. *Hydrobiologia* **129**:229.

Cochrane, J. D., and F. J. Kelly. 1986. Low-frequency circulation on the Texas-Louisiana Continental Shelf. *Journal of Geophysical Research* **91**:10645-10660.

Corbett, D. R., D. Vance, E. Letrick, D. Mallinson, and S. Culver. 2007. Decadal-scale sediment dynamics and environmental change in the Albemarle Estuarine System, North Carolina. *Estuarine, Coastal and Shelf Science* **71**:717-729.

Cressie, N., J. Frey, B. Harch, and M. Smith. 2006. Spatial Prediction on a River Network. *Journal of Agricultural, Biological, and Environmental Statistics* **11**:127-150.

Dent, C. L., and N. B. Grimm. 1999. Spatial Heterogeneity of Stream Water Nutrient Concentrations Over Successional Time. *Ecology* **80**:2283-2298.

Dinnel, S. P., and W. J. Wiseman Jr. 1986. Fresh water on the Louisiana and Texas shelf. *Cont. Shelf Res* **6**:765-784.

Eggleston, D. B., E. Johnson, and J. Hightower. 2004. Population Dynamics and Stock Assessment of the Blue Crab in North Carolina. Report Division of Marine Fisheries, Morehead City, NC.

Eggleston, D. B., N. B. Reyns, L. L. Etherington, G. Plaia, L. Xie. Climate impacts on large-scale estuarine blue crab settlement. *Fisheries Oceanography* (in press).

Gardner, B., P. J. Sullivan, and A. J. Lembo. 2003. Predicting stream temperatures: geostatistical model comparison using alternative distance metrics. *Canadian Journal of Fisheries and Aquatic Sciences* **60**:344-351.

Giese, G. L., H. B. Wilder, and G. G. Parker. 1979. Hydrology of major estuaries and sounds of North Carolina. *US Geological Survey Water-Supply Paper.*

Goldenberg, S. B., C. W. Landsea, A. M. Mestas-Nunez, and W. M. Gray. 2001. The Recent Increase in Atlantic Hurricane Activity: Causes and Implications. *Science* **293**:474-479.

Guan, H., J. L. Wilson, and O. Makhnin. 2005. Geostatistical Mapping of Mountain Precipitation Incorporating Autosearched Effects of Terrain and Climatic Characteristics. *Journal of Hydrometeorology* **6**:1018-1031.

Gundogdu, K. S., and I. Guney. 2007. Spatial analyses of groundwater levels using universal kriging. *Journal of earth system science* **116**:49-55.

Hamrick, J. M. 1996. User's manual for the environmental fluid dynamics computer code. *Special Report in Applied Marine Science and Ocean Engineering No. 331*. Virginia Institute of Marine Science/School of Marine Science, The College of William and Mary, Virginia.

Jensen, O. P., M. C. Christman, and T. J. Miller. 2006. Landscape-based geostatistics: a case study of the distribution of blue crab in Chesapeake Bay. *Environmetrics* **17**:605-621.

Jensen, O. P., and T. J. Miller. 2005. Geostatistical Analysis of the Abundance and Winter Distribution Patterns of the Blue Crab Callinectes sapidus in Chesapeake Bay. *Transactions of the American Fisheries Society* **134**:1582-1598.

Kinne, O. 1964. The effects of temperature and salinity on marine and brackish water animals. II. Salinity and temperature salinity combinations. *Oceanography and Marine Biology. An Annual Review* **2**:281–339.

Kitanidis, P. K. 1997. *Introduction to Geostatistics: Applications in Hydrogeology*. Cambridge University Press, Cambridge, UK.

Knott, D. M., and R. M. Martore. 1991. The short-term effects of Hurricane Hugo on fishes and decapod crustaceans in the Ashley River and adjacent marsh creeks, South Carolina. *Journal of Coastal Research* **SI8**:335-356.

Leecaster, M. 2003. Spatial analysis of grain size in Santa Monica Bay. *Marine Environmental Research* **56**:67.

Lilly, J. P. 1998. The Roanoke River and Albemarle Sound. in *Washington County, NC: a tapestry*, F. B. Jones and S. B. Phelps, eds. Jonsten Printing Company, Winston-Salem, NC.

Lin, J., L. Xie, L. J. Pietrafesa, J. S. Ramus, and H. W. Paerl. 2007. Water Quality Gradients across Albemarle-Pamlico Estuarine System: Seasonal Variations and Model Applications. *Journal of Coastal Research* **23**:213-229.

Lin, J., L. Xie, L. J. Pietrafesa, H. Xu, W. Woods, M. A. Mallin, and M. J. Durako. 2008a. Water quality responses to simulated flow and nutrient reductions in the Cape Fear River Estuary and adjacent coastal region, North Carolina. *Ecological Modeling* **212**:200.

Lin, J., H. Xu, C. Cudaback, and D. Wang. 2008b. Inter-annual variability of hypoxic conditions in a shallow estuary. *Journal of Marine Systems* **73**:169.

Little, L. S., D. Edwards, and D. E. Porter. 1997. Kriging in estuaries: as the crow flies, or as the fish swims? *Journal of Experimental Marine Biology and Ecology* **213**:1.

Lloyd, C. D. 2006. *Local models for spatial analysis*. CRC Press, Boca Raton, FL.

Mallin, M. A., and C. A. Corbett. 2006. How Hurricane Attributes Determine the Extent of Environmental Effects: Multiple Hurricanes and Different Coastal Systems. *Estuaries and Coasts* **29**:1046-1061.

Mallin, M. A., M. H. Posey, M. R. McIver, D. C. Parsons, S. H. Ensign, and T. D. Alphin. 2002. Impacts and Recovery from Multiple Hurricanes in a Piedmont Coastal Plain River System. *BioScience* **52**:999-1010.

Matheron, G. 1963. Principles of geostatistics. *Economic Geology* **58**:1246-1266.

Miller, J. M., J. P. Reed, and L. J. Pietrafesa. 1984. Patterns, mechanisms and approaches to the study of migrations of estuarine-dependent fish larvae and juveniles. Pp. 209-225 in *Mechanisms of Migration in Fishes*, J. D. McCleave, G. P. Arnold, J. J. Dodson and W. H. Neill, eds. Plenum Publishing Corporation, New York.

Molina, J. R. 2002. Estuarine Exchange Model of the Pamlico and Albemarle Sounds, North Carolina State University, Raleigh.

Paerl, H. W., J. D. Bales, L. W. Ausley, C. P. Buzzelli, L. B. Crowder, L. A. Eby, J. M. Fear, M. Go, B. L. Peierls, T. L. Richardson, and J. S. Ramus. 2001. Ecosystem impacts of three sequential hurricanes (Dennis, Floyd, and Irene) on the United States' largest lagoonal estuary, Pamlico Sound, NC. *Proceedings of the National Academy of Sciences* **98**:5655-5660.

Paerl, H. W., L. M. Valdes, B. L. Peierls, R. S. Weaver, T. Gallo, A. R. Joyner, and J. S. Ramus. 2005. Ecological effects of a recent rise in Atlantic hurricane activity on North Carolina's Pamlico Sound System: Putting Hurricane Isabel in perspective. in *Hurricane Isabel in perspective*, K. G. Sellner, ed. Chesapeake Research Consortium, CRC Publication 05-160, Edgewater, MD.

Paerl, H. W., L. M. Valdes, A. R. Joyner, B. L. Peierls, M. F. Piehler, S. R. Riggs, R. R. Christian, L. A. Eby, L. B. Crowder, J. S. Ramus, E. J. Clesceri, C. P. Buzzelli, and R. A. Luettich. 2006. Ecological Response to Hurricane Events in the Pamlico Sound System, North Carolina, and Implications for Assessment and Management in a Regime of Increased Frequency. *Estuaries and Coasts* **29**:1033-1045.

Paretzke, H., P. DeLuca, and A. Wambersie. 2006. 5--Sampling to Estimate Spatial Patterns. *Journal of the ICRU* **6**:49-64.

Patterson, H. D., and R. Thompson. 1971. Recovery of inter-block information when block sizes are unequal. *Biometrika* **58**:545-554.

Peterson, E. E., A. A. Merton, D. M. Theobald, and N. S. Urquhart. 2006. Patterns of Spatial Autocorrelation in Stream Water Chemistry. *Environmental Monitoring and Assessment* **121**:569-594.

Peterson, E. E., and N. S. Urquhart. 2006. Predicting Water Quality Impaired Stream Segments using Landscape-Scale Data and a Regional Geostatistical Model: A Case Study in Maryland. *Environmental Monitoring and Assessment* **121**:613-636.

Pietrafesa, L. J., and G. S. Janowitz. 1991. *Final Report on the Albemarle Pamlico Coupling Study*. NC Albemarle-Pamlico Estuarine Study.

Pietrafesa, L. J., G. S. Janowitz, T. Y. Choa, R. H. Weisberg, F. Askari, and E. Noble. 1986. The Physical Oceanography of Pamlico Sound. UNC Sea Grant Report. Report UNC-SG-WP-86-5. Sea Grant Program, Raleigh, North Carolina. 126 p.

Pietrafesa, L. J., J. M. Morrison, M. P. McCann, J. Churchill, E. Bohm, and R. W. Houghton. 1994. Water mass linkages between the Middle and South Atlantic Bights. *Deep-Sea Res* **41**:365–389.

Ping, J. L., C. J. Green, R. E. Zartman, and K. F. Bronson. 2004. Exploring spatial dependence of cotton yield using global and local autocorrelation statistics. *Field Crops Research* **89**:219.

Pritchard, D. W. 1954. A study of the salt balance in a coastal plain estuary. *Journal of Marine Research* **13**:133–144.

Pritchard, D. W. 1967. What is an estuary: Physical viewpoint. Pp. 3-5 in *Estuaries*, G. H. Lauff, ed. American Association for the Advancement of Science, Washington D.C.

Ramus, J., L. A. Eby, C. M. McClellan, and L. B. Crowder. 2003. Phytoplankton forcing by a record freshwater discharge event into a large lagoonal estuary. *Estuaries and Coasts* **26**:1344-1352.

Rathbun, S. L. 1998. Spatial Modeling in Irregularly Shaped Regions: Kriging Estuaries. *Environmetrics* **9**:109-129.

Reed, R. E., D. A. Dickey, J. M. Burkholder, C. A. Kinder, and C. Brownie. 2008. Water level variations in the Neuse and Pamlico Estuaries, North Carolina due to local and remote forcing. *Estuarine, Coastal and Shelf Science* **76**:431-446.

Reynolds-Fleming, J. V., and R. A. Luettich. 2004. Wind-driven lateral variability in a partially mixed estuary. *Estuarine, Coastal and Shelf Science* **60**:395-407.

Reyns, N. B. 2004. Biophysical dispersal dynamics of the blue crab in Pamlico Sound, North Carolina, North Carolina State University, Raleigh, NC, USA.

Rome, M. S., A. C. Young-Williams, G. R. Davis, and A. H. Hines. 2005. Linking temperature and salinity tolerance to winter mortality of Chesapeake Bay blue crabs (Callinectes sapidus). *Journal of Experimental Marine Biology and Ecology* **319**:129-145.

Schwartz, F. J., and A. F. Chestnut. 1973. *Hydrographic Atlas of North Carolina Estuarine and Sound Waters, 1972*, Chapel Hill, North Carolina: Sea Grant publication UNC-SG-73-12.

Searcy, S, D. B. Eggleston, J. Hare. 2007. Environmental influences on the relationship between juvenile and larval growth for Atlantic croaker, *Micropogonias undulates. Marine Ecology Progress Series* 349:81-88.

Sklar, F. H., and J. A. Browder. 1998. Coastal Environmental Impacts Brought About by Alterations to Freshwater Flow in the Gulf of Mexico. *Environmental Management* **22**:547-562.

Stanley, D. W., and S. W. Nixon. 1992. Stratification and Bottom-Water Hypoxia in the Pamlico River Estuary. *Estuaries* **15**:270-281.

State Climate Office of North Carolina. 2009a. http://www.nc-climate.ncsu.edu/climate/hurricane.php.

State Climate Office of North Carolina. 2009b. http://www.nc-climate.ncsu.edu/cronos/text_stations.php

Tabb, D. C., and A. C. Jones. 1962. Effect of Hurricane Donna on the Aquatic Fauna of North Florida Bay. *Transactions of the American Fisheries Society* **91**:375-378.

US Geological Survey (USGS). 2009a. North Carolina Drought Watch. http://nc.water.usgs.gov/drought/index.html

US Geological Survey (USGS). 2009b. USGS Water Date for North Carolina. http://nwis.waterdata.usgs.gov/nc/nwis/nwis

Weaver, J. C. 2005. The drought of 1998–2002 in North Carolina—Precipitation and hydrologic conditions. Report U.S. Geological Survey Scientific Investigations Report 2005–5053. Pp. 88 p.

Webster, P. J., G. J. Holland, J. A. Curry, and H. R. Chang. 2005. Changes in Tropical Cyclone Number, Duration, and Intensity in a Warming Environment. *Science* **309**:1844-1846.

Xia, M., L. Xie, and L. Pietrafesa. 2007. Modeling of the Cape Fear River Estuary plume. *Estuaries and Coasts* **30**:698-709.

Xie, L., and D. B. Eggleston. 1999. Computer Simulations of Wind-induced Estuarine Circulation Patterns and Estuary-shelf Exchange Processes: The Potential Role of Wind Forcing on Larval Transport. *Estuarine, Coastal and Shelf Science* **49**:221-234.

Xie, L., and L. J. Pietrafesa. 1999. Systemwide Modeling of Wind and Density Driven Circulation in Croatan-Albemarle-Pamlico Estuary System Part I: Model Configuration and Testing. *Journal of Coastal Research* **15**:1163-1177.

Xu, H., J. Lin, and D. Wang. 2008. Numerical study on salinity stratification in the Pamlico River Estuary. *Estuarine, Coastal and Shelf Science* **80**:74-84.

Table 1. Studies in which statistical models have been constructed to describe spatial distributions of water quality features with the system of interest and the parameter being modeled.

Reference	Model System	Response Variable
Little et al. (1997)	Murrells Inlet, SC	Nutrient Concentrations
Rathbun (1998)	Charleston Harbor, SC	Salinity and Dissolved Oxygen
Dent and Grimm (1999)	Verde River, AZ	Nutrient Concentrations
Gardner et al. (2003)	Beaverkill River, NY	Temperature
Cressie et al. (2006)	rivers across Southeast Queensland, Australia	Dissolved Oxygen
Peterson et al. (2006), Peterson and Urquhart (2006)	17 different rivers, MD	Nutrient Concentrations
Chehata et al. (2007)	Chesapeake Bay, VA	Salinity and Dissolved Oxygen

Table 2. Adjusted R^2 for eight linear regression models containing $dist_{sit}$ or $closest\_inlet\_dist_{it}$ with different combinations of spatial coordinate variables. $Dist_{sit}$ is calculated using Euclidian distance between location *it* and *s*, the geographic center of one of PS's major inlets. $Closest\_inlet\_dist_{it}$ is equal to the smallest $dist_{sit}$ variable and represents distance to the closest inlet)

Model: sal_{it} =	Adjusted R^2
$dist_{sit}$	0.3839
$dist_{sit} + easting_{it} + easting_{it}^2$	0.3994
$dist_{sit} + northing_{it} + northing_{it}^2 + northing_{it}^3$	0.4229
$dist_{sit} + easting_{it} + easting_{it}^2 + northing_{it} + northing_{it}^2 + northing_{it}^3 + northing_{it}*easting_{it} + northing_{it}^2*easting_{it} + northing_{it}*easting_{it}^2$	0.4251
$closest\_inlet\_dist_{it}$	0.3389
$closest\_inlet\_dist_{it} + easting_{it} + easting_{it}^2$	0.3440
$closest\_inlet\_dist_{it} + northing_{it} + northing_{it}^2 + northing_{it}^3$	0.4082
$closest\_inlet\_dist_{it} + easting_{it} + easting_{it}^2 + northing_{it} + northing_{it}^2 + northing_{it}^3 + northing_{it}*easting_{it} + northing_{it}^2*easting_{it} + northing_{it}*easting_{it}^2$	0.4250

Table 3. Adjusted R^2 for the seven linear regression models between salinity and each main effect explanatory variable or set.

Model: sal_{it} =	Adjusted R^2
$2mo\_FWII_{rit}$ set	0.3760
$closest\_inlet\_dist_{it}$	0.3389
$1wk\_FWII_{rit}$ set	0.2694
$category_t$	0.0491
$inverse\_days\_survey_t$	0.0347
no_storms_t	0.0286
$month_{it}$	0.0147

Table 4. Adjusted R^2 for the seven linear regression fits to evaluate the addition of spatial coordinates as explanatory variables to the overall salinity model. Each row lists the terms added to the model in that step, and includes all previously modeled terms in rows above.

Model: sal_{it} =	Adjusted R^2
$2mo\_FWII_{rit}$ + $closest\_inlet\_dist_{it}$ + $1wk\_FWII_{rit}$ + $inverse\_days\_survey_t$ + all $FWII_{rit}$ interactions	0.6601
+ $easting_{it}$ + $northing_{it}$	0.6963
+ $easting_{it}^2$ + $northing_{it}^2$	0.7204
+ $northing_{it}$*$easting_{it}$	0.7262
+ $northing_{it}^3$	0.7295
+ $northing_{it}$*$easting_{it}^2$ + $northing_{it}^2$*$easting_{it}$	0.7298
+ $northing_{it}^2$*$easting_{it}^2$	0.7297

Table 5. Formulas for the three isotropic spatial covariance functions used in this analysis (Exponential, Gaussian, and Spherical). For all: $\sigma_{n_t}^2$, σ_t^2, $\theta \geq 0$, and $-\infty < \rho < \infty$.

Covariance Function	Equation for element *ij* of $\mathbf{E}_T$	
Exponential	$\sigma_{n_t}^2 + \sigma_t^2$	if $d_{ij} = 0$
	$\sigma_{n_t}^2 + \sigma_t^2 \exp\left(\frac{-d_{ij}}{\theta_t}\right)$	if $d_{ij} > 0$
Gaussian	$\sigma_{n_t}^2 + \sigma_t^2$	if $d_{ij} = 0$
	$\sigma_{n_t}^2 + \sigma_t^2 \exp\left(\frac{-d_{ij}^2}{\theta_t^2}\right)$	if $d_{ij} > 0$
Spherical	$\sigma_{n_t}^2 + \sigma_t^2$	if $d_{ij} = 0$
	$\sigma_{n_t}^2 + \sigma_t^2\left[1 - \left(\frac{3d_{ij}}{2\rho_t}\right) + \left(\frac{3d_{ij}^3}{2\rho_t^3}\right)\right]$	if $d_{ij} > 0$

Table 6. Summary statistics of cross-validation analyses for salinity predictions generated by two OLS models, process and time, when one of three spatial covariance functions was included. Each spatial covariance model was evaluated with and without a nugget effect. The symbol "σ^2_n"indicates that a nugget was included. Stars (*) indicate rejection of the appropriate null hypothesis at the α=0.05 level of significance: H_{01}: σ^2_n=0; H_{02}: β_1=1; H_{03}: β_0=0. The exponential plus nugget process model is highlighted as it was chosen as the best model of PS salinity for our modeling context.

	Model Type	-2 log likelihood	AIC	BIC	RMSE (psu)	Slope/ β_1	Intercept/ β_0	R^2
PROCESS	IID	9935.9	9937.9	9943.5	2.9	0.98	0.84	0.74
	Exponential	7430.7	7584.7	7714.7	2.0	0.95	1.03	0.89
	Exponential + σ^2_n*	7424.0	7580.0	7711.7	2.0	0.96	0.96	0.89
	Gaussian	8198.0	8356.0	8489.5	2.3	0.94	1.37	0.84
	Gaussian + σ^2_n*	7532.0	7686.0	7816.0	2.1	0.94	1.15	0.87
	Spherical	7570.0	7722.0	7850.4	2.0	0.95	1.07	0.88
	Spherical + σ^2_n*	7571.6	7727.6	7859.3	2.0	0.96	0.93	0.89
TIME	IID	7077.5	7079.5	7084.9	2.6	0.83*	3.47*	0.83
	Exponential	Infinite						
	Exponential + σ^2_n	6217.1	6367.1	6493.7	2.1	0.92*	1.55*	0.87
	Gaussian	6281.0	6433.0	6561.3	2.2	0.90*	1.98*	0.86
	Gaussian + σ^2_n*	6214.0	6366.0	6494.4	2.2	0.91*	1.90*	0.86
	Spherical	6199.6	6315.6	6479.9	2.2	0.91*	1.86*	0.86
	Spherical + σ^2_n	6201.3	6357.3	6489.1	2.2	0.91*	1.86*	0.86

Table 7. Sixteen possible FWI scenarios derived from all combinations of *1wk_* and *2mo_FWI$_{rt}$* and corresponding time periods that exhibit each set of conditions. Only time periods that fit each scenario as defined in Section 3 are listed, the remaining 7 time periods were not classified. Boldfaced time periods are those in which hurricanes were present within 61 days of the survey. Time periods were ranked 1-40 by mean predicted salinity (1=lowest mean salinity; 40=highest).

2-month average FWI	1-week average FWI	Time period (mmyy)	Mean Salinity Rank
flood	flood	0603	1
		0999	11
	high		
	moderate	0687	13
		0689	14
	low		
high	flood	**0903**	2
		0690	12
	high	**0904**	9
	moderate	0698	3
		0693	5
		0697	6
	low		
moderate	flood	**0996**	8
	high	0696	15
		0900	17
	moderate	0605	4
		0989	10
		0601	15
		0600	19
		0604	20
		0688	25
		0990	28
		0692	31
	low	0694	24

Table 7 Continued

2-month average FWI	1-week average FWI	Time period (mmyy)	Mean Salinity Rank
low	flood	0987	23
	high	0695	35
	moderate	0905	21
	low	0997	26
		0699	29
		0901	33
		0902	34
		0993	36
		0602	37
		0988	38
		0994	40

FIGURE LEGENDS

Figure 1. Map of Pamlico Sound, NC and depth of the survey sampling area. The P195 trawl survey samples areas within Pamlico Sound only that are greater than 2 m deep. This map also shows the locations of PS's inlets: OR-Oregon Inlet, HA-Hatteras Inlet, and OC-Ocracoke Inlet. Parallel **A** is located at 35º 16' N latitude and meridian **B** is at 75º 42' W longitude, as referenced in Section 2.8. The green star is the location of Buxton, NC.

Figure 2. Observed bottom salinity vs. two-month relative freshwater influx index ($2mo\_FWII_{rit}$) from the Roanoke River. This figure includes all salinity observations from our temporal domain 1987-2006 and influx is in units of $m^3\ sec^{-1}\ km^{-1}$. Circles were drawn around four groups of values within the same time period that the researchers thought exhibited relationships with different slopes.

Figure 3. Sample covariogram calculated from OLS process model residuals for June 1994. Covariance is always in units of the response variable squared and is only examined for approximately half of the maximum lag distance separating any two pairs of sites. Here lag distance = 2.12 and max lag = 20.

Figure 4. Map images of (clockwise from upper left) predicted salinity from June 2005 as generated from our best-fitting model, observed salinity from the P195 June 2005 survey, and standard error (SE) of model-generated salinity predictions. June 2005 was considered to have moderate freshwater inflow in both the two-months and one-week prior to the survey.

Figure 5. Map images of (clockwise from upper left) predicted salinity as generated from our best-fitting model, observed salinity from the P195 survey, and standard error (SE) of model-generated salinity predictions for A: June 1999 and B: June 2002. Both time periods were considered to have low freshwater inflow in both the two-months and one-week prior to the survey.

Figure 6. Map images of (clockwise from upper left) predicted salinity as generated from our best-fitting model, observed salinity from the P195 survey, and standard error (SE) of model-generated salinity predictions for A: September 1999 and B: June 2003. Both time periods were considered to have extremely high freshwater inflow in both the two-months and one-week prior to the survey. In addition, September 1999 was associated with two land-falling hurricanes in close temporal proximity to the P195 survey.

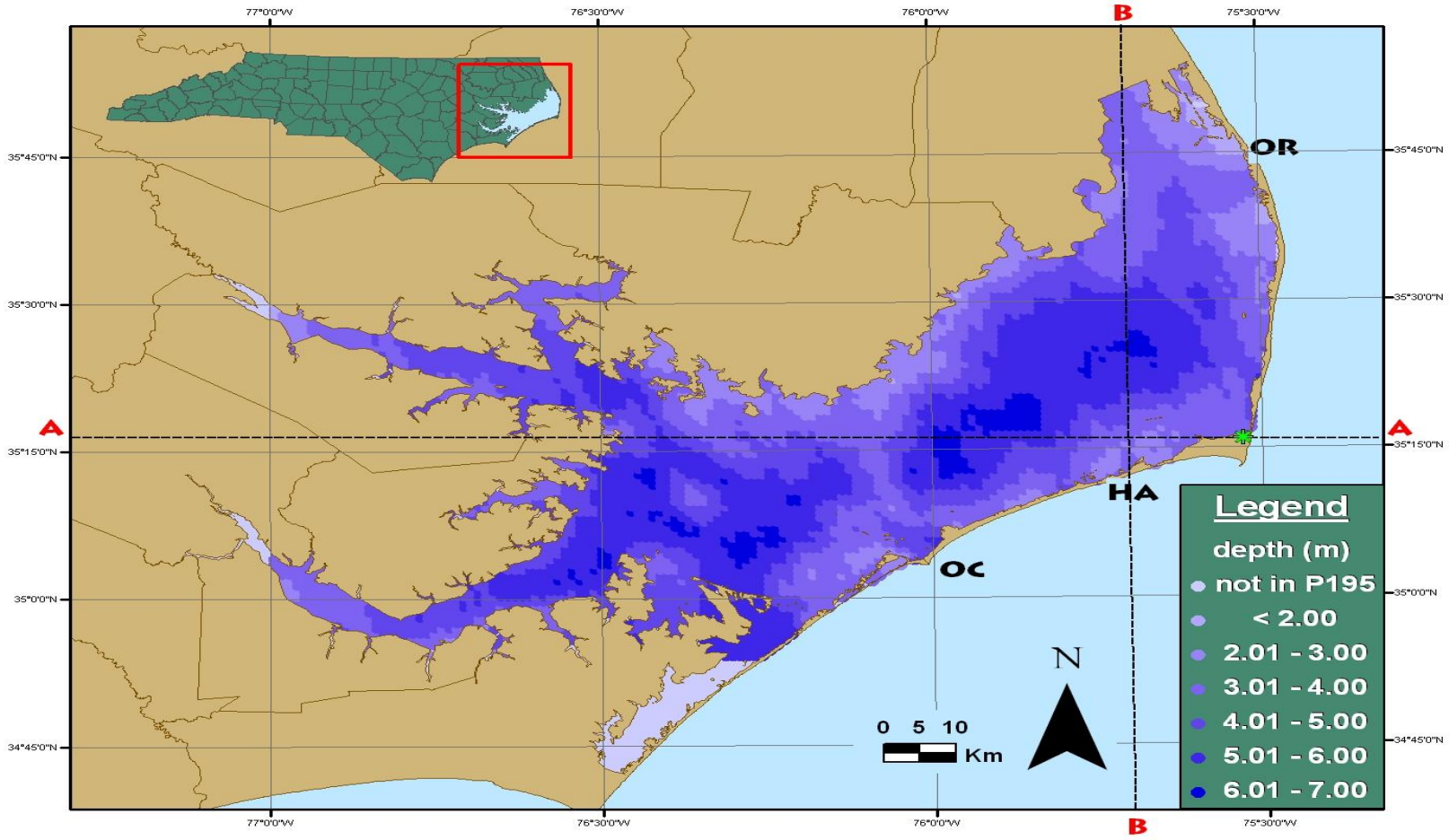

Figure 1. Map of Pamlico Sound, NC and depth of the survey sampling area.

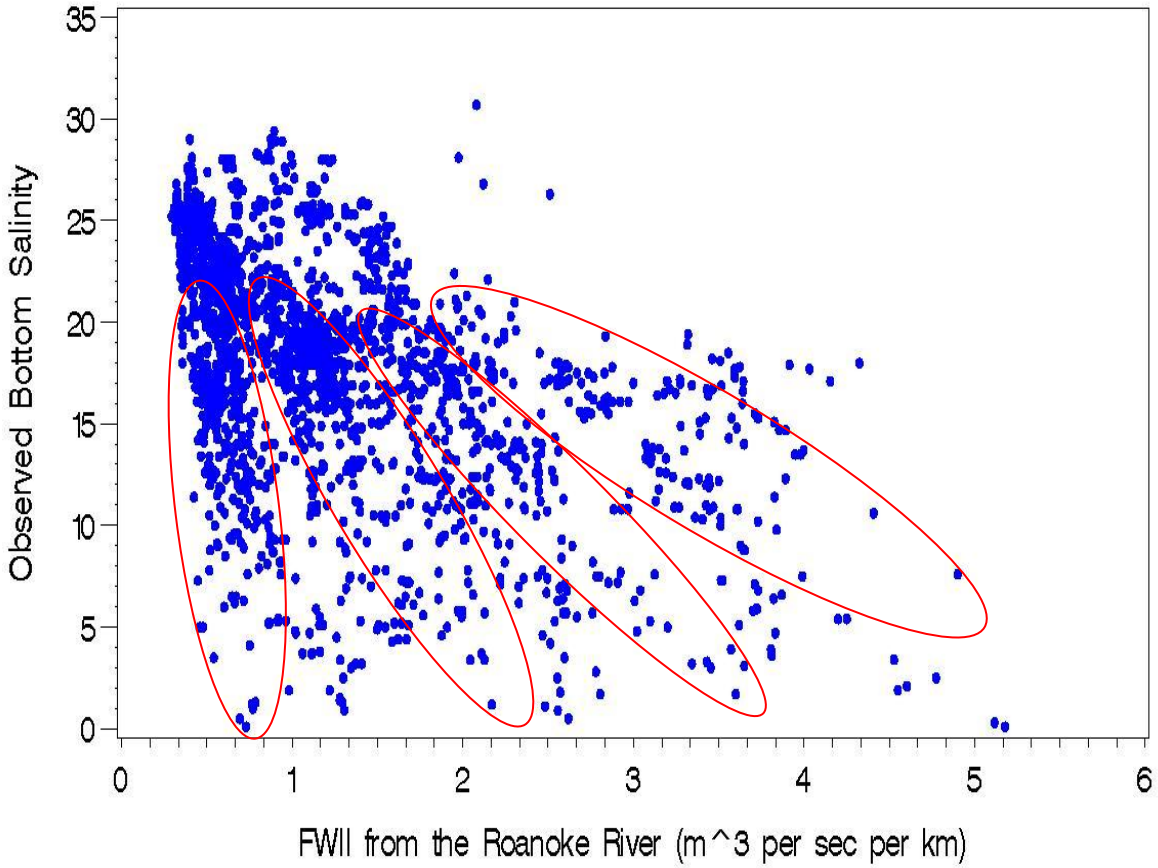

Figure 2. Observed bottom salinity vs. two-month relative freshwater influx index from the Roanoke River.

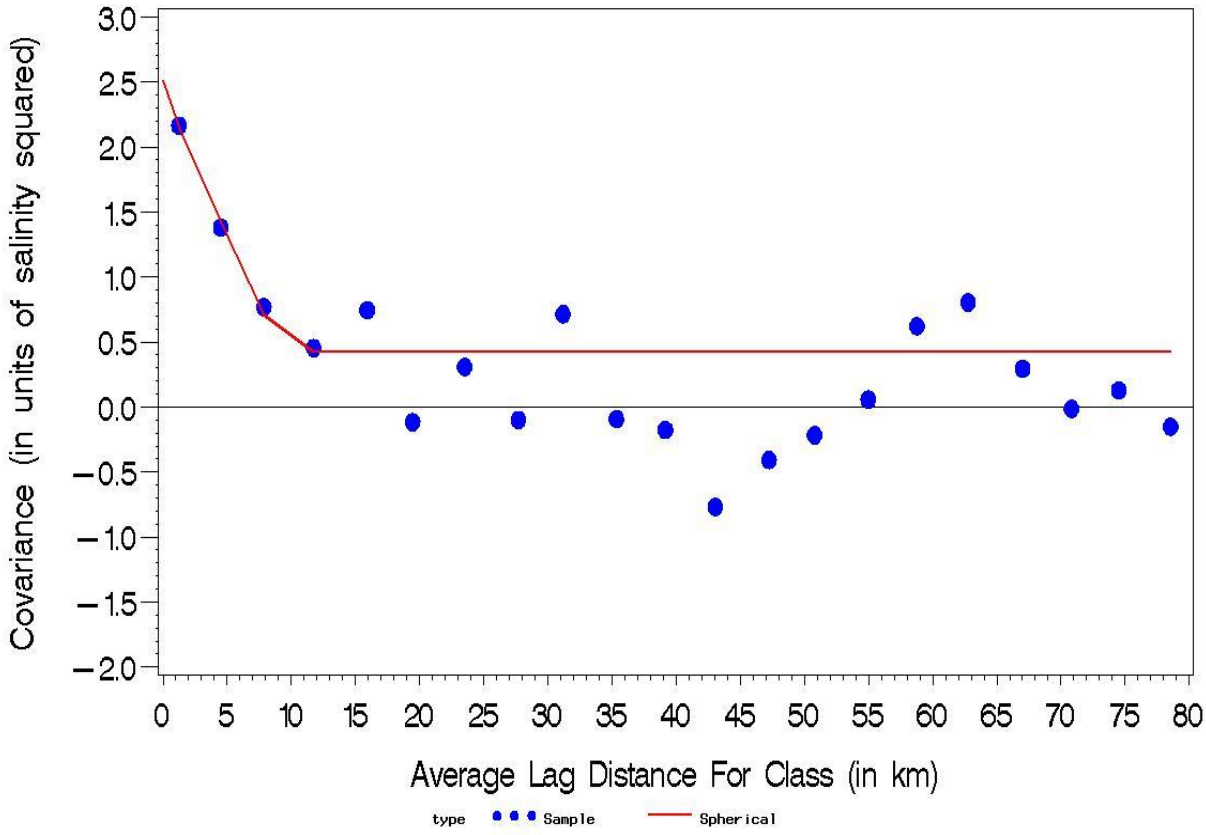

Figure 3. Sample covariogram calculated from OLS process model residuals for June 1994.

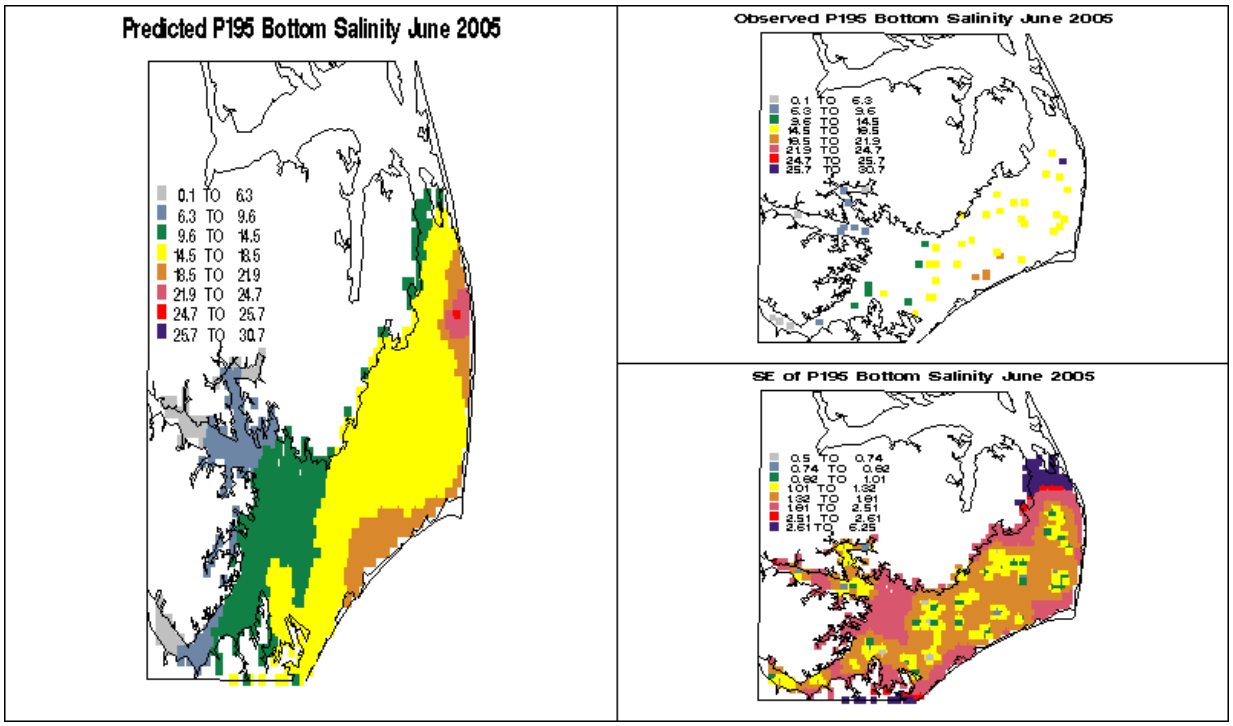

Figure 4. Map images of (clockwise from upper left) predicted salinity from June 2005, observed salinity from the P195 June 2005 survey, and standard error (SE) of model-generated salinity predictions.

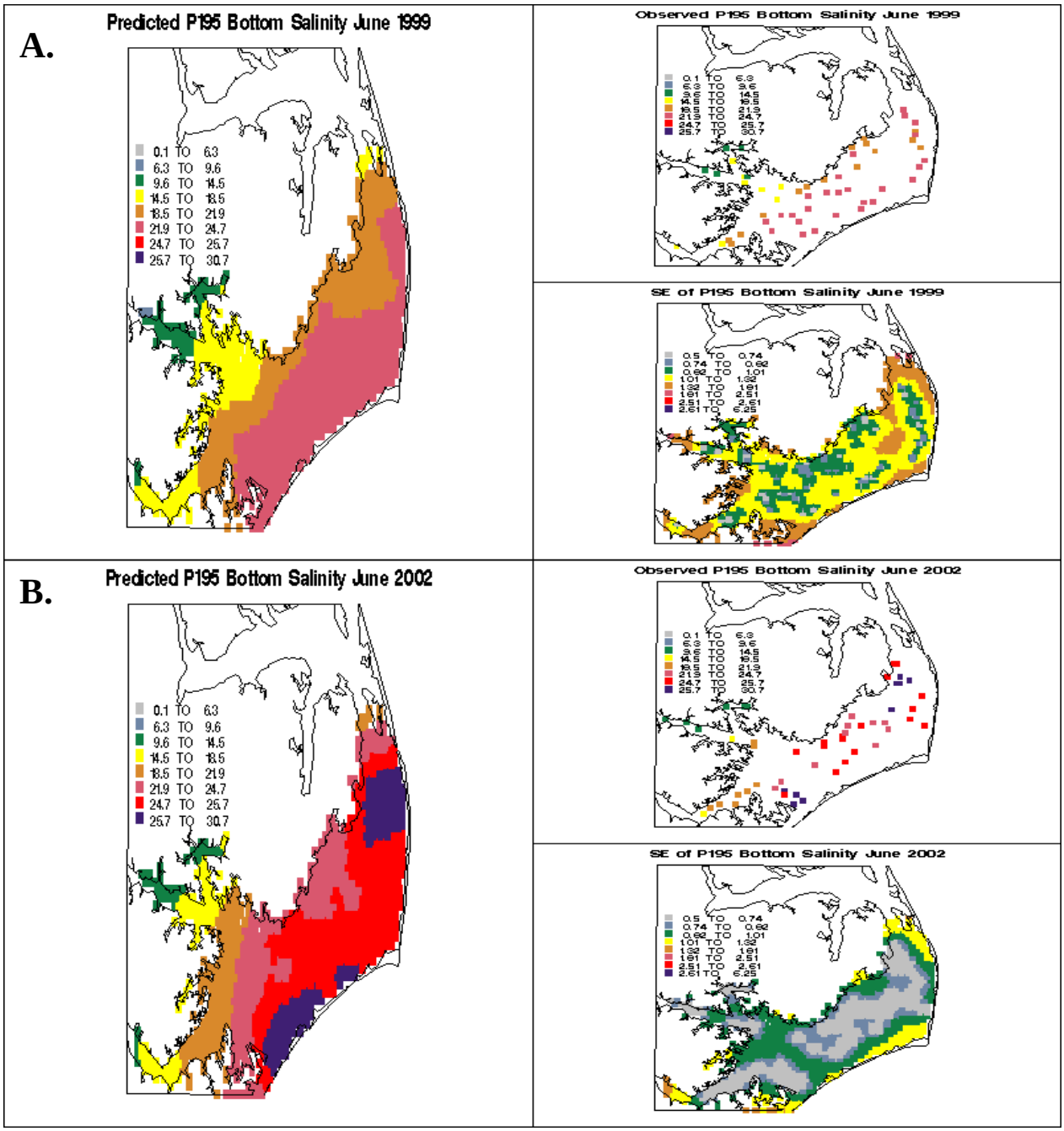

Figure 5. Map images of (clockwise from upper left) predicted salinity, observed salinity from the P195 survey, and standard error (SE) of model-generated salinity predictions for A: June 1999 and B: June 2002.

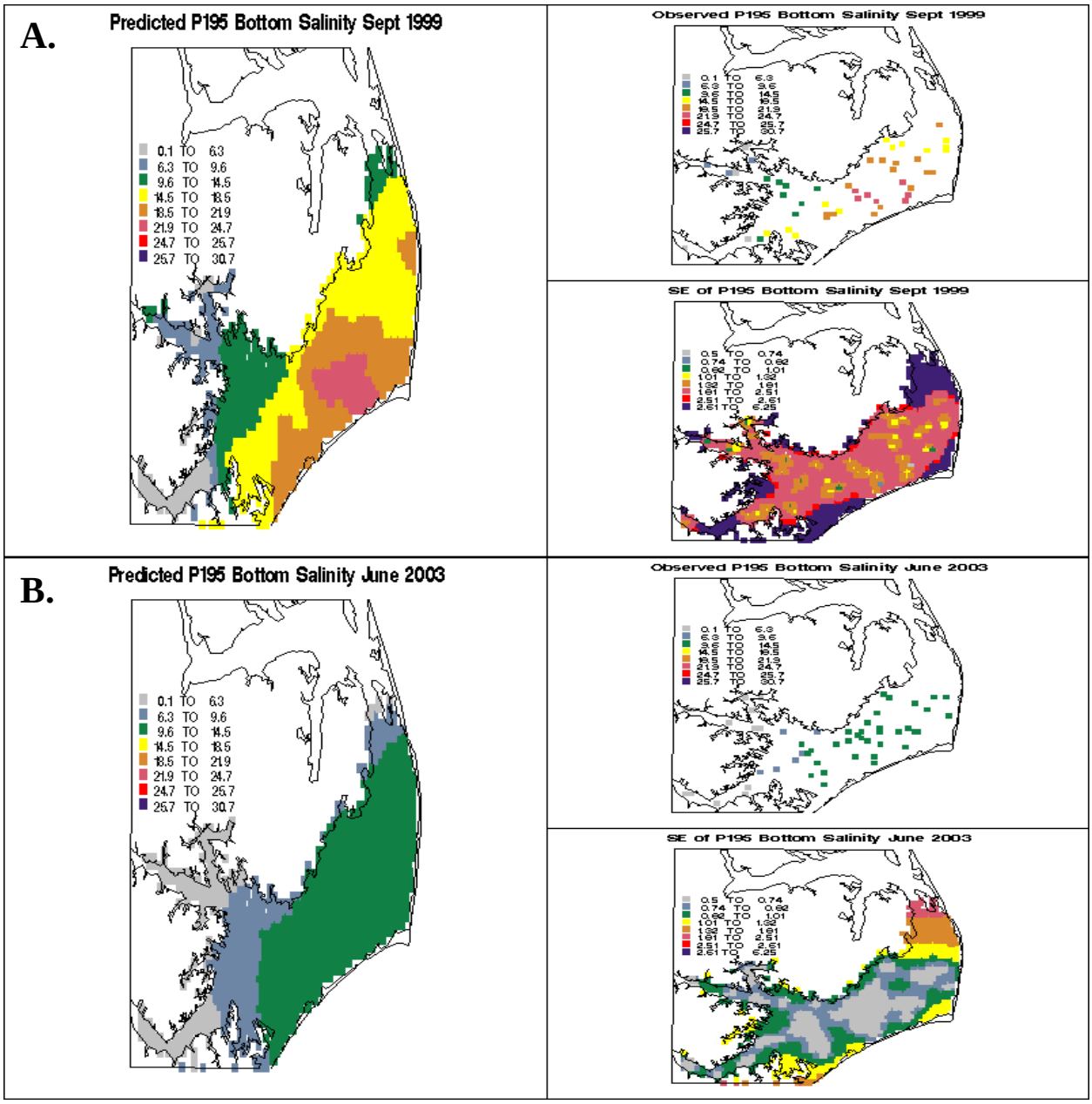

Figure 6. Map images of (clockwise from upper left) predicted salinity, observed salinity from the P195 survey, and standard error (SE) of model-generated salinity predictions for A: September 1999 and B: June 2003.

CHAPTER 2:

Environmental effects on blue crab spatial dynamics in Pamlico Sound, NC: implications for improving the accuracy of fishery-independent survey indices

ABSTRACT

Highly variable environmental conditions can alter spatial distribution patterns of estuarine species over time. These alterations can change fish catchability in survey and commercial gear, potentially biasing abundance estimates and masking or inflating the effects of overfishing. In this study, we created two statistical models to better account for potential environmental effects on fishery-independent indices of mature female blue crab spawning stock biomass (SSB) over space and time. These models will aid management efforts geared toward sustaining North Carolina blue crab spawning stock, which has declined to historic lows since 2000. Model output will providing relatively (1) accurate indices of SSB over time, which is important for establishing catch limits, and (2) accurate maps of the spatial distribution of SSB over time, which is important for identifying important estuarine habitat and potential migration corridors. We also employ new analytical methods to correctly model the probability distribution of blue crab (*Callinectes sapidus*) SSB as zero-inflated gamma, due to excessive zeros that are characteristic of trawl survey data.

1. INTRODUCTION

Amidst concern over the ecological repercussions of global climate change, the number of studies documenting spatial shifts in population distributions in response to environmental variation continues to grow (Kareiva et al. 1993, Southward et al. 1995, Walther et al. 2002). For managers of commercially valuable species, even temporary distribution shifts can be problematic. Environmental change can cause larger proportions of a population to concentrate or aggregate within certain areas of preferred habitat (Loneragan and Bunn 1999). Inadvertent over- or under-sampling of aggregations by fishery–independent assessment surveys can bias stock abundance estimates and mask underlying trends in population size (Beverton and Holt 1957, Hilborn and Walters 2003). Directed overexploitation of animal aggregations by harvesters can result in rapid population declines (e.g. Peruvian anchovy: Csirke 1989; Atlantic Cod: Rose and Kulka 1999).

In North Carolina, blue crab (*Callinectes sapidus*) not only support the state's most profitable fishery, valued at $28 million in 2008 (NCDMF 2009a), but they also have considerable impact on estuarine community structure, serving as dominant predators in benthic environments (Hines et al. 1990, Mansour and Lipcius 1991). Immediately following the landfall of two sequential hurricanes (Dennis and Floyd) in September 1999, a mass migration of crabs out of upriver tributaries resulted in a population that was more concentrated in mainstem Pamlico Sound (Eby and Crowder 2002, Eggleston et al. 2004). That same fall, a 369% increase in mean statewide blue crab commercial catch efficiency was noted relative to the previous 12-year average (Burkholder et al. 2004). A 70%

reduction of adult and post-larval abundance between 2000 and 2005 (Eggleston et al. in press) and continued declines in annual landings from 2000-2007 (NCDMF 2009b) both suggest that blue crab population abundance is historically low. To facilitate species recovery, the NC Marine Fisheries Commission (MFC) designated protection of the spawning stock, the subpopulation of all sexually mature female crab, as a "primary concern" in the 2004 revision of the Blue Crab Fishery Management Plan (BC FMP) (NCDMF 2004).

For successful natural resource management of species like the blue crab, it is critical to establish target amounts of removable biomass and levels of exploitation that are sustainable. To set these respective targets, estimates of relative population size over time and population distribution patterns over space are essential. The objective of this analysis is to better inform these two estimates by accounting for variability in a species' physical environment. To accomplish this task, we created two statistical models that account for the effects of environmental factors on SSB and spatial dynamics of blue crab in Pamlico Sound (PS), NC as an example. The analytical methods used in this study can be applied to a wide range of mobile species and ecosystems in which mobile fishery species alter their spatial dynamics in response to environmental conditions.

To correct for environmentally induced bias in stock abundance estimates generated from a fisheries-independent trawl survey, we modeled the expected value of the probability distribution of blue crab spawning stock biomass (SSB) at each space-time sample location as function of environmental factors. Changes in these factors over time affect the proportion of the population available to be caught in the survey. We used output from this model to calculate annual means of environmentally-adjusted SSB that are more suitable to

track relative population size over time than estimates of SSB not adjusted for physical conditions.

To investigate potential spatial shifts in the population distribution of mature female blue crabs, we again modeled the mean of the probability distribution of blue crab SSB at a given space-time location. This second model, however, included additional environmental factors that did not change over time, but could still affect the spatial distribution of crab within the survey area. If we can identify locations or conditions with a high probability of observing an aggregation, adaptive management options that include select-area fishery closures could be a plausible approach in conserving SSB. Given the general difficulties in estimating population size of mobile marine animals (Hilborn and Walters 2002), the potential for continued environmental change (Goldenberg 2001, Weaver 2005), and the number of currently overexploited stocks (Rosenberg 2006), results of this study should be applicable to a wide range of mobile fishery species and ecosystems.

1.1. Model species

Blue crab can be found throughout estuaries on the East and Gulf Coasts of the United States. Their physiological tolerance for a wide range of salinities (Guerin and Stickle 1992), temperatures (Tagatz 1969), and dissolved oxygen concentrations (Bell 2008) permits survival across the spectrum of physical conditions observed in these dynamic systems. Despite this tolerance, blue crab acclimation to abrupt environmental change can still take several weeks and incurs substantial metabolic cost (Tagatz 1969, Levinton 2001). Both Bell et al. (2003) and Paerl et al. (2006) have noted that in PS, rapid environmental change typically stimulates crab movement, which can result in large-scale temporary

displacements at the population level. In other estuaries, rapid environmental change associated with hurricane-induced freshwater influx has drastically altered observed blue crab spatial distribution patterns (Anderson et al. 1973, Knott and Martore 1991).

Blue crab spatial distribution also varies by life history stage. In theory, the annual down-estuary spawning migration of mature females should be a fairly predictable shift in spatial distribution of this portion of the population; however in practice, many details surrounding the migration process remain unclear. It is known that inseminated females travel across PS after mating in mesohaline and oligohaline upriver regions during summer to release larvae near inlets (Millikin & Williams 1984, Tankersley et al. 1998). This process facilitates the offshore transportation of larvae, which is necessary to minimize osmotic stress during development (Carr et al. 2004). The factors or conditions that prompt migration, however, are still under debate. Anguilar et al. (2005) hypothesized that down-estuary migration is triggered in an individual female either after a pre-determined temporal lag following insemination or by biotic or abiotic cues. Potential abiotic cues include seasonal decreases in temperature (Anguilar et al. 2005), salinity (Tankersley et al. 1998), or photoperiod (Hench et al. 2004).

1.2. Current fishery regulations

The NC blue crab fishery is managed through limits on effort, gear, and landings, but two regulations specifically address spawning stock protection. In 1965, spawning sanctuaries closed to commercial crabbing from March 1 to August 31 were established at the five major inlets connecting Pamlico Sound to the Atlantic Ocean: Oregon, Hatteras, Ocracoke, Bardens, and Drum. These spatial closures, intended to protect females during

clutch maturation and larval release, still stand despite reports that they are both infrequently enforced and too small to protect a significant proportion of the spawning population (Medici et al. 2006, Eggleston et al. 2009).

Managers were prompted to consider additional methods of spawning stock conservation following the large decline in post-1999 crab abundance and the significant spawning stock-recruitment relationship documented by Eggleston et al. (2004). As a result, the 2004 revision of the BC FMP included a provision that granted the MFC the right to invoke a female upper size limit of 6 ¾ inches (17.15 cm) between September 1 and April 30 as an emergency rule should annual catch-per-unit-effort (CPUE) of mature females by the September NCDMF PS Trawl Survey Program 195 ("the survey") fall below the 90% confidence interval (CI) of mean CPUE from 1987-2003 for two consecutive years (NCDMF 2004). Since larger crabs produce more eggs per brood than smaller mature females and are thought to contribute more to successive generations (NCDMF 2004), annual CPUE for this regulation was calculated by averaging the per-station sum of carapace widths (CWs) of individual mature females, thus creating an index of relative abundance that was "adjusted" for crab size. Figure 1 depicts this highly-variable annual mean "adjusted CPUE" index from 1987-2003. The upper size limit was implemented for the first time in January 2006, and because adjusted CPUE has yet to rise above the lower the 90% CI for two consecutive years, the limit remains in effect despite a general lack of enforcement (S. McKenna, NCDMF, pers. comm. 2009).

1.3. Survey catchability and previous work

Because total fish biomass is often unobservable, blue crab is one of many commercial species managed using fishery-independent CPUE as a relative index of population size. This assumes that CPUE is proportional to biomass and that this proportionality, or catchability, is constant over time (Arreguin-Sanchez 1996). A number of researchers (Harley et al. 2001, Walters and Martell 2002, Francis et al. 2003, and others) have questioned this assumption. They argue that, because assessment surveys frequently do not cover the full spatial range of the targeted stock, catchability is actually a function of the proportion of the population that is in the survey area at the time of the survey.

Due to sampling limitations, the NCDMF P195 survey excludes many regions of viable crab habitat immediately adjacent to the survey sample area. These include both shallow (< 2 m deep) areas on the western shore of PS and in upriver tributaries known to be important crab nursery habitats (Etherington and Eggleston 2003) and the entirety of Albemarle Sound where over a quarter of NC's annual blue crab commercial harvest is caught (NCDMF 2009b). We know from previous work that (*i*) spatial patterns of many abiotic variables in PS (temperature: C. Durham, unpublished data; salinity: Chapter 1 of this work; dissolved oxygen: Bell 2008) are highly variable over successive annual surveys, (*ii*) mature female crabs are especially responsive to abiotic change (Tagatz 1969, 1971), and they may require certain abiotic conditions in order to extrude a clutch (Rittschof et al., *in submission*), and (*iii*) crab movement between survey and non-survey areas is not restricted (Medici et al. 2006). In light of this evidence, it is illogical to assume that the same proportion of the mature female population resides within the survey area every June or

September, regardless of environmental conditions. More than likely, the survey area contains a greater population proportion during time periods when conditions are "favorable," resulting in increased catchability, increased CPUE for the survey overall, and an inflated estimate of relative population size. Under less favorable conditions, the opposite should be true, causing relative population size to be underestimated.

Observing that the spatial distribution of crab shifts with changes in the distribution of PS salinity, Eggleston et al. (2004) proposed replacing adjusted CPUE with a new index of annual "salinity-adjusted SSB" to monitor relative blue crab spawning stock size over time. Annual salinity-adjusted SSB means for this index were obtained through an analysis of covariance (ANCOVA) where per-station SSB, calculated by converting crab CW lengths to biomass weights, was modeled as a linear function of salinity with normally distributed errors. It is apparent when comparing annual mean salinity-adjusted SSB from 1987-2003 to mean unadjusted SSB from 1987-2006 (Figure 2) that overall variability across the time series of annual estimates decreases when mean SSB is adjusted for salinity. When both adjustment indices are directly compared (Figures 1 and 2), it is clear that they depict slightly different trends in relative spawning stock size over time, and that these slight differences have a sizeable impact on resulting management decisions (e.g., using the salinity-adjusted SSB index in 2004 would have resulted in immediate implementation of the upper female size limit regulation). Ultimately, managers chose not to adopt the salinity-adjusted SSB index, citing its failure "to incorporate other factors (water temperature, rainfall, storm events, etc.) also thought to affect the annual spatial distribution of mature female crab" (NCDMF 2004).

In preparation for the next BC FMP revision (scheduled for 2010), we model blue crab SSB at a given space-time (*it*) location (hereafter, SSB_{it}) as a function of salinity and other abiotic variables to address the MFC's concerns about including all pertinent variables in an adjusted index to monitor the spawning stock. We improve Eggleston et al.'s (2004) salinity-adjusted index by correctly modeling the probability distribution of SSB as zero-inflated gamma (ZIG), allowing a non-linear relationship between $salinity_{it}$ and SSB_{it}, and considering additional variables that are dynamic over both time and space (e.g. temperature, dissolved oxygen) that could also affect survey catchability. We will refer to this as the "adjustment" model. We created a second model of SSB_{it} to provide the MFC with the ability to identify areas for spatial closures that might conserve larger proportions of the spawning population than do current sanctuaries. This model, which we refer to as the "aggregation" model, includes additional variables that might affect the spatial distribution of SSB but are temporally static (e.g. depth, distance from a survey site to the nearest inlet), and therefore do not affect survey catchability. With the aggregation model, we map the mean of the conditional probability distribution of SSB at unsampled locations across PS during each survey time period. With these maps, we identify areas where there is a greater chance of observing either high SSB or an SSB hyper-aggregation (i.e. extremely high SSB) in a given time period and show whether there is consistency in the locations with a high probability of an aggregation. If consistent locations are observed, these areas could be considered as potential sanctuary sites. Information gained from these models will greatly assist PS blue crab management efforts, and natural resource managers in other systems could perform similar analyses by using these general methods.

2. METHODS

Both models of SSB_{it} were constructed similarly. In Section 2.1, we describe the data and choose an appropriate probability distribution to model SSB. In Sections 2.2 and 2.3, we identify abiotic factors that at a given time are thought to affect either the proportion of the population of mature females within the survey area or the probability distribution of SSB_{it}, create variables to represent each factor, examine relationships between each and SSB_{it}, and explain decisions regarding whether or not to consider them in either model. (A summary of these decisions can be found in Table 5.) Factors were grouped according to temporal variability, and time was considered its own group. We describe the variable-selection procedure for the adjustment model in Section 2.4 and for the aggregation model in Section 2.5, reporting the results of each final model in Section 3.

2.1. Data sources

The primary objective of NCDMF's PS Trawl Survey Program 195 ("the survey") is to assess the abundance of blue crab, shrimp, and resident finfish species at every space-time sample location. A description of survey sampling design can be found in Chapter 1; Section 2.1.1 along with a list of environmental variables measured at each site and the notation used to represent various scales of space and time in the data series. We continue to use previously defined reference notation in this chapter because blue crab and salinity were both collected at the same space-time locations. Figure 3 depicts both the measured depth at all 2,100 space-time locations in our observed dataset and the extent of the survey area's spatial domain.

A double-rigged 9.1 m Mongoose trawl with a 1.9 cm mesh cod end is used to collect biological samples at each survey site. After a standard 20-minute tow time, the size (mm) of all individuals caught is recorded. Blue crabs are sexed, and females are rated for maturity (e.g. immature, mature, sponging). To calculate biomass, the CW of all female crabs, except those rated as "immature females," was converted to a weight (g) using a ratio established by Miller and Houde (1999). SSB_{it} is the sum of these weights per site i in time period t.

To later predict the mean of the probability distribution of SSB at unsampled locations, we created a lattice data set of latitude and longitude coordinate pairs at evenly spaced 1 nmi (1.85 km) increments across the survey area's spatial domain. The value of salinity at each pair of coordinates was predicted using the salinity model documented in Chapter 1. To obtain predictions of temperature and depth at each coordinate pair, we preformed ordinary kriging using observed survey data. We employed a SAS macro (*%uk_optimal_cov*) that fits 10 theoretical spatial covariance functions (Exponential, Gaussian, Spherical, Linear, and Power, all with and without a nugget) to the data in each time period using restricted maximum likelihood estimation (REML). The macro then selects the best-fitting model given the data from each time period and uses corresponding spatial covariance parameter estimates to interpolate the response variable at designated prediction locations.

2.2. Statistical theory and general modeling assumptions

Because the objectives of this work are similar to those of Eggleston et al. (2004), we examined the salinity-adjusted SSB model in more detail. We document this investigation

for the reader as it exemplifies the importance of identifying and examining key assumptions made when fitting certain models.

The ANCOVA model used to calculate salinity-adjusted SSB can be written as a regression of the following form:

$$(1) \qquad SSB_{it} = \alpha_t + \beta * sal_{it} + \varepsilon_{it} \qquad \varepsilon_{it} \sim N(0, \sigma^2)$$

where α_t denotes the intercept, which is specific to an individual time period *t*, β is the regression coefficient for salinity estimated by the model, sal_{it} is the value of salinity at site *i* in time period *t*, and ε_{it} is the error at a space-time location. Errors are modeled as normally distributed (*N*) with mean zero and variance σ^2. Here, mean SSB ($\overline{SSB}$) is modeled as a linear function of explanatory variables. Each SSB_{it} observation is adjusted for salinity by subtracting $\beta * \overline{sal}$, or the global mean salinity over all sites and time periods. Annual salinity-adjusted means shown on Figure 2 are the time period-specific means of the adjusted observations. With this model construction, both SSB_{it} and ε_{it} are assumed, conditional on the values of the explanatory variables, to be normally distributed with constant variance for all values of *it*. It is also assumed that the relationship between SSB_{it} and sal_{it} is linear.

We performed an exploratory data analysis (EDA) to decide if these assumptions were satisfied. A frequency histogram of the response variable invalidated the assumption of normality. As illustrated in Figure 4, the probability distribution of SSB_{it} is not symmetric and bell-shaped; rather, it is zero-inflated and skewed right. Because this distributional non-normality made it difficult to determine the functional form for the relationship between SSB_{it} and sal_{it} using a scatter plot, we binned month-specific SSB_{it} by salinity and calculated the

mean and variance in each bin both including and excluding zeros (Table 1). Focusing on September bins, mean SSB_{it} appears to increase and then decrease with increasing levels of salinity, thus violating the assumption of a linear relationship. The constant variance assumption is violated by a similar trend in the variance of SSB_{it} across bins (Table 1). (We refer to this use of binning to learn about functional forms as a "tabular EDA" and we use it to examine relationships between SSB_{it} and other explanatory variables in subsequent sections.)

In light of the above analysis, we expand upon the work of Eggleston et al. (2004) by reconsidering these three assumptions when modeling the conditional probability distributions of blue crab SSB in this work. The term "conditional probability distribution" means that as opposed to modeling a single zero-inflated skew right probability distribution, we actually model multiple zero-inflated skew right probability distributions of SSB conditional on (that is, as a function of) the values of explanatory variables. This conditional modeling accounts for the fact that under some temperature and salinity combinations, for example, there may be a higher probability that zero crabs are present. To give another example, there may be certain locations in the sound where crabs are more likely to aggregate in large numbers. Probability distributions at these locations would in general be more skew right.

We account for SSB non-normality by using a generalized linear model (GLM), in which the expected value of the response (SSB_{it}) is related to a linear combination of explanatory variables though a link function, and by specifying a zero-inflated gamma (ZIG) mixture distribution for SSB_{it}. With any mixture, the distribution of the random variable is a

weighted sum of multiple probability density functions (pdfs or "mixture components") that each has an assigned a probability weight, with the sum of all weights equal to one. A ZIG mixture joins a degenerate zero distribution (ZI) with weight π, with π interpreted as the probability that SSB is zero, to a gamma ($\mathbf{\Gamma}$) distribution with probability 1- π. (Appendix 1 contains a complete derivation of the ZIG pdf.) Using a ZIG mixture in a GLM allowed us to examine the effects of multiple explanatory variables on both mixture components by modeling the linear predictor of π, the logistic transform of the probability that SSB_{it} is 0, and the linear predictor of μ, the inverse transform of the expected value of all non-zero SSB_{it} observations, as separate functions. (During variable selection, explanatory variables in the "ZI component" are used to model the linear predictor of π. Variables in the "Γ component" will model the linear predictor of μ.). To permit non-linearity in the relationship between SSB_{it} and any explanatory variable (including sal_{it}), we performed additional tabular EDAs and included variables of higher polynomial order when SSB_{it} increased and then decreased (or decreased and then increased) across bins.

It is worth noting that equation 1 additionally necessitates the assumption that, conditional on the values of the explanatory variables, both SSB_{it} and ε_{it} are independently distributed for all values of *it*. This assumption is also likely violated because observations of SSB_{it} are collected over space and time, and space-time data frequently exhibits spatial or space-time correlation. The models constructed in these analyses do not account for spatial correlation because at this time the SAS® software package does not have procedures that allow the modeling of spatial random effects in zero-inflated mixture models. In modeling the mean of the conditional probability distribution of SSB as opposed to an individual

observation of SSB_{it}, this omission should not seriously affect results, since spatial correlation in this analysis should be present only in error structure to more accurately estimate deviations from the mean.

2.3. Explanatory variables considered:

2.3.1. Group 1: Time period and month

The probability distribution of SSB_{it} likely varies temporally on inter- and intra-annual scales. This variability results from space-time differences both in the factors described below as well as in other factors, abiotic or biotic (e.g. year class strength, fishing mortality rate), not considered in this study. To account for factors not considered, we included the effect of time period in the model as a set of 40 binomial random variables, one for each time period in the temporal domain. $Time\_period_{it}$ thus represents spatial differences in mean SSB per time period after accounting for the effects of other explanatory variables in the model and similar to Eggleston et al.'s (2004) ANCOVA model, provides a different intercept for every time period. We additionally considered the interaction of $month_{it}$ with other explanatory variables (discussed below), because it appeared inappropriate to assume that the relationship between an explanatory variable and SSB_{it} was the same throughout the year.

2.3.2. Group 2: Temporally dynamic variables

- **Salinity and Temperature**

Salinity and temperature can to alter crab spatial distribution in PS, and different sources believe that seasonal decreases in each might be responsible for cueing female spawning migration (see Section 1.1). Thus, year-to-year fluctuations in these variables

might affect not only the spatial distribution of SSB_{it} across the survey area in a particular time period, but also the proportion of the population of mature females within the survey area at a given time. The previous salinity tabular EDA indicated a potential non-linear relationship between SSB_{it} and sal_{it} that could vary by month (Table 1), so we entertained sal_{it}, sal_{it}^2, and their interactions with $month_{it}$ in both adjustment and aggregation models. A second tabular EDA revealed a similar month-specific relationship between SSB_{it} and $temp_{it}$ (Table 2). These results warranted the examination of $temp_{it}$, $temp_{it}^2$, $temp_{it}*month_{it}$, and $temp_{it}^2*month_{it}$ in both models. Both sal_{it} and $temp_{it}$, in addition to all other explanatory variables considered in this analysis, were centered before they were squared or interacted with $month_{it}$ by subtracting their mean.

- **Dissolved Oxygen**

Bell et al. (2003) observed that decreases in DO concentration frequently incited movement of mature females in PS. While many researchers believe DO is critical to the determination of blue crab spatial distribution patterns (Breitburg 2002, Eby and Crowder 2002, and others), we were unable to include it as an explanatory variable due to data limitations. However, this omission should not seriously impact the results of either model. Decreasing concentrations of DO should not affect the proportion of the mature female crab population within the survey area in a given time period (and thus, not affect the adjustment model), because hypoxic ([DO] < 2 mg/L) conditions typically occur in deep-water areas where stratification of the water column is possible (G. Bell, pers. comm.), and the survey area contains all PS areas deeper than two meters. In addition, the spatiotemporal extent of hypoxic conditions when they are observed is frequently finer than the sampling resolution of

the survey (Bell et al. 2003), making any relationship between DO_{it} *and* SSB_{it} difficult to detect in our dataset. Without a detectable relationship, this factor would have been excluded from the aggregation model during variable selection procedures.

- **Rainfall, Freshwater Influx, and Storm Events**

During the 2004 BC FMP revision, NCDMF scientists identified rainfall, freshwater influx (FWI), and storm events as additional factors that could affect the spatial distribution of SSB in PS. While all three were associated with the same process believed to spur blue crab spatial distribution shifts (i.e. the rapid freshening and/or cooling of PS waters), we suspect that crabs were not responding to these factors individually, but rather to the abiotic change they collectively produced. For this reason, we include salinity and temperature instead of rainfall, FWI and storm events as the former factors integrate changes produced by the latter.

2.3.3. Group 3: Temporally static

- **Distance to inlet**

Previous research has indicated that mature female crabs migrate to the nearest inlet to spawn (Medici et al. 2006, Eggleston et al. 2009). Therefore, the $closest\_inlet\_dist_{it}$ variable created during salinity modeling (Ch. 1; Sect. 2.5) might exhibit a negative relationship with SSB_{it} during the spawning season. Unfortunately, results from a number of studies have produced conflicting theories as to how and when spawning migration begins. It is currently unclear whether mature females (*a*) travel back and forth across the estuary with each brood, up to seven times per season (Tankersley et al. 1998, R. Howell, pers. comm.), (*b*) migrate down-estuary once and remain in the eastern sound throughout the

season as they produce multiple broods (Medici et al. 2006), or (*c*) continue eastward migration with each successive brood, eventually leaving the sound and spawning in the coastal ocean (Hench et al. 2004, Forward et al. 2005). This combined research led us to wonder whether the SSB responsible for producing the September peak in post-larval abundance (Eggleston et al. in press) was (*a*) moving down-estuary toward the nearest inlet in late August/September, (*b*) accumulating throughout the spawning season in the eastern half of PS, or (*c*) residing just outside of PS, having traveled down-estuary in summer. In light of these questions, and because month-specific non-linear relationships between $closest\_inlet\_dist_{it}$ and SSB_{it} were observed with tabular EDA (Table 4), we entertained four distance to closest inlet variables. The objective here was not to determine which hypothesis was correct but to account for all three when considering potential functional forms of the relationship between $closest\_inlet\_dist_{it}$ and SSB_{it}.

$Closest\_inlet\_dist_{it}$ is included to investigate a linear relationship between SSB and distance to the nearest inlet, irrespective of month. If (*b*) is true, more mature females could be located near the inlets in both June and September if they are actively spawning at these times. The interaction between $month_{it}$ and $closest\_inlet\_dist_{it}$ accounts for differences in the June and September relationships between SSB_{it} and $closest\_inlet\_dist_{it}$. If (*a*) is true, we might see a linear relationship between SSB_{it} and $closest\_inlet\_dist_{it}$ in September but not in June.

$Closest\_inlet\_dist_{it}^2$ investigates a possible non-linear relationship between this factor and SSB_{it}. If (*b*) is true, peak SSB might occur at some intermediate distance from the closest inlet in both June and September if crabs remain in the eastern portion of the sound for the

entire season and only move toward the inlet immediately prior to larval release. The interaction between $month_{it}$ and $closest\_inlet\_dist_{it}^2$ accounts for differences in the June and September relationships between SSB_{it} and $closest\_inlet\_dist_{it}^2$. If (*c*) is true, we might expect to observe peak SSB at intermediate distances from the closest inlet in June, as crabs begin to migrate. In September, as crabs inseminated in late summer prepare to over-winter en-route to inlets and complete migration the following spring, we might observe peak SSB at distances farther from the inlet. In this scenario, by September the SSB producing the maximum post-larval abundance is already concentrated offshore outside of the survey area.

- **Depth**

In the Chesapeake Bay, post-copulatory female crabs follow deep basin corridors (>10 m) to the bay mouth to spawn (Lipcius et al. 2003). Medici et al. (2006) suggested that mature females in PS might also use migration corridors to orient towards inlets, which might yield a positive relationship between SSB_{it} and $depth_{it}$ during the spawning season. Again, in light of conflicting evidence regarding the exact timing of the blue crab spawning migration and the results of a tabular EDA examining SSB_{it} in different depth bins (Table 5), we considered four depth variables. $Depth_{it}$ accounts for a possible linear relationship between SSB_{it} and $depth_{it}$ irrespective of month if crabs are continually migrating. The interaction between $month_{it}$ and $depth_{it}$ accounts for month-specific differences in the SSB_{it} / $depth_{it}$ relationship in the event that the majority of mature females migrate in one month only. $Depth_{it}^2$ addresses a possible non-linear relationship between SSB_{it} and $depth_{it}$, if females are either en-route to inlets or temporarily residing in eastern PS waiting for successive brood maturation. In this case, the largest values of SSB would occur at

intermediate depths and shift to deeper depths only when spawning is imminent. The interaction between $month_{it}$ and $depth_{it}^2$ again accounts for month-specific relationship differences. If mature females are actively releasing larvae or just beginning migration in June, the largest values of SSB should occur at both deep and shallow depths. If they are in the process of migrating in September but preparing to over-winter, the largest values of SSB might occur at intermediate depths.

- **Spatial coordinates (northing and easting)**

The location of survey sites could account for variability in SSB_{it} not explained by other factors. Thus, we chose to evaluate $northing_{it}$, $easting_{it}$, $northing_{it}$*$easting_{it}$ in the aggregation model. Because redundancies in the proportion of variability in SSB explained by these spatial coordinate variables and other, more process-based variables are likely; we consider them in a separate final step and include them only if they explain additional variability not accounted for by other variables already selected for the model.

2.4. Coding a generalized linear mixture model

Zero-inflated gamma models are not included in any off-the-shelf statistical software packages. The SAS® proc NLMIXED procedure (SAS Institute© 2009), however, allows the user to specify a non-standard probability distribution by writing code to represent the likelihood function. Appendix 2 gives sample NLMIXED code for a model that includes sal_{it}, sal_{it}^2, and a single intercept for all time periods in both the ZI and Γ mixture components.

We used a variation of this simple model, replacing the single intercept in both ZI and Γ with time-period-specific intercepts ($time\_period_{it}$), to choose parameter starting values for

all model runs used to perform variable selection in the exercises that follow. Testing multiple starting values is important to ensure that the fitting algorithm converges to the true global minimum rather than a local minimum of the -2 log-likelihood (-2ll). We ran this simple model for a wide variety of intercept starting values, sometimes specifying a single starting value to be used for all time periods, other times specifying different starting values for each time period's intercept. To determine what values to try, we used a logical thought process based upon the data, but we also considered arbitrarily chosen values. Starting values for the slope coefficients of all explanatory variables were set equal to zero, which is the value they would have if they had no effect on the response. We ultimately chose the intercept starting values that gave us the smallest -2ll while satisfying all model constraints. Based on this exercise, the remainder of analyses here will use one starting value for all time period intercepts in ZI and another for all intercepts in Γ.

Prior work (Stefansson 1996) suggests that the probability of zero SSB_{it} should be a function of explanatory variables just as is the relative value of SSB_{it}. Examining tabular EDA output for all explanatory variables in Γ (Tables 1-4), the proportion of zeros appeared to increase with depth in September; decrease with salinity in June; increase, then decrease with salinity and temperature in September; and decrease, then increase with temperature and distance to the nearest inlet in June. We used our simple model to determine whether the inclusion of explanatory variables and time-specific intercepts in the ZI component improved model results enough to offset the increase in model complexity and decrease in error degrees of freedom. Table 6 gives fit statistics for the six model parameterizations used to make this decision. All models were fit to a base dataset that contained a randomly-chosen

90% of the total number of observations (N_B=1890), and parameter estimates obtained were used to predict SSB_{it} in a test dataset containing the remaining 10% of the observations that were withheld from model fitting procedures (N_E=210). Seven criteria were used to evaluate model fit. Three, –2ll, Akaike's information criterion (AIC), and Bayesian information criterion (BIC), were base dataset model fit statistics. These criteria identify the best-fitting model given the data; better fitting models in general have lower –2ll, AIC, and BIC when compared appropriately. The remaining four criteria, root mean squared error (RMSE) between predicted and observed SSB_{it}, and the slope, intercept, and coefficient of determination (R^2) of the regression of observed SSB_{it} on predicted SSB_{it}, were calculated from test dataset predictions. These criteria indicate which model generates the most accurate predictions of withheld data. More accurate predictions have lower RMSE, slopes closer to one, intercepts closer to zero, and R^2 closer to one. Because test dataset criteria were virtually identical for all six models (Table 6), models were compared using BIC. BIC and AIC are both appropriate for comparing likelihood models with different numbers of explanatory variables because they penalize model complexity (i.e. the number of parameters in model). BIC was chosen in this instance because it has a larger penalty than AIC, and therefore tends to favor less-complex models than AIC. Because models that included time-period specific intercepts in ZI had smaller BICs than models that did not, and because the model with the overall smallest BIC contained salinity in ZI, we decided to include all explanatory variables in both components.

2.5. Variable selection I: Adjustment model

The fully-parameterized adjustment model included eight potential explanatory variables (sal_{it}, sal_{it}^2, sal_{it}*$month_{it}$, sal_{it}^2*$month_{it}$, $temp_{it}$, $temp_{it}^2$, $temp_{it}$*$month_{it}$, and $temp_{it}^2$*$month_{it}$) and different time-specific intercepts ($time\_period_{it}$) in both the ZI and Γ mixture components (96 variables total). Using previously identified starting values, we fit this full model (Model **I**) to the base dataset, generated SSB_{it} predictions, and recorded the parameter estimates and corresponding p-values for each explanatory variable (Table 8) in addition to the same seven evaluation criteria used previously (Table 7). In Table 8, we observed that parameter estimates for both $temp_{it}^2$ and $temp_{it}^2$*$month_{it}$ in the ZI component were not significantly different from zero using a t-test with α=0.05. Thus, we performed a hand-iterated backwards elimination variable selection procedure. With each iteration, we removed the insignificant explanatory variable whose test statistic was closest to zero and then re-fit the model until the highest order of all terms included was significant. After two removal steps, the resulting model (Table 7, Model **II**) had significant parameter estimates for all highest-order terms or interactions (Table 9). We selected this as the final adjustment model because it had a smaller BIC than the full model and identical test dataset criteria (Table 7). We re-ran Model **II** using the full dataset to obtain predictions of π and μ for every SSB_{it} observation. To calculate an environmentally-adjusted SSB index, we predicted π and μ at a single hypothetical location h in every time period t where sal_{ht} and $temp_{ht}$ were set equal to the mean value of sal_{it} and $temp_{it}$ observed over the entire data series. The annual (or in this case, time period) mean adjusted SSB was equal to the mean of the conditional probability distribution of SSB at this hypothetical location, calculated by the

formula $(1- \pi_{ht})*\mu_{ht}$. Figures 5 and 6 depict this new environmental adjustment for SSB over time in June and September time periods, respectively. The series titled "grand mean 87-03" in both figures is the mean of environmentally-adjusted annual means from an additional fit of the final model to only data collected between 1987 and 2003. With this additional fit, we can directly compare this new SSB adjustment to both previous adjustment attempts (i.e. adjusted CPUE: NCDMF 2004 and salinity-adjusted SSB: Eggleston et al. 2004).

To examine trends over time in these two adjustment time series, we fit a reduced model to the full dataset that included the same explanatory variables as the final adjustment model, but instead estimated only two intercepts in ZI and Γ: one for samples collected in June ($june* year_{it}$) and another for samples collected in September ($sept* year_{it}$). $Year_{it}$ is a class variable corresponding to the year in which a specific space-time location was sampled (where $year_{it}$ = 1987:2006), and both *june* and *sept* are indicator variables that equal 1 if the space-time location is sampled in that month and 0 otherwise. Parameter estimates for intercept variables in this new temporal trends model are listed in Table 10.

2.6. Variable selection II: Aggregation model

The aggregation model used the final adjustment model as a base and additionally included 11 temporally-static process variables ($closest\_inlet\_dist_{it}$, $closest\_inlet\_dist_{it}^2$, $closest\_inlet\_dist_{it}*month_{it}$, $closest\_inlet\_dist_{it}^2*month_{it}$, $depth_{it}$, $depth_{it}^2$, $depth_{it}*month_{it}$, and $depth_{it}^2*month_{it}$) and three spatial coordinate variables ($northing_{it}$, $easting_{it}$, and $northing_{it}*easting_{it}$). We selected candidate variables from each group using the same methods documented in adjustment model variable selection. After the addition of the temporally-static variable group, the reduced model (Table 11, Model **B**) fit the observed

data better than the full model (Model **A**), when fit was judged based on test dataset evaluation criteria and BIC.

When the spatial coordinate variable group was added to the reduced aggregation model from the previous step (Model **B**), we noticed that some previously significant parameter estimates were now insignificant. To determine whether or not to retain the variables corresponding to these newly insignificant estimates, we performed two different backwards elimination routines and calculated model evaluation criteria for each. The first routine removed only insignificant spatial coordinate terms at successive iterations and retained all previously-selected process variables (Model **C**), while the second removed both insignificant spatial coordinate terms and insignificant process variables in decreasing polynomial order (Model **D**). Both models **C** and **D** have a lower BIC, a lower RMSE, and a larger R^2 than model **B**, the process model without spatial coordinate variables, indicating that both parameterizations improve model fit based on evaluation criteria (Table 11). Even though model **D** has the smaller BIC of the two, model **C** has the smaller RMSE when predicting to the test dataset and a larger R^2 between observed and predicted SSB_{it}. Because it was of greater concern to us to select the model that generated the most accurate predictions (i.e. those that were the closest to actual observations in the test dataset), we ultimately chose model **C** as the best aggregation model for our objectives. We fit this model to the full dataset and generated predictions of both π_{at} and μ_{at} at lattice dataset locations, where the subscript a indexes a specific unsampled spatial location in the lattice dataset nested within a particular time period (a=1, ... ,1346). With these predictions, we created retrospective maps for each time period of the mean of the conditional probability

distribution of SSB (hereafter, $\overline{SSB_{at}}$), which where $\overline{SSB_{at}} = (1 - \pi_{at}) * \mu_{at}$. ($\overline{SSB_{at}}$ is considered the mean of the conditional probability distribution of SSB at unsampled locations because spatial coordinate variables are included in the final aggregation model. The "*at*" subscript is used to remind readers that this mean is unique for every space-time location, however, it is also conditional on the values of other explanatory variables in the model.)

3. RESULTS

3.1. Adjustment model

The presence of significant interactions between $month_{it}$ and both $temp_{it}$ and sal_{it} in ZI and Γ (Table 9) signifies that the effect of both temperature and salinity on the probability of SSB=0 and the mean of the probability distribution of non-zero values of SSB varied according to month. Interpretation of the absolute effect of either explanatory variable on the overall mean of the SSB probability distribution, however, is not straightforward. If SSB had been normally distributed, it might have been modeled using standard linear regression. In this case, the mean of the SSB probability distribution would be a linear function of the explanatory variables and a positive parameter estimate for salinity would indicate that mean SSB increased with salinity.

Using a GLM, it is not the mean, but rather the linear predictor of the mean that is a linear function of the explanatory variables. To infer relationships between explanatory variables and the mean, the linear predictor must be transformed using the appropriate link function. Using a ZIG mixture distribution model, the mean of the overall SSB probability

distribution is a function of the means of two component distributions where the mean of each component is a different linear function of explanatory variables. In combining these two frameworks, the overall mean of the SSB probability distribution is a function of the mean of each component distribution, which is itself a different transformation of the linear predictor for that component. Thus the combined effects of temperature and salinity on month-specific SSB were examined using contour plots. These plots were constructed from predictions of SSB generated from estimated model parameters and the intercept values for a single time period using hypothetical conditions that spanned the range of observed temperatures and salinities in each month group.

The contour plot for June SSB predictions illustrates that predicted SSB is largest at intermediate values of temperature and high values of salinity, but that these optimal settings are each conditional on the values of the other variable (Figure 5). For example, predicted SSB is highest at intermediate temperatures in general, but within this optimal temperature range, SSB predictions increase with increasing salinity. Although this figure is generated using an intercept estimated for a single time period, these same patterns would be observed in contour plots generated for all June time periods. Using a different intercept would not change the shape of the contours; it would merely alter the absolute value assigned to each one. We can thus report that in June time periods, predicted SSB is largest when temperature is between 23.5° and 26.5°C and salinity is above 28.

It is clear when examining the contour plot of September SSB predictions why it was important to include interactions between both temperature and salinity and month in the adjustment model (Figure 6). This figure is visually quite different from the June SSB

contour plot (Figure 5), indicating that the effects of salinity and temperature on SSB in September are different from their effects on SSB in June. In September, predicted SSB increases as both salinity and temperature decrease, but these relationships are still conditional on the value of the other factor. As was true for the June contour plot, these same patterns would be observed in contour plots created for all September time periods. Thus, in September time periods, predicted SSB is largest when temperatures less than 21°C and salinities less than 14.

Annual means of June and September environmentally-adjusted SSB were graphed separately over time (Figures 7 and 8). In addition to the mean, each figure includes the upper and lower 95% CI for the mean estimate and the "grand adjustment mean" or the mean of annual adjusted means from 1987 to 2003 along with its 90% CI. This specific year range and confidence level were selected to match those used when the adjusted CPUE index was last examined by the NC MFC to consider an upper size limit for mature female blue crabs. After adjustment, the relative population size of mature female crab in PS exhibited different patterns over each monthly time series (Figures 7 and 8).

The June adjustment (Figure 7) varies over time with an occasional strong year class (1990-91, 1999, 2004) occurring every four or more years separated by groups of years (1988-89, 1992-98, 2000-03) with similar values of mean adjusted SSB (average range between adjusted SSB means in a group: 0.42 kg). A general negative trend in relative population size over time is also visually apparent in this series. Before 2000, means of adjusted June SSB were above the lower 90% CI (1.02 kg) for the grand adjustment mean in 10 out of 14 years. From 2000-2006, mean adjusted June SSB was above this CI in only one

year (2004) and it was still below the grand adjustment mean (1.37 kg). Results from the temporal trends model corroborated this observed negative trend. Despite decreases in both the probability of observing SSB=0 and in the mean of all non-zero SSB observations (indicated by parameter estimates in Table 10 for *june* year*$_{it}$ in ZI and Γ, respectively), time period-specific calculations of $(1-\pi_{ht})*\mu_{ht}$ showed that the entire ZIG distribution mean was decreasing over time. Comparing annual mean unadjusted SSB in June time periods with this annual June SSB adjustment, it is visually apparent that the overall range of the adjustment time series is smaller than that of the unadjusted series (Figure 9), due to the portion of SSB variability explained by the model. Mean adjusted June SSB was larger than unadjusted June SSB in 13 of the 20 time periods examined, indicating that the unadjusted index underestimated relative mean SSB in June time periods more than it overestimated it.

Mean adjusted September SSB (Figure 8) was visually quite different from mean adjusted June SSB (Figure 7). The September adjustment time series appears to have two phases: pre- and post-1999. Nine out of twelve years prior to 1999 had annual adjusted SSB means that were at or above the 1987-2003 grand mean (0.91 kg), and all yearly means were above the lower 90% CI for the grand mean (0.71 kg; Figure 8). Beginning in 1999, not only were all annual adjusted SSB means below the grand mean, but the entire 95% CI was below the lower 90% CI for the grand mean (Figure 8). The mean of annual means from 1999-2006 (0.31 kg) is 3.5 times smaller than the mean of annual means from 1987-1998 (1.14 kg; Figure 8). Similarly, parameter estimates from the temporal trends model for *sept* year*$_{it}$ in both ZI and Γ indicated that annual mean adjusted SSB was decreasing over time (i.e. an increasing probability of SSB=0 coupled with a decreasing mean SSB for all non-zero

observations). Again, adjusted SSB was larger than unadjusted SSB in the majority (16 out of 20) of September time periods (Figure 10). All four time periods where mean SSB was adjusted down (1996, 1999, 2003, and 2004) were time periods are where a hurricane made landfall in coastal NC in the sixty days prior to survey sampling. Only five time periods in our series contained hurricanes in the two months before the survey was performed. SSB was adjusted up in the fifth time period (September 1998), however the difference between the unadjusted and adjusted means was small (0.06 kg; Figure 10).

3.2. Aggregation model

Parameter estimates for the final aggregation model are listed in Table 12. Despite preferential selection of process-based variables for the model, we chose to refrain from interpreting all parameter estimates individually. Relationships between explanatory variables and SSB_{it} are much less straightforward than in the adjustment model due to increased model complexity. This decision was justified considering both the aggregation model's intended purpose (to predict $\overline{SSB_{at}}$ at unsampled locations) and the understanding that no single explanatory variable alone determines the spatial distribution of SSB. Thus, we were more interested in the model's performance as a whole than in the significance of any single variable, assuming that all variables selected for the final model were important predictors of $\overline{SSB_{at}}$.

Examining predictions for each mixture component separately, the mean of all 53,840 π predictions (0.31) was similar to the proportion of zeros in the observed data set (0.30). The largest difference between the mean of π for an individual time period and the

proportion of zero observations in that time period was 0.004. The overall range of π predictions was large (0.003:0.96), but the middle 50% (interquartile) of these predictions ranged from 0.11 to 0.46, indicating that the majority (> 50%) of sites had a 11-46% predicted chance of observing SSB=0. Similarly, at the majority of all prediction locations where SSB was not zero, mean SSB was between 0.75 to 1.34 kg, as this was the value of the interquartile range of predicted μ across all time periods (overall mean μ=1.22 kg). Time period-specific means of μ predictions were also similar to observed mean SSB_{it} per time period calculated from all non-zero observations with a RMSE of 0.069 kg between the two. $\overline{SSB_{at}}$ predictions calculated from both components had an overall mean of 0.95 kg and an interquartile range of 0.42 to 1.14 kg, while their standard errors had mean 0.17 kg and interquartile range of 0.09 to 0.18 kg. Coefficients of variation (CVs), calculated by dividing standard errors by their respective $\overline{SSB_{at}}$ predictions, indicated that more than 99.5% of $\overline{SSB_{at}}$ predictions were significantly different from zero (i.e. they had standard errors that were less than half of their means or CVs<0.5) using an α of 0.05.

We examined the spatial distribution of $\overline{SSB_{it}}$ by creating two sets of time-period specific PS maps. To compare the magnitude of predictions among all time periods in either June or September, the maps in the first set have the same legend based on percentiles (%) of the probability distribution of predicted $\overline{SSB_{at}}$ across all time periods: minimum value to 5%; 5-10%; 10-25%; 25-50%; 50-75%; 75-90%; 90-95%; and 95% to maximum value. To locate areas with the largest and smallest predictions within each time period separately, the maps in the second set have different legends for each time period that were based on the

probability distribution of predicted $\overline{SSB_{at}}$ from that time period alone using the same percentile groups. Maps in this second set facilitate the examination of possible changes in the spatial distribution of $\overline{SSB_{at}}$ under different environmental conditions. We selected two time periods from June (1992 and 2003) and three from September (1998, 1999, and 2000) to illustrate trends in space and time.

3.2.1. June

We chose to compare an early time period (1992) with a late one (2003) to look for differences in the spatial distributions of predicted $\overline{SSB_{at}}$ as mean June environmentally-adjusted SSB decreased over time. In 1992 (Figure 11A), greater than 85% of $\overline{SSB_{at}}$ predictions ranged from 0.72 to 2.31 kg as is visually indicated by the amount of PS area that is colored orange, pink, and red. The transition of the color ramp from cool to warm colors illustrates that $\overline{SSB_{at}}$ increases moving northeast (NE) across PS. Predictions were highest in the vicinity of Oregon Inlet on both the eastern and western shores of PS, but decreased slightly in waters adjacent to the inlet. Smallest predictions of $\overline{SSB_{at}}$ were located in the Neuse River (NR) and near both Hatteras and Ocracoke Inlets.

The same general spatial pattern was observed in 2003 (Figure 11B): increasing $\overline{SSB_{at}}$ moving from southwest (SW) to NE, with smallest values predicted in Neuse River and near both southerly inlets. As expected, predictions in this time period are smaller overall. Two-thirds of SSB predictions in June 2003 were between 0.23 and 0.72 kg, while predictions near Hatteras and Ocracoke Inlets and in NR were less than 0.14 kg.

Despite the fact that 1992 had on average lower observed temperatures, higher observed salinities, and lower FWI in both the two months and one week before the survey, the spatial distribution pattern of $\overline{SSB_{at}}$ is strikingly similar when map legends are based on percentiles of predictions within an individual time period (Figure 12). The same general spatial patterns were evident in all June time period maps, regardless of prevailing abiotic conditions or total observed SSB. Two summary maps further illustrate this pattern while identifying potential aggregation areas: the first shows predictions of SSB at or above the 99th percentile for their time period (Figure 13A) and the second includes all predictions, regardless of time period, larger than 7 kg, or the 99th percentile of all June SSB_{it} observations (Figure 13B). In both maps, the largest predictions of $\overline{SSB_{at}}$ occur in the northern regions of PS (north of 35.5°N latitude) near, but not adjacent to, Oregon Inlet.

3.2.2. September

The pre- and post-1999 framework for interpreting the September adjusted SSB time series in Section 3.1, motivates the following comparison of spatial patterns of $\overline{SSB_{at}}$. Recall from Figure 8 that 1998 (1.05 kg) was the last year that the September adjusted SSB fell above the 1987-2003 grand mean, that mean adjusted SSB decreased by a factor of two (0.44 kg) between 1998 and 1999, and that this decline continued to and beyond September 2000 (0.39 kg), albeit at a slower rate. This decline in annual relative SSB over successive Septembers is visually apparent when comparing maps with the same legend of $\overline{SSB_{at}}$ for these three time periods (Figure 14). The most noticeable decrease occurred in 2000, when

predictions at almost every space-time location were one or two percentile groups lower than predictions at the same locations in either of the other two time period maps (Figure 14).

As was the case in June, despite variable abiotic conditions and differences in observed SSB, spatial distribution patterns of $\overline{SSB_{at}}$ predictions were similar in all September time periods. The largest predictions of $\overline{SSB_{at}}$ in 1998, 1999, and 2000 all occur in the NE corner of PS and in the Pamlico River (Figure 15). The SW-NE pattern of increasing $\overline{SSB_{at}}$ identified in June time periods can still be observed in September time period maps, but an area of low predicted $\overline{SSB_{at}}$ in central PS that extends southward to Ocracoke and Hatteras Inlets interrupts the gradient (Figure 15). The spatial distribution of predictions above the 99th percentile for their time period are more dispersed in September summary maps (Figure 16A) than they were in June summary maps (Figure 13A), but these high predictions still occupy the same general areas as those larger than 5 kg (the 99th percentile of all September SSB_{it} observations; Figure 16B). Both September summary maps indicate potential aggregation areas near Croatan Sound and on the NW shore of PS, between Pains and Wysocking Bays on the western shore of PS, and near the mouth of the Pamlico River (Figure 16). Predictions of $\overline{SSB_{at}}$ are relatively high in Pamlico and Pungo Rivers within certain time periods (Figure 16A), but do not appear to be absolutely high when compared to predictions in all September time periods (Figure 16B).

4. DISCUSSION

We created two models each of which addresses a management need for mobile blue crabs in Pamlico Sound, NC. The first adjusts for temporally dynamic abiotic variables that affect catchability so that the adjusted annual mean is a reliable index of the year-to-year variability of blue crab spawning stock biomass. When the September environmentally-adjusted SSB index is examined over time, it does not contradict conclusions drawn from the previous salinity-adjustment analysis (Eggleston et al. 2004) and instead corroborated anecdotal evidence that the size of the blue crab population has declined over the past 20, especially post-1999. A variant of this model that specifically investigated temporal trends in each monthly time series indicated that blue crab spawning stock size is indeed decreasing over time in both June and September time periods.

Second, to model the spatial distribution of SSB, we additionally incorporated temporally static abiotic variables. Separate examinations of June and September maps of $\overline{SSB_{at}}$ show that the highest predictions consistently occur in the same PS areas. These results suggest additional areas for consideration of no-take sanctuaries to protect the population of mature female crabs more effectively during the spawning season. Information gained from these two models will help improve management efforts designed to sustain blue crab spawning stock biomass over time. In addition, the approach taken in this study can be applied to a wide range of fishery-independent surveys whose target species also varies in space and time in response to environmental variables, thereby affecting their availability to survey gear.

This analysis improves on previous blue crab SSB modeling efforts by incorporating the actual probability distribution of the data. The application of models that address zero inflation in ecological datasets has become increasingly popular in recent history (Maunder and Punt 2004, Martin et al. 2005). Both the GENMOD and COUNTREG procedures in SAS Version 9.2 allow the specification of a zero-inflated Poisson or a zero-inflated negative binomial model with a few lines of additional coding (SAS Institute Inc. 2009), though these two models are appropriate for discrete data only. Models that deal with zero-inflated continuous data, a common outcome of fisheries stock assessment surveys, however, are less common. A few researchers (Stefansson 1996, Syrjala 2000) have addressed this issue using the delta method, a two-step process where the probability of obtaining a zero catch and the CPUE given that the catch is non-zero is modeled separately. Candidate probability distributions for non-zero observations include log-normal (Syrjala 2000) and gamma (Stefansson 1996). While similar to Stefansson's (1996) delta-gamma model, the ZIG mixture model used here maximizes the likelihood of both mixture components concurrently. Fitting the two distributions simultaneously was the more appropriate procedure in this case because the quantity of interest was the mean of the entire mixture, as opposed to separate means of the zero and non-zero mixture components (Tu 2002). This simultaneous fitting procedure also allows for estimation of standard prediction errors for the overall distribution mean, as opposed to just estimating standard errors for π and μ separately.

4.1. Possible model improvements

Though this work represents a significant update to Eggleston et al. (2004), there remains room for improvement. We modeled relationships between explanatory variables

and SSB using linear and quadratic terms in the linear predictors for π and μ. While the increasing and then decreasing (or decreasing and then increasing) relationships seen in the tabular EDA's provide some support for the use of these functional forms, improvements to this model might consider more flexible functional forms, possibly using non-parametric techniques. Further expansion of the methods might include modeling spatial correlation. Including spatial random effects in zero-inflated mixture distributions is an area of active development in the statistical community; such an expansion would represent a non-trivial research project.

4.2. Adjustment model outcomes

This analysis demonstrates that relationships exist between observed SSB_{it} and both sal_{it} and $temp_{it}$. By adjusting annual mean SSB for mean temperature and salinity, we produce a valid index to track changes in relative SSB over time. Comparing this September SSB environmental adjustment (Figure 8) to NCDMF's adjusted CPUE (Figure 1), the index on which the mature female upper slot limit management rule was based, we see a very different story of blue crab spawning stock size over time. Instead of a relative stock size between the grand mean and the lower 90% CI for seven out of the nine years between 1987 and 1995 (Figure 1), there is now a time series in which relative stock size is at or above the mean in eight out of the same nine years (Figure 6). There is still a peak in 1996 in the September environmentally-adjusted SSB time series, but it is much smaller relative to other environmentally-adjusted SSB means (Figure 8) than the 1996 peak in the adjusted CPUE time series was compared to the other adjusted CPUE means (Figure 1). Differences between the two adjustments are most apparent beginning in 1999. The adjusted CPUE

index predicts relative spawning stock size to be below the 90% CI for four (non-consecutive) years between 2000 and 2004, interrupted by a large increase in adjusted CPUE in 2003 almost equal to the mean from 1996 (Figure 1). Not only is each annual environmentally-adjusted SSB mean from 1999 to 2006 below the lower 90% CI for the grand mean, but in all cases the entire 95% CI is below the grand mean (Figure 8).

Comparing these two figures (Figures 1 and 8) clearly illustrates the need for an environmentally-adjusted SSB index. Looking just at the index of adjusted CPUE, it appears in general as if relative spawning stock size was relatively invariable at the beginning of the time series and was more variable towards the end, with both years of relatively high CPUE (1996-1999, 2003) and relatively low SSB (2000-2002, 2004) (Figure 1). This figure does not depict a population in decline; but rather a population that is more inter-annually variable at the end of the time series than at the beginning. Looking at the September environmentally-adjusted SSB time series (Figure 8), one sees a relative population that, although variable with a few years of high mean adjusted SSB, was consistently between 0.5 and 1.5 kg annually before 1999, and has since been less than 0.5 kg in every year. This graph portrays a population in decline. It is unknown whether an immediate enaction of the upper slot limit regulation in 2004 would have made a difference, since according the September environmentally-adjusted SSB time series (Figure 8) the stock had already been at historic lows for five consecutive years. However, if this environmental adjustment had been available to managers during the 2004 BCFMP revision, it might have caused more concern over the health of the population.

The interpretation of our September SSB environmental adjustment time series (Figure 8) matches Eggleston et al.'s (2004) interpretation of the salinity-adjusted SSB time series (Figure 2). Both figures (2 and 8) illustrate a marked decline in blue crab relative population size in the late 1990s and a subsequent lack of recovery to prior abundance levels. While Eggleston's salinity adjustment makes it appear that mean adjusted SSB increases slightly in 2003 from record lows in 2000-2002 (Figure 2), the environmental SSB adjustment shows no such increase (Figure 8). According to the latter, the population has been at a record low level since 1999. This result is most likely due to the fact that both temperature and salinity were low in September 1999 (possibly as a result of hurricane-induced FWI), causing a larger proportion of the population to occur within the survey area and resulting in an observed mean SSB that over-estimates true population size. This finding also corroborated anecdotal evidence from fishers who were observing masses of blue crabs moving from the river into the mainstem sound following Hurricane Floyd. In fact, because the September 1999 survey was delayed for two weeks until hurricane floodwaters receded, it left blue crabs exposed to intense fishing pressure for two weeks longer than they were prior to any other September survey. It is thus likely that mean unadjusted SSB was even lower than it might have been if samples had been collected immediately after the hurricane.

Land-falling hurricanes were observed in the 60 days prior to survey sampling in five September time periods. Mean unadjusted SSB overestimated the size of the spawning stock in four of these time periods (1996, 1999, 2003 and 2004; Figure 8). These four time periods also had the largest combined FWI during both the two months and the week before survey sampling. Because there was a September time period that had a hurricane but did not have

high FWI (1998) and a time period that had high FWI but no hurricane (2000), there appears to be an interactive effect of high FWI and hurricane presence that causes a greater proportion of the population of mature females to occur within the survey area, inflating the unadjusted estimate of spawning stock size. While explanatory variables corresponding to site-specific FWI and time period-specific storm events are unnecessary in this analysis (see Section 2.3.2), a further examination of the relationships between observed SSB and both FWI and hurricane presence is warranted.

4.3. Aggregation model outcomes

The aggregation model provides information about the spatial distribution of observed SSB, regardless of the proportion of the mature female population that is present within the survey area. Comparing groups of maps from time periods that exhibited similar conditions of each temporally dynamic environmental variable (e.g. maps with low mean PS salinity, high mean PS temperature, high overall FWI, hurricane presence, etc.) did not reveal any consistent patterns in locations of high or low $\overline{SSB_{at}}$. This illustrates the point that patterns of observed spatial distribution cannot be attributed to a single environmental factor in isolation. Rather, observed spatial distributions are the result of interactions between multiple factors. Areas of high and low predicted $\overline{SSB_{at}}$ are observed in the same absolute spatial locations across all June and all September time periods (Figures 12 and 15), regardless of an individual time period's range of predicted $\overline{SSB_{at}}$ or the proportion of the mature female population within the survey area. Time periods in both month groups have consistently high predictions of $\overline{SSB_{at}}$ in locations that occur on survey area borders (Figures

13 and 16). These areas of high mean $\overline{SSB_{at}}$ likely continue to locations outside the survey area, indicating that there are large portions of the population also outside the survey area. This observation provides further evidence to support the aforementioned belief that the survey area does not contain the same proportion of the population at all times and thus further validates the need for an adjusted population index.

Predicted $\overline{SSB_{at}}$ was lowest in upriver regions of NR and near Ocracoke and Hatteras Inlets in both June and September maps (Figures 12 and 15, respectively), with low predictions radiating from the inlets to include regions in the SE corner of PS in September. Recall that these inlet areas are the locations of blue crab spawning sanctuaries. Additional results from at least two other studies (Medici et al. 1996 and Eggleston et al. 2009) are consistent with the finding that mature female crabs do not aggregate near inlets. While tracking mature female crab in and around inlet sanctuaries in August 2003, Medici et al. (1996) noted that only females with late-stage egg masses (< 3 days from hatching) exhibited directed movement towards inlets. All other mature females, even those with early-stage egg masses, appeared to move randomly and were recaptured inside and outside of spawning sanctuaries with similar frequency. Using sampling methods modeled after those used in the NCDMF Program 195 trawl survey, Eggleston et al. (2009) observed that mature female abundance inside inlet sanctuaries in June, August, and September 2002 was not different from abundance observed outside the sanctuaries. This combined information will hopefully prompt managers to reconsider the siting of select area closures for the blue crab fishery.

5. CONCLUSIONS

We successfully created statistical models to better inform management of the North Carolina blue crab fishery by accounting for both differences in environmental conditions over time and employing new analysis methods to correctly model the probability distribution of observed blue crab spawning stock biomass. The adjustment model validated conclusions drawn from previous analyses and field observations that the size of the NC blue crab spawning stock has decreased over the past 20 years. The aggregation model identified areas in Pamlico Sound with both high and low probability of observing mature female crab, which will assist an evaluation of the efficacy of current spawning sanctuaries at protecting mature female crabs. This information can facilitate effective policy during the 2010 revision of the NC blue crab FMP. In a broader context, it is important to consider the effect of environmental change on the spatial distribution of any mobile species when assessing population abundance over time. Data for factors known to affect species spatial distributions (salinity, temperature, DO, current speed and direction, etc.) are often already collected during assessment surveys at the same space-time locations as biological samples; it should be straightforward to use both the methods presented in this study to explore potential relationships and the statistical code to perform a similar analysis with any surveyed species.

6. REFERENCES

Aguilar, R., A. H. Hines, T. G. Wolcott, D. L. Wolcott, M. A. Kramer, and R. N. Lipcius. 2005. The timing and route of movement and migration of post-copulatory female blue crabs, *Callinectes sapidus* Rathbun, from the upper Chesapeake Bay. *Journal of Experimental Marine Biology and Ecology* **319**:117.

Anderson, A. M., W. J. Davis, M. P. Lynch, and J. R. Schubel. 1973. *Effects of Hurricane Agnes on the Environment and Organisms of Chesapeake Bay*. The Chesapeake Bay Research Council, Johns Hopkins University, Baltimore, MD.

Arreguin-Sanchez, F. 1996. Catchability: a key parameter for stock assessment. *Reviews in Fish Biology and Fisheries* **6**:221-242.

Bell, G. W. 2008. The impact of episodic hypoxia on blue crabs (*Callinectes sapidus*): from molecules to populations, North Carolina State University, Raleigh, NC, USA.

Bell, G. W. 2002. Behavioral response of free-ranging blue crabs to episodic hypoxia, North Carolina State University, Raleigh, NC, USA.

Bell, G. W., D. B. Eggleston, and D. L. Wolcott. 2003. Behavioral responses of free-ranging blue crabs to episodic hypoxia. I. Movement. *Marine Ecology Progress Series* **259**:215-225.

Breitburg, D. 2002. Effects of Hypoxia, and the Balance between Hypoxia and Enrichment, on Coastal Fishes and Fisheries. *Estuaries* **25**:767-781.

Burkholder, J., D. Eggleston, H. Glasgow, C. Brownie, R. Reed, G. Janowitz, M. Posey, G. Melia, C. Kinder, R. Corbett, D. Toms, T. Alphin, N. Deamer, and J. Springer. 2004. Comparative impacts of two major hurricane seasons on the Neuse River and western Pamlico Sound ecosystems. *Proceedings of the National Academy of Sciences* **101**:9291-9296.

Carr, S. D., R. A. Tankersley, J. L. Hench, R. B. Forward, and R. A. Luettich. 2004. Movement patterns and trajectories of ovigerous blue crabs *Callinectes sapidus* during the spawning migration. *Estuarine, Coastal and Shelf Science* **60**:567-579.

Csirke, J. 1989. Changes in the catchability coefficient in the Peruvian anchoveta (*Engraulis ringens*) fishery. P. 207–219 in *Proceedings of the ICLARM Conference on the Peruvian Upwelling Ecosystem: Dynamics and Interactions*, D. Pauly, P. Muck, J. Mendo and I. Tsukayama, eds., Manila, Philippines.

Eby, L. A., and L. B. Crowder. 2002. Hypoxia-based habitat compression in the Neuse River Estuary: context-dependent shifts in behavioral avoidance thresholds. *Canadian Journal of Fisheries and Aquatic Sciences* **59**:952-965.

Eggleston, D. B., N. B. Reyns, L. L. Etherington, G. Plaia, L. Xie. (in press). Tropical storm and environmental forcing on regional blue crab settlement. *Fisheries Oceanography.*

Eggleston, D. B., G. W. Bell, and S. P. Searcy. 2009. Do blue crab spawning sanctuaries in North Carolina protect the spawning stock? *Transactions of the American Fisheries Society* **138**:581-592.

Eggleston, D. B., E. Johnson, and J. Hightower. 2004. Population Dynamics and Stock Assessment of the Blue Crab in North Carolina. Report Division of Marine Fisheries, Morehead City, NC.

Etherington, L. L., and D. B. Eggleston. 2003. Spatial dynamics of large-scale, multistage crab (*Callinectes sapidus*) dispersal: determinants and consequences for recruitment. *Canadian Journal of Fisheries and Aquatic Sciences* **60**:873-887.

Forward, R. B., J. H. Cohen, M. Z. Darnell, and A. Saal. 2005. The circatidal rhythm in vertical swimming of female blue crabs, *Callinectes sapidus*, during their spawning migration: a reconsideration. *Journal of Shellfish Research* **24**:587-590.

Francis, R. I. C., R. J. Hurst, and J. A. Renwick. 2003. Quantifying annual variation in catchability for commercial and research fishing. *Fishery Bulletin* **101**:293-304.

Guerin, J. L., and W. B. Stickle. 1992. Effects of salinity gradients on the tolerance and bioenergetics of juvenile blue crabs (*Callinectes sapidus*) from waters of different environmental salinities. *Marine Biology* **114**:391-396.

Harley, S. J., R. A. Myers, and A. Dunn. 2001. Is catch-per-unit-effort proportional to abundance? *Canadian Journal of Fisheries and Aquatic Sciences* **58**:1760-1772.

Hench, J. L., R. B. Forward Jr., S. D. Carr, D. Rittschof, and R. A. Luettich Jr. 2004. Testing a selective tidal-stream transport model: Observations of female blue crab (*Callinectes sapidus*) vertical migration during the spawning season. *Limnology and Oceanography* **49**:1857-1870.

Hilborn, R., and C. Walters. 2003. *Quantitative Fisheries Stock Assessment*. Kluwer Academic Publications, New York.

Hines, A. H., A. M. Haddon, and L. A. Wiechert. 1990. Guild structure and foraging impact of blue crabs and epibenthic fish in a subestuary of Chesapeake Bay. *Marine Ecology Progress Series* **67**:105-126.

Johnson, E. 2004. Population dynamics and stock assessment of the blue crab in North Carolina, North Carolina State University, Raleigh, NC, USA.

Kareiva, P. M., J. G. Kingsolver, and R. B. Huey. 1993. *Biotic interactions and global change*. Sinauer Assoc. Press, Sundarland, MA.

Knott, D. M., and R. M. Martore. 1991. The short-term effects of Hurricane Hugo on fishes and decapod crustaceans in the Ashley River and adjacent marsh creeks, South Carolina. *Journal of Coastal Research* **SI8**:335-356.

Levinton, J. S. 2001. *Marine Biology: Function, Biodiversity, Ecology*. Oxford University Press, New York.

Lipcius, R. N., W. T. Stockhausen, R. D. Seitz, and P. J. Geer. 2003. Spatial dynamics and value of a marine protected area and corridor for the blue crab spawning stock in Chesapeake Bay. *Bulletin of Marine Science* **72**:453-469.

Loneragan, N. R., and S. E. Bunn. 1999. River flows and estuarine ecosystems: Implications for coastal fisheries from a review and a case study of the Logan River, southeast Queensland. *Austral Ecology* **24**:431-440.

Mansour, R. A., and R. N. Lipcius. 1991. Density-dependent foraging and mutual interference in blue crabs preying upon infaunal clams. *Marine Ecology Progress Series* **72**:239-246.

Martin, T. G., B. A. Wintle, J. R. Rhodes, P. M. Kuhnert, S. A. Field, S. J. Low-Choy, A. J. Tyre, and H. P. Possingham. 2005. Zero tolerance ecology: improving ecological inference by modeling the source of zero observations. *Ecology Letters* **8**:1235-1246.

Maunder, M. N., and A. E. Punt. 2004. Standardizing catch and effort data: a review of recent approaches. *Fisheries Research* **70**:141-159.

Medici, D. A., T. G. Wolcott, and D. L. Wolcott. 2006. Scale-dependent movements and protection of female blue crabs (*Callinectes sapidus*). *Canadian Journal of Fisheries and Aquatic Sciences* **63**:858-871.

Miller, T. J., and E. D. Houde. 1999. Blue crab target setting. Technical Report [UMCES] CBL TS-177-99. Chesapeake Biological Laboratory, Solomons, MD.

Millikin, M. R., and A. B. Williams. 1984. Synopsis of biological data on the blue crab, *Callinectes sapidus* Rathbun. FAO Fisheries Synopsis No. 138, NOAA Tech Report. NMF 51: 1-38.

North Carolina Division of Marine Fisheries (NCDMF). 2009a. Commercial Statistics Index. Website: http://www.ncfisheries.net/statistics/comstat/index.html

NCDMF. 2009b. Trip Ticket Program commercial fishing statistics. North Carolina Division of Marine Fisheries, Morehead City.

NCDMF. 2004. North Carolina fishery management plan, blue crab, 2004. North Carolina Division of Marine Fisheries, Morehead City.

Paerl, H. W., L. M. Valdes, A. R. Joyner, B. L. Peierls, M. F. Piehler, S. R. Riggs, R. R. Christian, L. A. Eby, L. B. Crowder, J. S. Ramus, E. J. Clesceri, C. P. Buzzelli, and R. A. Luettich. 2006. Ecological Response to Hurricane Events in the Pamlico Sound System, North Carolina, and Implications for Assessment and Management in a Regime of Increased Frequency. *Estuaries and Coasts* **29**:1033-1045.

Posey, M. H., T. D. Alphin, H. Harwell, and B. Allen. 2005. Importance of low salinity areas for juvenile blue crabs, *Callinectes sapidus* Rathbun, in river-dominated estuaries of southeastern United States. *Journal of Experimental Marine Biology and Ecology* **319**:81-100.

Reyns, N. B., D. B. Eggleston, and R. A. Luettich. 2007. Dispersal dynamics of post-larval blue crabs, *Callinectes sapidus*, within a wind-driven estuary. *Fisheries Oceanography* **16**:257-272.

Rittschof, D., M. Z. Darnell, K. M. Darnell, M. Goldman, M. B. Ogburn, and R. McDowell. March 10–13, 2009. Informing Managers: Blue Crab Spawning Biology and Stock Assessment. In *Proceedings of the 25th Lowell Wakefield Fisheries Symposium: Biology and Management of Exploited Crab Populations under Climate Change*, Anchorage, Alaska.

Rose, G., and D. Kulka. 1999. Hyperaggregation of fish and fisheries: how catch-per-unit-effort increased as the northern cod (*Gadus morhua*) declined. *Canadian Journal of Fisheries and Aquatic Sciences* **56**:118-127.

Rosenberg, A. A., J. H. Swasey, and M. Bowman. 2006. Rebuilding US fisheries: progress and problems. *Frontiers in Ecology and the Environment* **4**:303-308.

SAS Institute, Inc. 2009. SAS 9.2 Help and documentation, Cary, NC: SAS Institute Inc., 2002-2009.

Southward, A. J., S. J. Hawkins, and M. T. Burrows. 1995. Seventy years' observations of changes in distribution and abundance of zooplankton and intertidal organisms in the western English Channel in relation to rising sea temperature. *Journal of Thermal Biology* **20**:127.

Stefánsson, G. 1996. Analysis of groundfish survey abundance data: combining the GLM and delta approaches. *ICES Journal of Marine Science* **53**:577–588.

Syrjala, S. E. 2000. Critique on the use of the delta distribution for the analysis of trawl survey data. *ICES Journal of Marine Science* **57**:831–842.

Tagatz, M. 1971. Osmoregulatory ability of blue crabs in different temperature-salinity combinations. *Chesapeake Science* **12**:14.

Tagatz, M. E. 1969. Some Relations of Temperature Acclimation and Salinity to Thermal Tolerance of the Blue Crab, *Callinectes sapidus*. *Transactions of the American Fisheries Society* **98**:713-716.

Tankersley, R. A., M. G. Wieber, M. A. Sigala, and K. A. Kachurak. 1998. Migratory Behavior of Ovigerous Blue Crabs *Callinectes sapidus*: Evidence for Selective Tidal-Stream Transport. *Biological Bulletin* **195**:168-173.

Tu, W. 2002. Zero-inflated data. Pp. 2387-2391 In *Encyclopedia of Environmetrics*, A. H. El-Shaarawi and W. W. Piegorsch, eds. John Wiley & Sons, Ltd., Chichester, West Sussex, UK.

Walters, C. J., and S. J. D. Martell. 2004. *Fisheries Ecology and Management*. Princeton University Press, Princeton, NJ, USA.

Walther, G.-R., E. Post, P. Convey, A. Menzel, C. Parmesan, T. J. C. Beebee, J.-M. Fromentin, O. Hoegh-Guldberg, and F. Bairlein. 2002. Ecological responses to recent climate change. *Nature* **416**:389-395.

Table 1. Characteristics of the June and September distribution of SSB_{it} in different bins of salinity. Listed is the number of observations in the bin out of a total of 1053 for June (N_J) or 1047 for September (N_S), the mean and variance of SSB_{it} for the bin, the number of observations where SSB_{it}=0, and the proportion of zero observations in the bin (calculated by dividing # 0's by either N_J or N_S).

				With Zeros		Without Zeros			
Bin #	**Month**	**Salinity range**	**N**	**Mean SSB**	**Variance SSB**	**Mean SSB**	**Variance SSB**	**# 0's**	**% 0's**
1	6	0-5	36	0.49	0.37	0.80	0.35	14	38.9
2	6	5-10	85	0.65	0.85	0.86	0.94	20	23.5
3	6	10-15	197	0.92	2.53	1.19	2.96	45	22.8
4	6	15-20	421	1.43	10.24	1.75	11.94	76	18.1
5	6	20-25	252	1.58	9.36	1.97	10.92	50	19.8
6	6	25-30	62	1.42	7.99	1.63	8.84	8	12.9
1	9	0-5	30	1.03	1.58	1.24	1.64	5	16.7
2	9	5-10	67	1.85	15.62	2.43	19.18	16	23.9
3	9	10-15	156	1.03	10.06	1.74	15.88	64	41.0
4	9	15-20	334	0.72	2.66	1.22	3.89	136	40.7
5	9	20-25	339	0.55	1.28	0.97	1.87	148	43.7
6	9	25-30	121	0.40	0.43	0.64	0.54	46	38.0

Table 2. Characteristics of the June and September distribution of SSB_{it} in different bins of temperature. Listed is the number of observations in the bin, the mean and variance of SSB_{it} for the bin both including and excluding observations where SSB_{it}=0, and the number and proportion of zero observations per bin (# 0's / N_J or N_S). We see different non-linear relationships between mean SSB and temperature in the two months; in June, mean SSB increases from bins 1-2 and decreases from bins 2-5. In September, mean SSB begins high in bin 1, decreases in bins 2-4, and increases again from bins 4-5. Month-specific non-linear relationships can similarly be observed across bins of percent zeros.

				With Zeros		Without Zeros			
Bin #	**Month**	**Temp range (°C)**	**N**	**Mean SSB**	**Variance SSB**	**Mean SSB**	**Variance SSB**	**# 0's**	**% 0's**
1	6	< 23	104	0.72	3.54	0.98	4.55	27	26.0
2	6	23-24	102	1.99	32.27	2.51	39.43	21	20.6
3	6	24-25	246	1.37	7.49	1.72	8.81	50	20.3
4	6	25-26	281	1.37	5.42	1.64	6.05	47	16.7
5	6	> 26	320	1.07	2.36	1.36	2.60	68	21.3
1	9	< 23	152	1.14	11.73	1.68	16.45	49	32.2
2	9	23-24	127	0.71	2.26	1.14	3.16	48	37.8
3	9	24-25	198	0.70	3.13	1.31	5.07	92	46.5
4	9	25-26	326	0.59	1.18	1.00	1.59	133	40.8
5	9	> 26	244	0.80	4.28	1.29	6.30	93	38.1

Table 3. Characteristics of the June and September distribution of SSB_{it} in different bins of distance to the closest inlet. Listed is the number of observations in the bin, the mean and variance of SSB_{it} for the bin both including and excluding observations where SSB_{it}=0, and the number and proportion of zero observations per bin (# 0's / N_J or N_S). We see different relationships between mean SSB and distance to the closest inlet in the two months. In June, we observe a non-linear relationship as mean SSB increases from bins 1-2 and decreases from bins 2-5. In September, we observe a linear relationship with mean SSB beginning high in bin 1 and decreasing in bins 2-5. A non-linear relationship can similarly be observed across bins of percent zeros in June, but there appears to be no discernable relationship in September.

				With Zeros		Without Zeros			
Bin #	**Month**	**Distance range (km)**	**N**	**Mean SSB**	**Variance SSB**	**Mean SSB**	**Variance SSB**	**# 0's**	**% 0's**
1	6	< 18.5	217	1.11	3.02	1.42	3.42	47	21.7
2	6	18.5 – 37.0	509	1.49	11.99	1.85	14.28	101	19.8
3	6	37.0 – 55.6	157	1.42	4.80	1.67	5.24	24	15.3
4	6	55.6 – 74.1	114	0.95	2.08	1.12	2.28	18	15.8
5	6	> 74.1	56	0.29	0.17	0.49	0.19	23	41.1
1	9	< 18.5	216	0.82	10.03	1.62	18.49	106	49.1
2	9	18.5 – 37.0	505	0.82	3.07	1.25	4.13	173	34.3
3	9	37.0 – 55.6	148	0.63	1.75	1.09	2.55	63	42.6
4	9	55.6 – 74.1	123	0.65	1.09	1.05	1.34	47	38.2
5	9	> 74.1	55	0.43	0.48	0.82	0.61	26	47.3

Table 4. Characteristics of the June and September distribution of SSB_{it} in different bins of depth. Listed is the number of observations in the bin, the mean and variance of SSB_{it} for the bin both including and excluding observations where SSB_{it}=0, and the number and proportion of zero observations per bin (# 0's / N_J or N_S). We see different relationships (or a lack thereof) between mean SSB and distance to the closest depth in the two months. In June, there appears to be no discernable relationship with either mean SSB or the percent zeros per bin. In September, we observe non-linear relationship with both mean SSB and percent zeros.

				With Zeros		Without Zeros			
Bin #	**Month**	**Depth range (m)**	**N**	**Mean SSB**	**Variance SSB**	**Mean SSB**	**Variance SSB**	**# 0's**	**% 0's**
1	6	2 – 3	122	1.36	5.02	1.66	5.63	22	18.0
2	6	3 – 4	272	1.07	3.34	1.39	3.90	63	23.2
3	6	4 – 5	272	1.62	14.12	1.87	15.87	37	13.6
4	6	5 – 6	265	1.11	5.94	1.40	7.12	56	21.1
5	6	> 6	122	1.26	7.22	1.77	9.25	35	28.7
1	9	2 – 3	125	0.95	9.53	1.43	13.72	42	33.6
2	9	3 – 4	248	1.15	7.47	1.70	10.16	81	32.7
3	9	4 – 5	286	0.83	2.66	1.26	3.50	98	34.3
4	9	5 – 6	278	0.45	0.79	0.89	1.17	136	48.9
5	9	> 6	110	0.22	0.26	0.47	0.43	58	52.7

Table 5. Summary of the decisions regarding whether or not to consider each variable in either the adjustment or the aggregation models. An "X" in the column signifies the consideration of an individual variable for a particular model.

	Variable	Model it was considered in:	
		Adjustment	**Aggregation**
Group 1	$time\_period_{it}$	**X**	**X**
	$month_{it}$	as an interaction only	
Group 2	sal_{it}, sal_{it}^2, $sal_{it}*month_{it}$, $sal_{it}^2*month_{it}$	**X**	**X**
	$temp_{it}$, $temp_{it}^2$, $temp_{it}*month_{it}$, $temp_{it}^2*month_{it}$	**X**	**X**
	DO_{it}, $rainfall_{it}$, $1wk\_$ and $2mo\_FWII_{it}$, $storm\_events_t$		
Group 3	$depth_{it}$		**X**
	$closest\_inlet\_dist_{it}$		**X**
	$northing_{it}$, $easting_{it}$, $northing_{it}*easting_{it}$		**X**

Table 6. Fit statistics for models used to examine the effects of including explanatory variables in the ZI mixture component. Boldface type indicates rejection of the appropriate null hypothesis at the α=0.05 level of significance: H_{01}: α_t =0; H_{02}: β_{sal} =0; H_{03}: β_{sal2}=0; H_{04}: β_1=1; H_{05}: β_0=0. There are 40 total time period variables, the number of those where H_{01} was rejected is listed in parentheses.

# of variables in model	Predictors in ZI	Predictors in Γ	-2 ll	AIC	BIC	RMSE (kg)	Slope/ β_1	Intercept/ β_0	R^2
85	**time period (28)** **sal** sal2	**time period (40)** sal **sal2**	5322.7	5492.7	5964.0	1.67	0.99	**-0.59**	0.19
84	**time period (29)** **sal**	**time period (40)** sal **sal2**	5322.7	5490.7	5956.4	1.67	0.99	**-0.59**	0.19
83	**time period (30)**	**time period (40)** sal **sal2**	5331.4	5497.4	5957.6	1.67	0.99	**-0.59**	0.19
46	sal sal2	**time period (40)** sal **sal2**	5650.6	5742.6	5997.7	1.67	0.98	**-0.59**	0.19
45	sal	**time period (40)** sal **sal2**	5650.6	5740.6	5990.1	1.67	0.98	**-0.59**	0.19
44		**time period (40)** sal **sal2**	5653.1	5741.1	5985.0	1.67	0.98	**-0.59**	0.19

Table 7. Fit statistics for the full adjustment model (**I**) and the final adjustment model (**II**). "df" is the total number of model degrees of freedom, or the total number of predictor variables in the model minus one. RMSE is calculated based on SSB in kg. Boldface type indicates rejection of the appropriate null hypothesis at the α=0.05 level of significance: H_{01}: α_t =0; H_{02}: β_{ZI} =0 for any explanatory variables in the ZI component; H_{03}: β_{Γ} =0 for any explanatory variables in the Γ component; H_{04}: β_1=1; H_{05}: β_0=0. There are 40 total time period variables, the number of those where H_{01} was rejected is listed in parentheses.

	df	Predictors in ZI	Predictors in Γ	-2 ll	AIC	BIC	RMSE (kg)	Slope/ β_1	Intercept/ β_0	R^2
I	95	**time period (26)** sal sal2 sal*month **sal2*month** temp temp2 **temp*month** temp2*month	**time period (40) sal** sal2 **sal*month sal2*month** temp **temp2 temp*month temp2*month**	5236.9	5430.9	5968.7	1.67	0.82	-0.37	0.21
II	93	**time period (29)** sal sal2 sal*month **sal2*month** temp **temp*month**	**time period (40) sal** sal2 **sal*month sal2*month** temp **temp2 temp*month temp2*month**	5238.3	5428.3	5955.0	1.67	0.82	-0.37	0.21

Table 8. Parameter estimates and corresponding p-values for explanatory variables when the full adjustment model (Model **I**) was fit. Boldface type indicates that the estimate for that variable was statistically different from zero using a t-test with an α=0.05 level of significance.

	Variable	Parameter Estimate	Standard Error	T-test statistic	p-value
ZI component	sal	0.024	0.027	0.86	0.3903
	sal2	0.003	0.002	1.29	0.1985
	sal*month	0.026	0.034	0.75	0.4536
	sal2*month	**-0.007**	**0.003**	**-2.31**	**0.0207**
	temp	-0.118	0.086	-1.36	0.1738
	temp2	-0.018	0.021	-0.87	0.3865
	temp*month	**0.324**	**0.113**	**2.86**	**0.0042**
	temp2*month	0.011	0.031	0.36	0.7215
Γ component	**sal**	**-0.015**	**0.004**	**-3.96**	**<.0001**
	sal2	-0.001	0.000	-1.41	0.1596
	sal*month	**0.050**	**0.007**	**6.86**	**<.0001**
	sal2*month	**0.002**	**0.001**	**3.27**	**0.0011**
	temp	-0.014	0.013	-1.07	0.2867
	temp2	**0.015**	**0.005**	**2.71**	**0.0068**
	temp*month	**0.104**	**0.025**	**4.08**	**<.0001**
	temp2*month	**-0.030**	**0.011**	**-2.68**	**0.0074**

Table 9. Parameter estimates and corresponding p-values for explanatory variables when the final adjustment model (Model **II**) was fit. Boldface type indicates that the estimate for that variable was statistically different from zero using a t-test with an α=0.05 level of significance.

	Variable	Parameter Estimate	Standard Error	T-test statistic	p-value
ZI component	sal	0.025	0.027	0.92	0.3588
	sal2	0.003	0.002	1.33	0.1846
	sal*month	0.025	0.034	0.73	0.4672
	sal2*month	**-0.008**	**0.003**	**-2.39**	**0.0170**
	temp	-0.079	0.076	-1.05	0.2933
	temp*month	**0.292**	**0.104**	**2.82**	**0.0049**
Γ component	**sal**	**-0.015**	**0.004**	**-3.96**	**<.0001**
	sal2	-0.001	0.000	-1.39	0.1634
	sal*month	**0.050**	**0.007**	**6.86**	**<.0001**
	sal2*month	**0.002**	**0.001**	**3.27**	**0.0011**
	temp	-0.014	0.013	-1.08	0.2797
	temp2	**0.015**	**0.005**	**2.74**	**0.0063**
	temp*month	**0.103**	**0.025**	**4.08**	**<.0001**
	temp2*month	**-0.030**	**0.011**	**-2.62**	**0.0088**

Table 10. Parameter estimates and corresponding p-values for intercepts used to examine temporal trends in annual environmentally-adjusted SSB over time. Boldface type indicates that the estimate for that variable was statistically different from zero using a t-test with an α=0.05 level of significance.

	Variable	Parameter Estimate	Standard Error	T-test statistic	p-value
ZI	**june*year**	**-0.080**	**0.0074**	**-10.86**	**<.0001**
	sept*year	0.010	0.0063	1.60	0.1101
Γ	**june*year**	**0.076**	**0.0043**	**17.70**	**<.0001**
	sept*year	**0.066**	**0.0044**	**15.19**	**<.0001**

Table 11. Fit statistics for four different iterations of the aggregation model. **A** denotes the full model with only process-based variables. **B** is the process-only model after backwards elimination. After both the addition of spatial coordinate variables and a second backwards elimination, **C** is the final aggregation model if all previous variables were retained, and **D** is the final model if newly-insignificant non-spatial coordinate terms were also removed. "df" is the total number of model degrees of freedom, or the total number of predictor variables in the model minus one. RMSE is calculated based on SSB in kg. Boldface type indicates rejection of the appropriate null hypothesis at the α=0.05 level of significance: H_{01}: α_t =0; H_{02}: β_{ZI} =0 for any explanatory variables in the ZI component; H_{03}: β_{Γ} =0 for any explanatory variables in the Γ component; H_{04}: β_1=1; H_{05}: β_0=0. There are 40 total time period variables, the number of those where H_{01} was rejected is listed in parentheses.

Table 11 Continued

	df	Predictors in ZI	Predictors in Γ	-2 ll	AIC	BIC	RMSE (kg)	Slope (β_1)	Intercept (β_0)	R^2
A	110	**time period (34)** sal sal2 sal*month sal2*month temp temp*month **closest_inlet_dist** closest_inlet_dist^2 closest_inlet_dist*month closest_inlet_dist^2*month **depth depth^2 depth *month** depth^2*month	**time period (39)** sal **sal2 sal*month sal2*month** temp **temp2 temp*month temp2*month** closest_inlet_dist **closest_inlet_dist^2 closest_inlet_dist*month** closest_inlet_dist^2*month **depth** depth^2 **depth *month depth^2*month**	5048.4	5270.4	5885.8	1.64	0.84	-0.32	0.20
B	106	**time period (34) sal** sal2 sal*month **sal2*month** temp **temp*month** closest_inlet_dist **closest_inlet_dist^2 depth depth^2 depth *month**	**time period (39)** sal **sal2 sal*month sal2*month** temp **temp2 temp*month temp2*month** closest_inlet_dist **closest_inlet_dist^2 closest_inlet_dist* month depth** depth^2 **depth *month depth^2*month**	5052.4	5266.4	5859.7	1.64	0.83	-0.31	0.20
C	109	**time period (32)** sal sal2 sal*month **sal2*month** temp temp*month closest_inlet_dist **closest_inlet_dist^2** depth **depth^2 depth *month north**	**time period (40)** sal sal2 **sal*month sal2*month** temp temp2 **temp*month** temp2*month **closest_inlet_dist closest_inlet_dist^2** closest_inlet_dist* month depth **depth^2 depth *month depth^2*month north east**	4828.7	5048.7	5658.6	1.56	1.02	-0.43	0.24
D	103	**time period (32)** sal **sal2 sal*month** closest_inlet_dist **closest_inlet_dist^2** depth **depth^2 depth *month north**	**time period (40)** sal sal2 **sal*month sal2*month** temp **temp*month closest_inlet_dist closest_inlet_dist^2** depth **depth^2 depth *month depth^2*month north east**	4839.2	5047.2	5623.8	1.58	0.98	-0.36	0.21

Table 12. Parameter estimates and corresponding p-values for explanatory variables when the final aggregation model (Model **C**) was fit. Boldface type indicates that the estimate for that variable was statistically different from zero using a t-test with an α=0.05 level of significance.

	Variable	Parameter Estimate	Std. Error	T-test statistic	p-value
ZI component	sal	0.047	0.036	1.32	0.19
	sal2	-0.001	0.003	-0.24	0.81
	month*sal	0.037	0.036	1.03	0.30
	month*sal2	**-0.008**	**0.004**	**-2.14**	**0.03**
	temp	0.045	0.085	0.54	0.59
	month*temp	-0.068	0.117	-0.58	0.56
	closest_inlet_dist	-0.016	0.011	-1.44	0.15
	closest_inlet_dist2	**0.003**	**0.001**	**6.24**	**<.0001**
	depth	0.089	0.084	1.06	0.29
	depth2	**0.147**	**0.047**	**3.16**	**0.002**
	month*depth	**0.246**	**0.109**	**2.27**	**0.02**
	north	**-0.055**	**0.006**	**-9.12**	**<.0001**
Γ component	sal	-0.006	0.005	-1.22	0.22
	sal2	0.0001	0.0003	0.18	0.86
	month*sal	**0.045**	**0.010**	**4.7**	**<.0001**
	month*sal2	**0.002**	**0.001**	**2.8**	**0.01**
	temp	0.024	0.015	1.6	0.11
	temp2	0.010	0.006	1.71	0.09
	month*temp	**0.073**	**0.023**	**3.16**	**0.002**
	month*temp2	-0.017	0.012	-1.37	0.17
	closest_inlet_dist	**-0.011**	**0.002**	**-4.61**	**<.0001**
	closest_inlet_dist2	**0.001**	**0.0001**	**4.37**	**<.0001**
	month* closest_inlet_dist	0.004	0.004	1.19	0.24
	depth	-0.008	0.007	-1.14	0.26
	depth2	**-0.020**	**0.006**	**-3.18**	**0.002**
	month*depth	**0.111**	**0.031**	**3.63**	**0.0003**
	month*depth2	**0.100**	**0.017**	**5.74**	**<.0001**
	north	**-0.008**	**0.001**	**-5.66**	**<.0001**
	east	**-0.006**	**0.001**	**-4.13**	**<.0001**

FIGURE LEGENDS

Figure 1. Adjusted CPUE for mature females collected in the Program 195 September survey from 1987-2004. CPUE is in units of total carapace width (CW) of mature females caught per station divided by number of tows in a time period. This figure is reproduced from the BC FMP (NCDMF 2004).

Figure 2. Index of annual salinity-adjusted SSB means over time overlaying mean unadjusted SSB from the September survey over time. The pink line depicts the mean of the unadjusted annual means from 1987-2003. The orange line depicts the mean of the annual salinity-adjusted means from 1987-2003.

Figure 3. Map of depths at survey locations sampled over the entire space-time domain. In this figure, N=2100. Colors depict the observed depth in meters at each station with cool colors representing shallower depths and warm colors indicating deeper depths.

Figure 4. Frequency histogram of the distribution of SSB (in g/tow).

Figure 5. Contour plots of predicted June SSB from the adjustment model as a function of temperature and salinity.

Figure 6. Contour plots of predicted September SSB from the adjustment model as a function of temperature and salinity.

Figure 7. Annual mean environmentally-adjusted SSB for June. Figure depicts adjustment over time for samples collected in June. Blue broken lines represent the 95% CI for each individual annual mean. The purple line depicts the mean of yearly means from 1987-2003, and the broken purple lines enclose the 90% CI for this grand mean.

Figure 8. Annual mean environmentally-adjusted SSB for September. Figure depicts adjustment over time for samples collected in September. Blue broken lines represent the 95% CI for each individual annual mean. The purple line depicts the mean of yearly means from 1987-2003, and the broken purple lines enclose the 90% CI for this grand mean.

Figure 9. Difference between unadjusted and environmentally-adjusted mean SSB across June time periods.

Figure 10. Difference between unadjusted and environmentally-adjusted mean SSB across September time periods.

Figure 11. Map images of predicted $\overline{SSB_{at}}$ as generated from the best-fitting aggregation model for A: June 1992 and B: June 2003. Legend quantiles are based on the distribution of $\overline{SSB_{at}}$ predictions across all time periods and are the same for both maps.

Figure 12. Map images of predicted $\overline{SSB_{at}}$ as generated from the best-fitting aggregation model for A: June 1992 and B: June 2003. Legend quantiles are based on the distribution of $\overline{SSB_{at}}$ predictions within each time periods and are thus different for both maps.

Figure 13. Summary maps of $\overline{SSB_{at}}$ predictions across all June time periods. Predictions in map A were at or above the 99th percentile of all predations in their individual time period, while predictions in map B were all those larger than 7 kg, or the 99th percentile of all June SSB_{it} observations, regardless of time period.

Figure 14. Map images of predicted $\overline{SSB_{at}}$ as generated from the best-fitting aggregation model for A: September 1998, B: September 1999, and C: September 2000. Legend quantiles are based on the distribution of $\overline{SSB_{at}}$ predictions across all time periods and are the same for all three maps.

Figure 15. Map images of predicted $\overline{SSB_{at}}$ as generated from the best-fitting aggregation model for A: September 1998, B: September 1999, and C: September 2000. Legend quantiles are based on the distribution of $\overline{SSB_{at}}$ predictions within each time periods and are thus different for all three maps.

Figure 16. Summary maps of $\overline{SSB_{at}}$ predictions across all September time periods. Predictions in map A were at or above the 99th percentile of all predations in their individual time period, while predictions in map B were all those larger than 5 kg, or the 99th percentile of all September SSB_{it} observations, regardless of time period

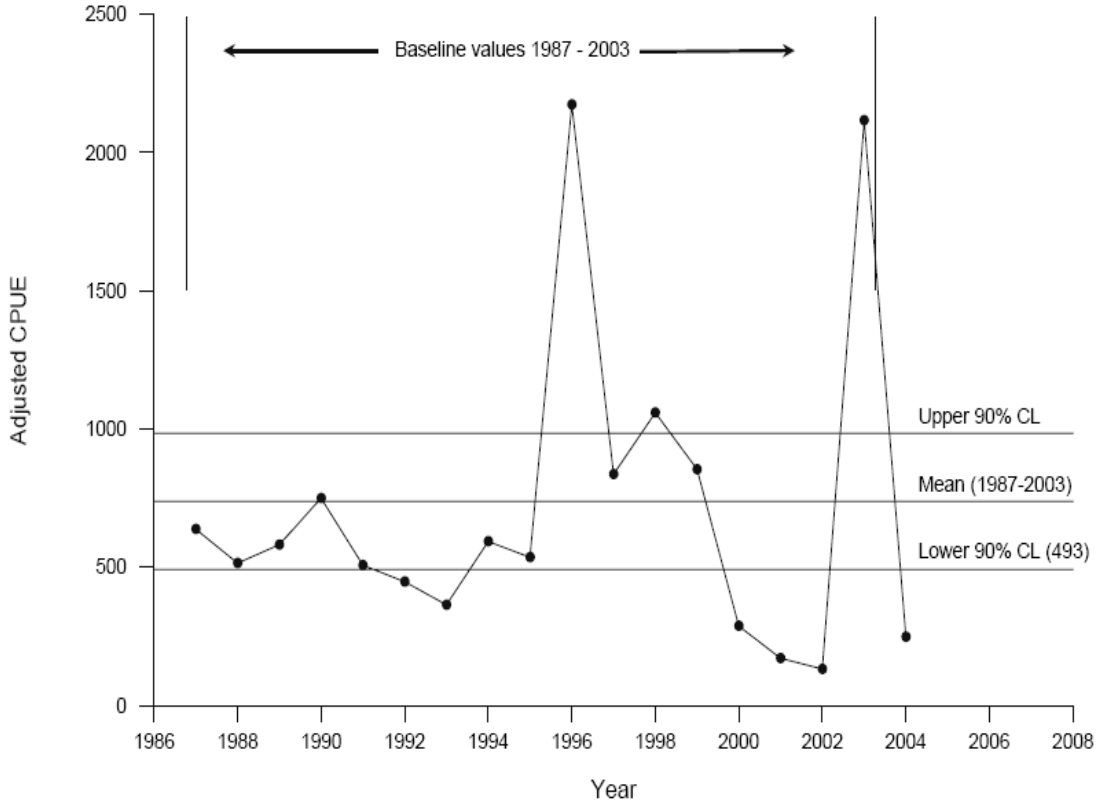

Figure 1. Adjusted CPUE for mature females collected in the Program 195 September survey from 1987-2004.

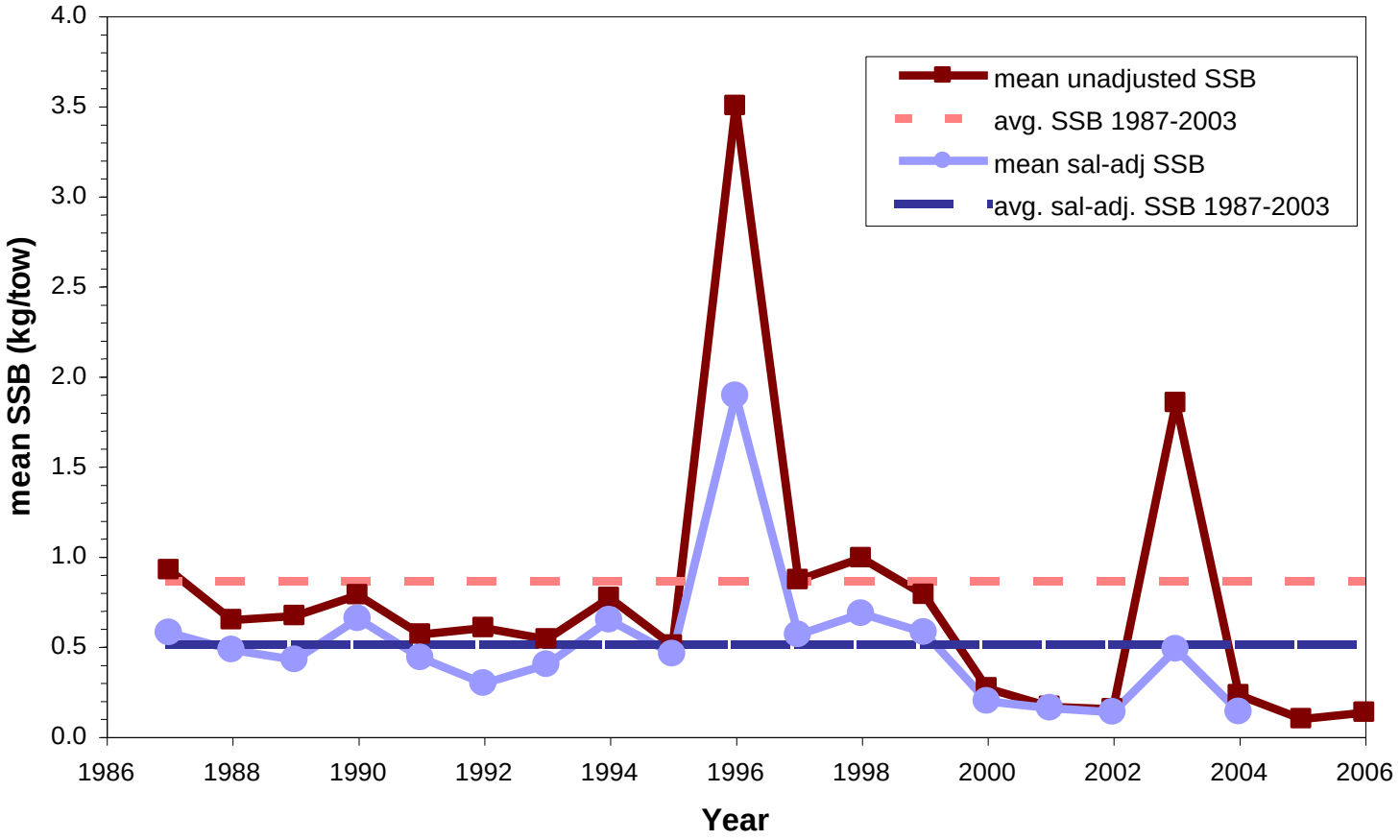

Figure 2. Index of annual salinity-adjusted SSB means over time overlaying mean unadjusted SSB from the September survey over time.

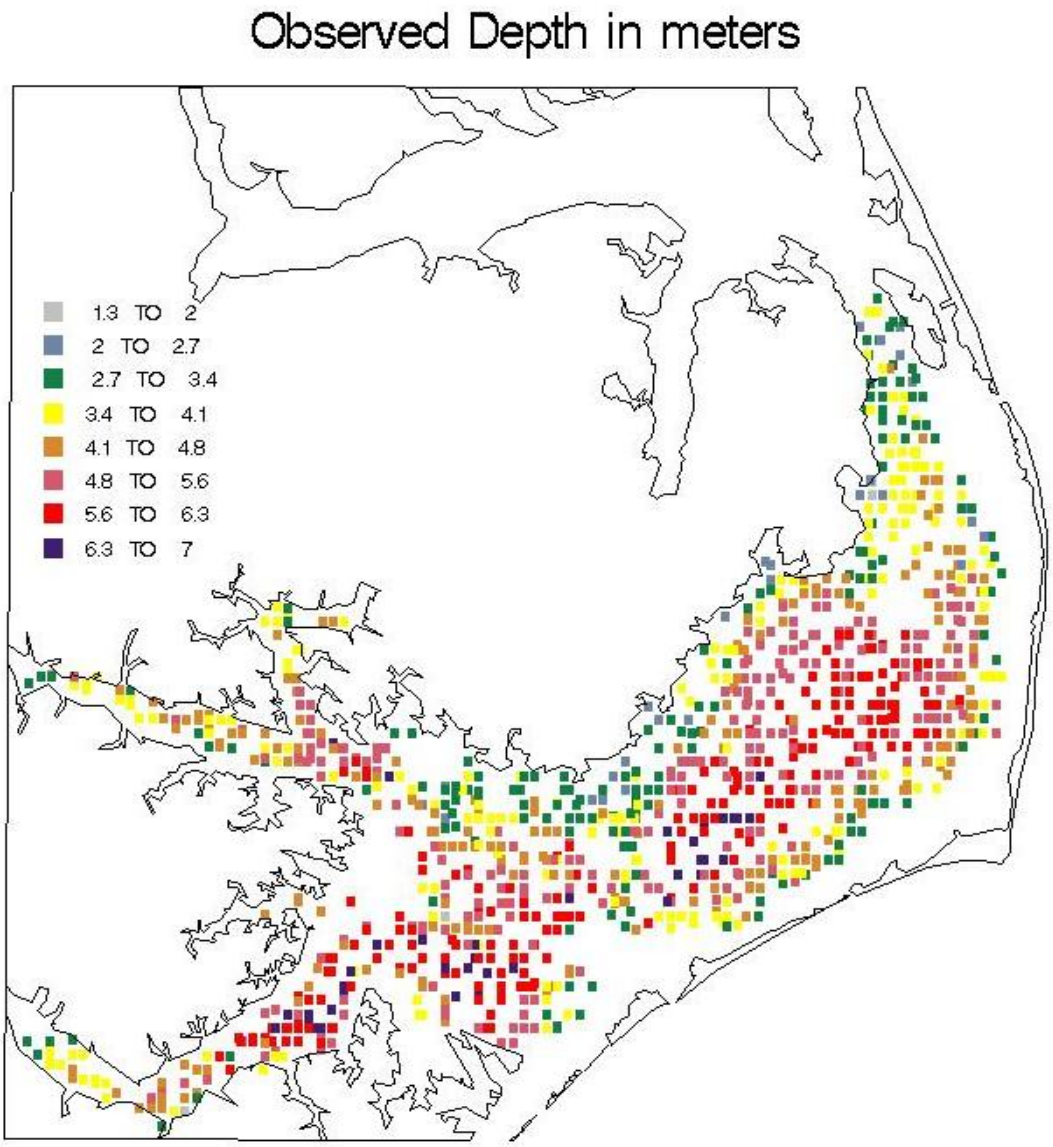

Figure 3. Map of depths at survey locations sampled over the entire space-time domain.

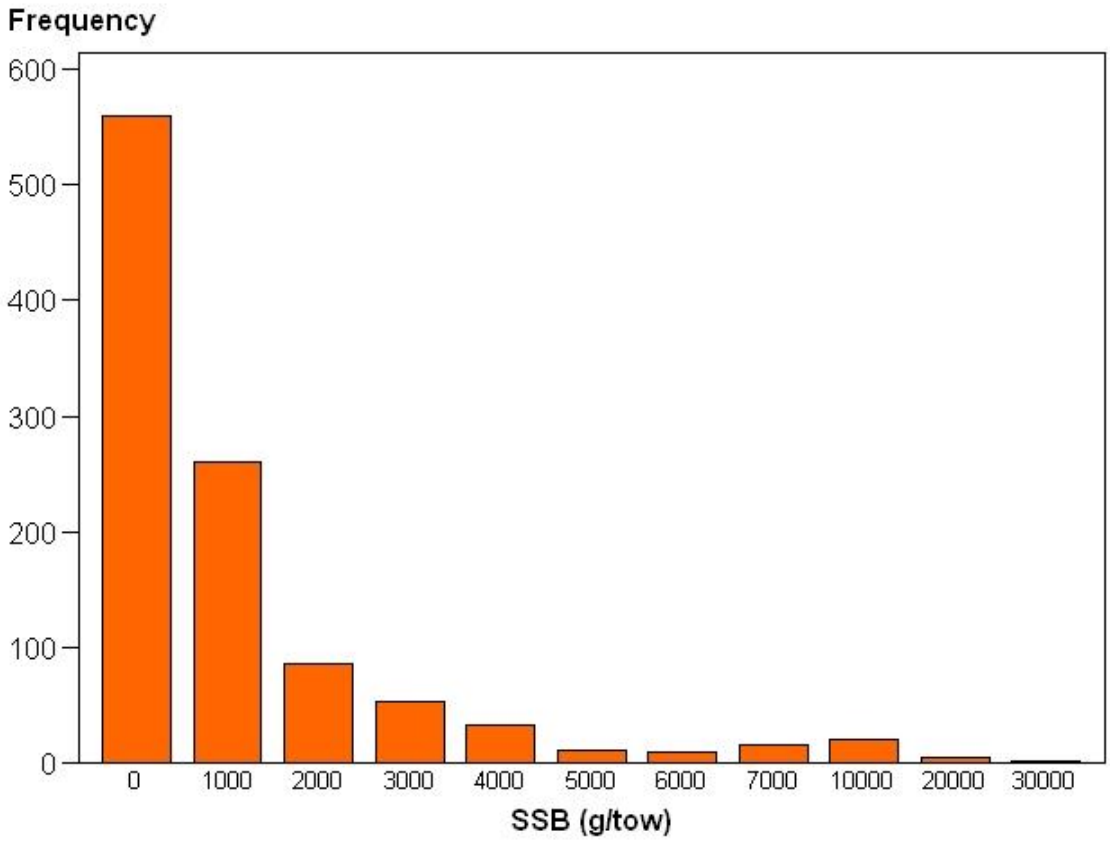

Figure 4. Frequency histogram of the distribution of SSB (in g/tow).

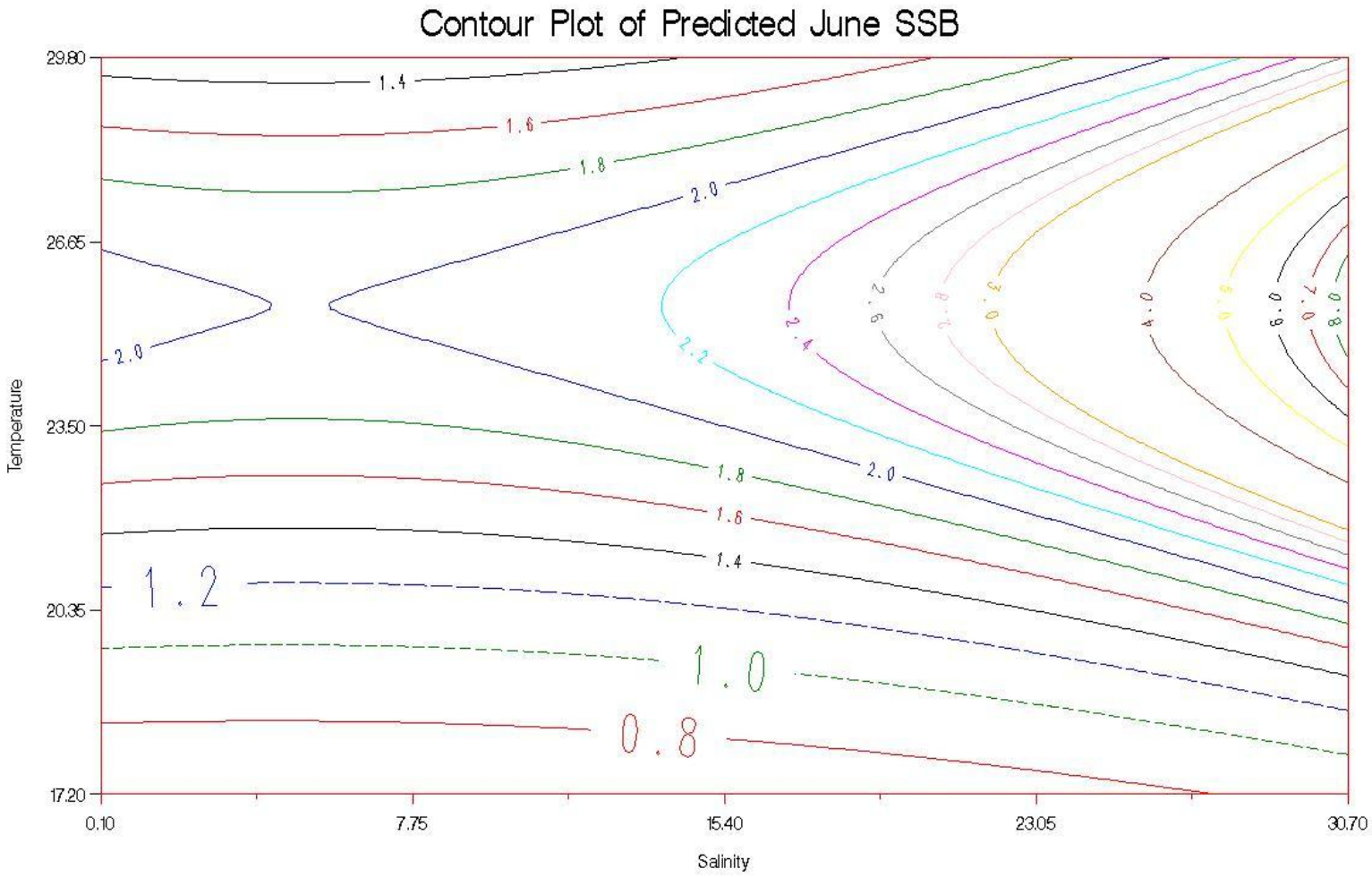

Figure 5. Contour plots of predicted June SSB from the adjustment model as a function of temperature and salinity.

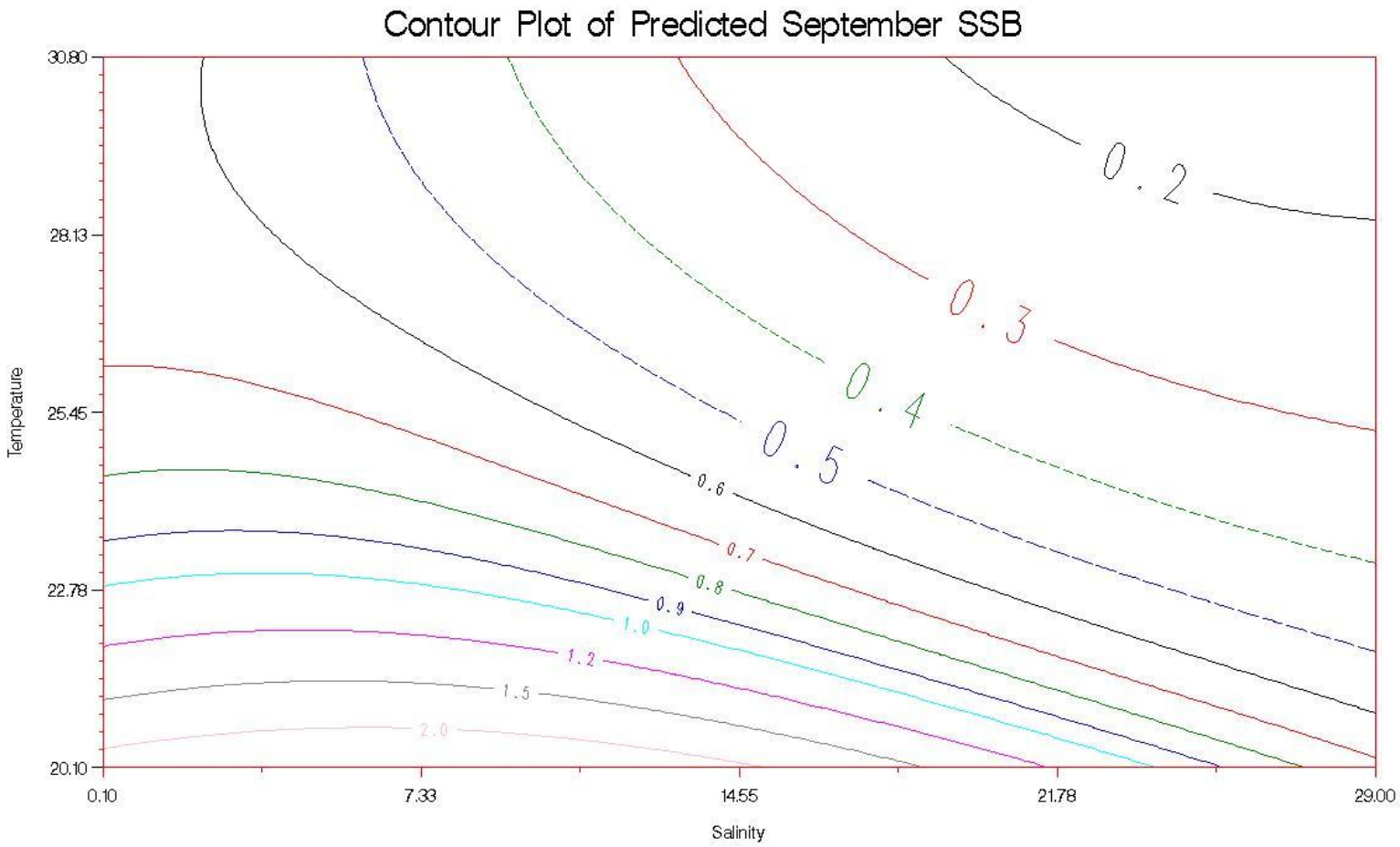

Figure 6. Contour plots of predicted September SSB from the adjustment model as a function of temperature and salinity.

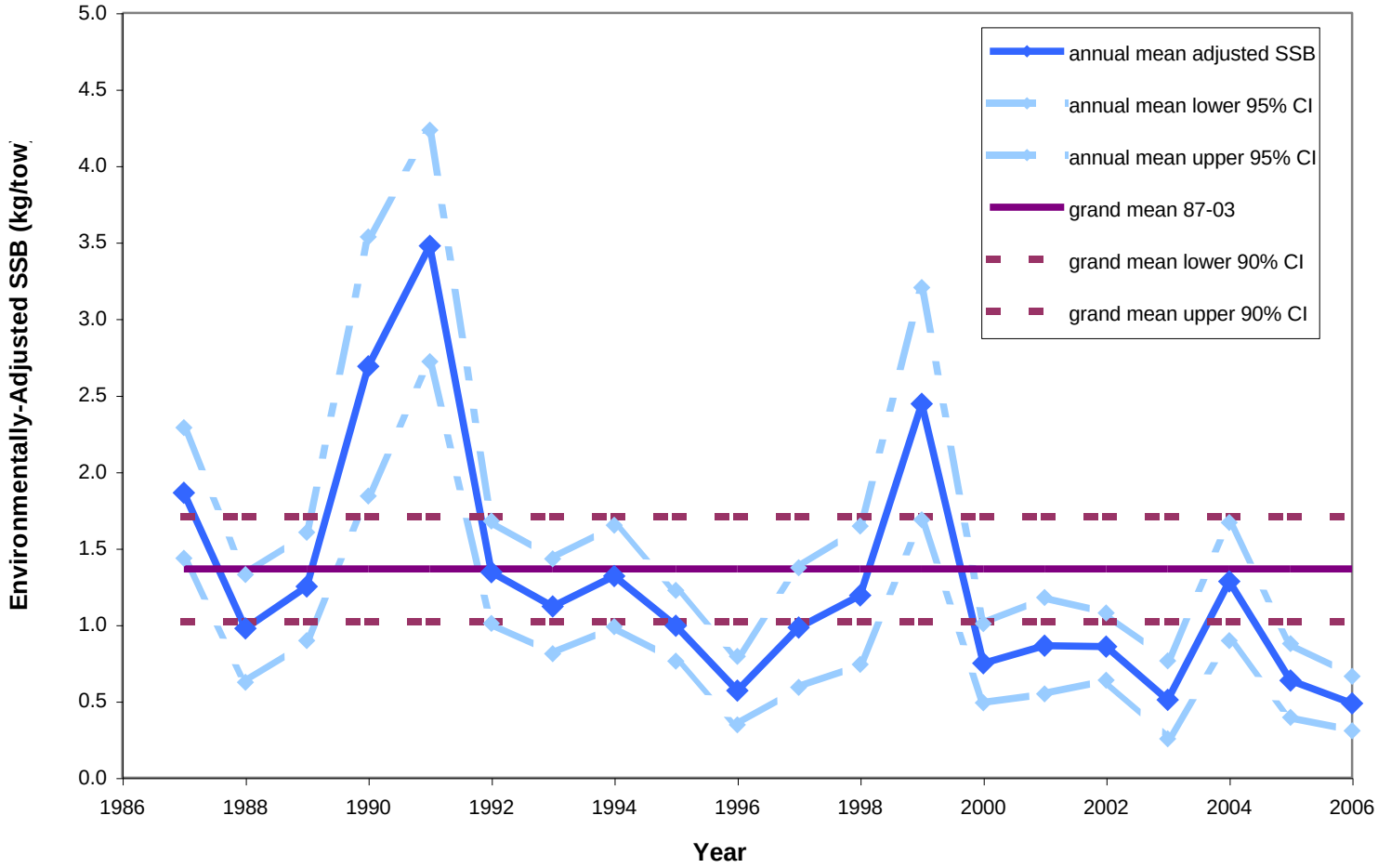

Figure 7. Annual mean environmentally-adjusted SSB for June.

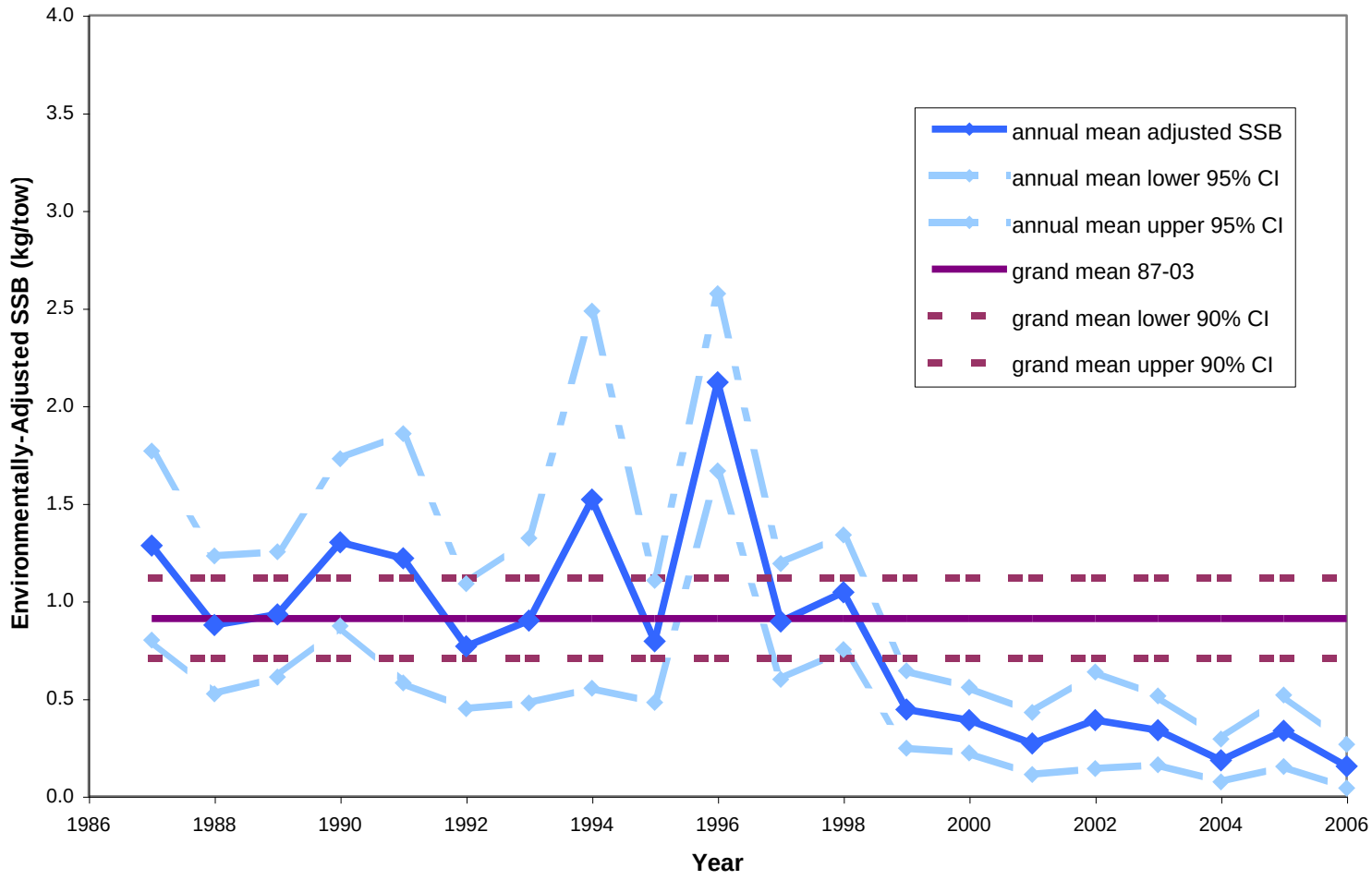

Figure 8. Annual mean environmentally-adjusted SSB for September.

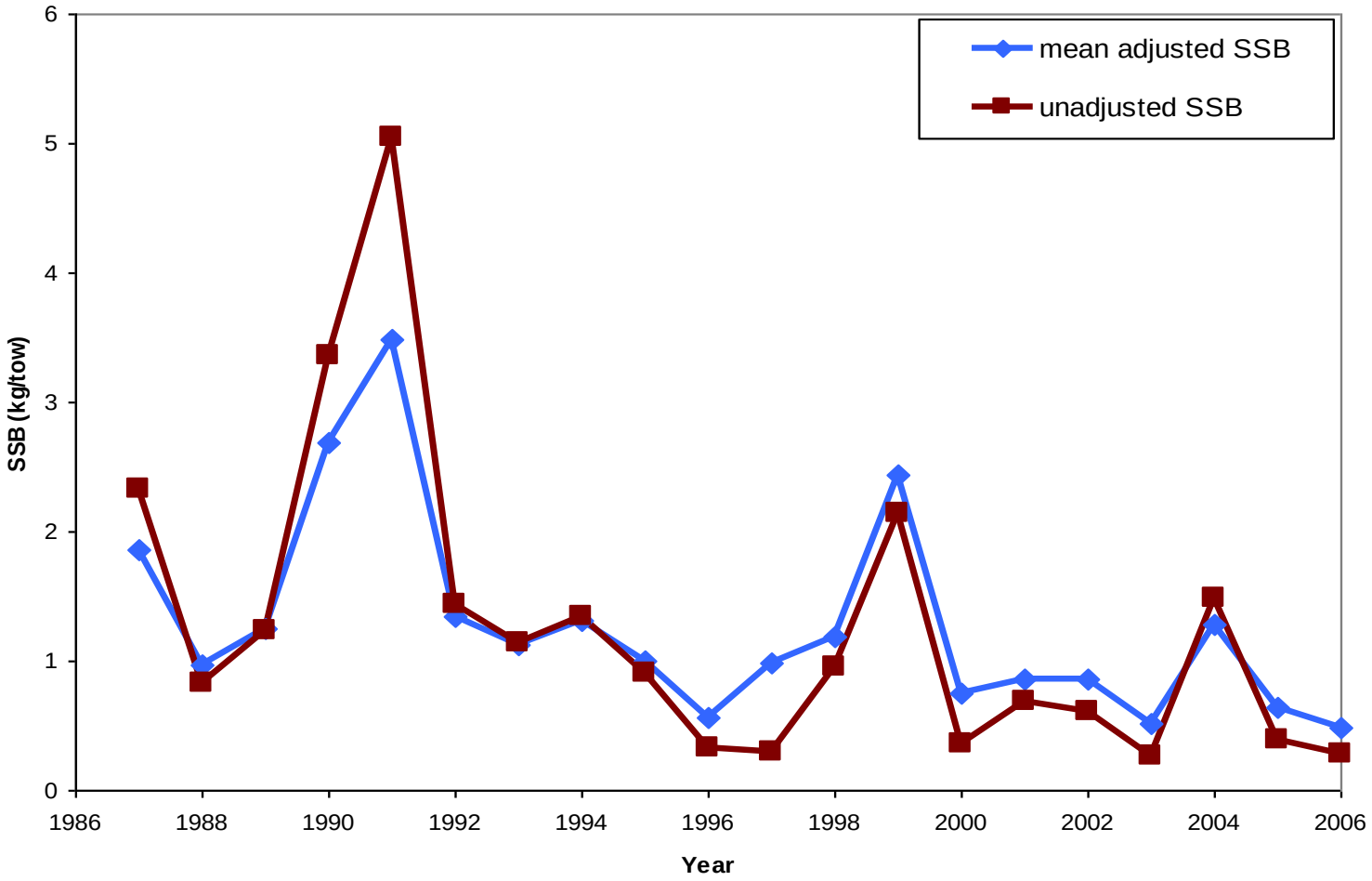

Figure 9. Difference between unadjusted and environmentally-adjusted mean SSB across June time periods.

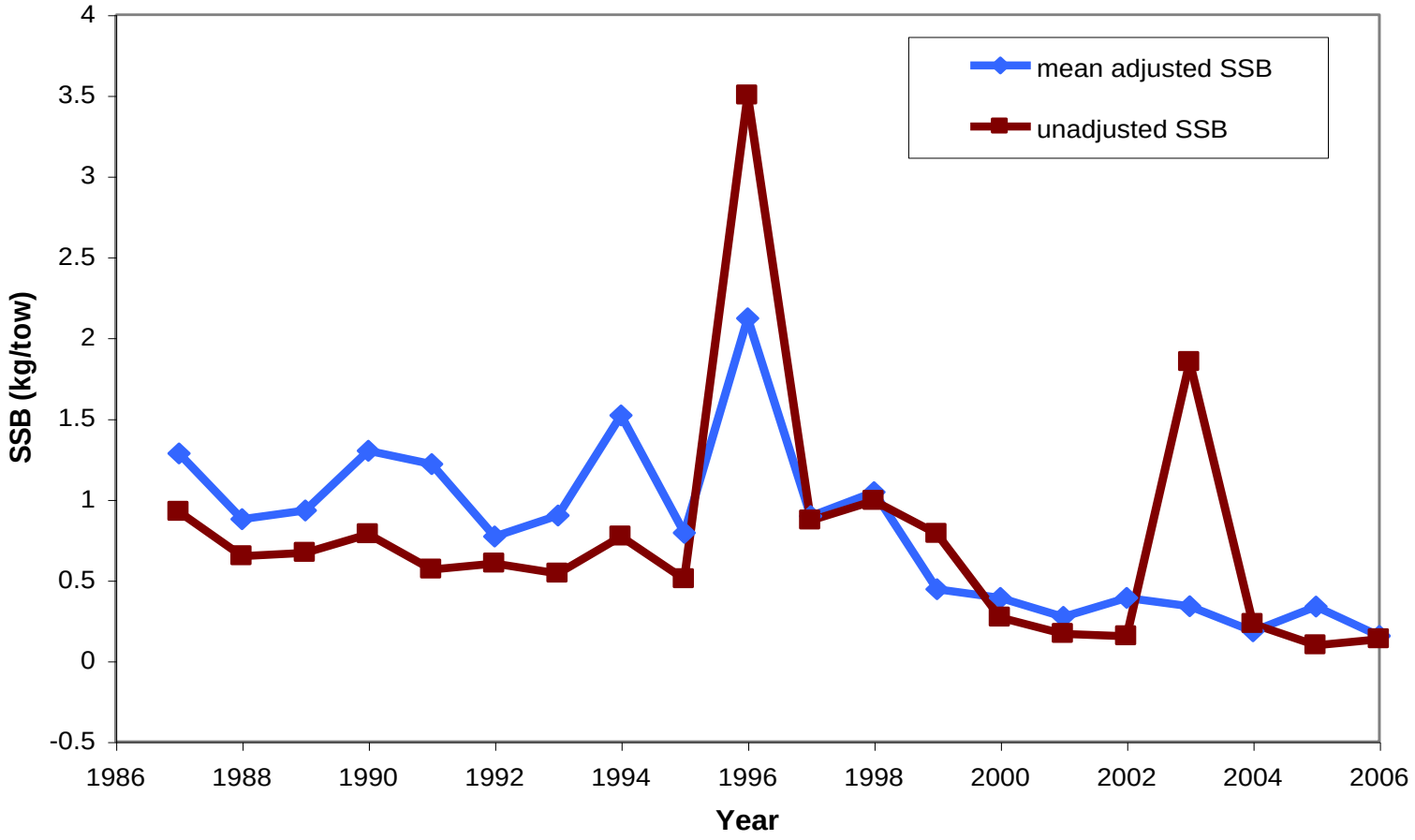

Figure 10. Difference between unadjusted and environmentally-adjusted mean SSB across September time periods.

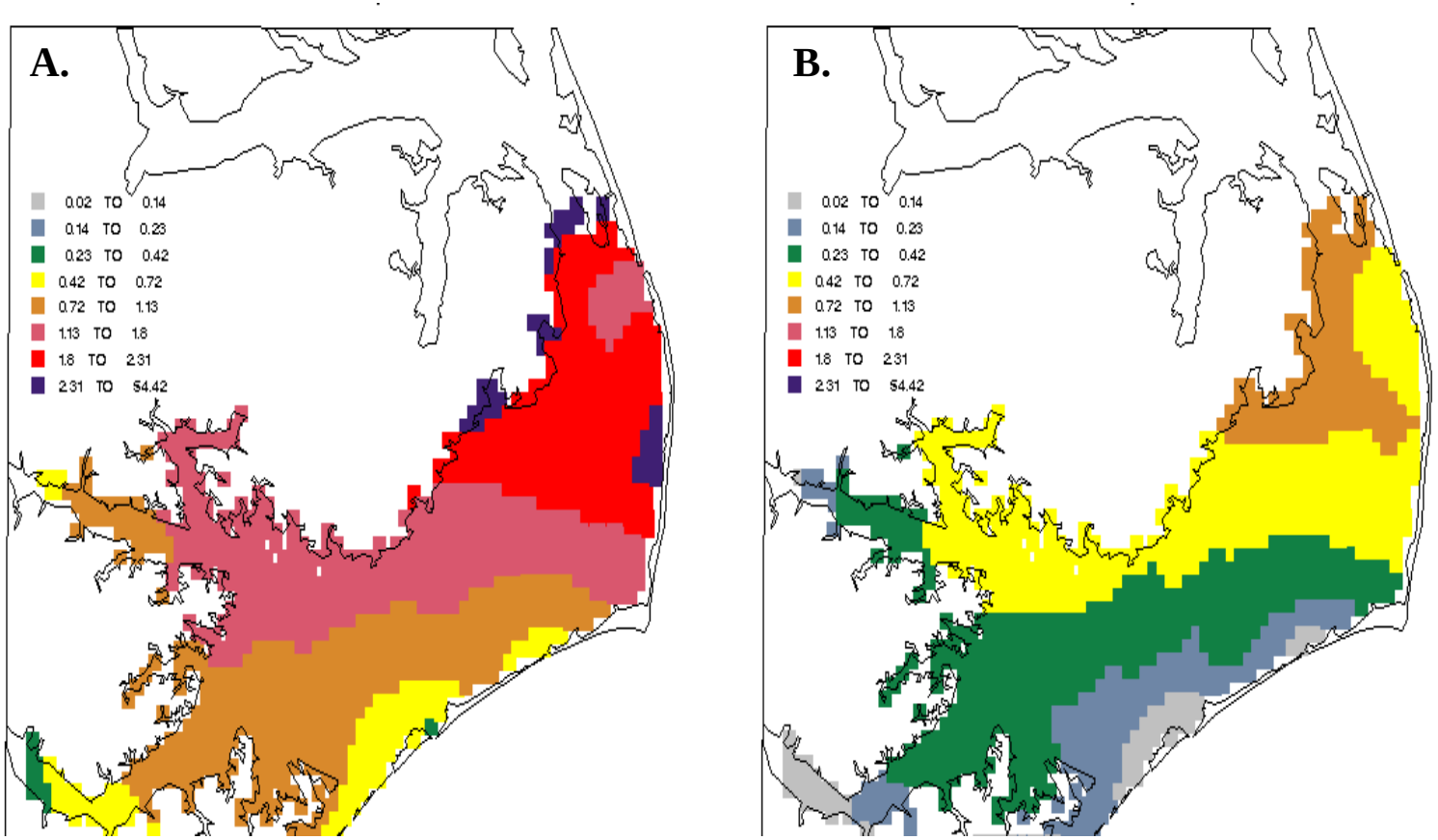

Figure 11. Map images of predicted $\overline{SSB_{at}}$ as generated from the best-fitting aggregation model for A: June 1992 and B: June 2003 where legend quantiles are the same for both maps.

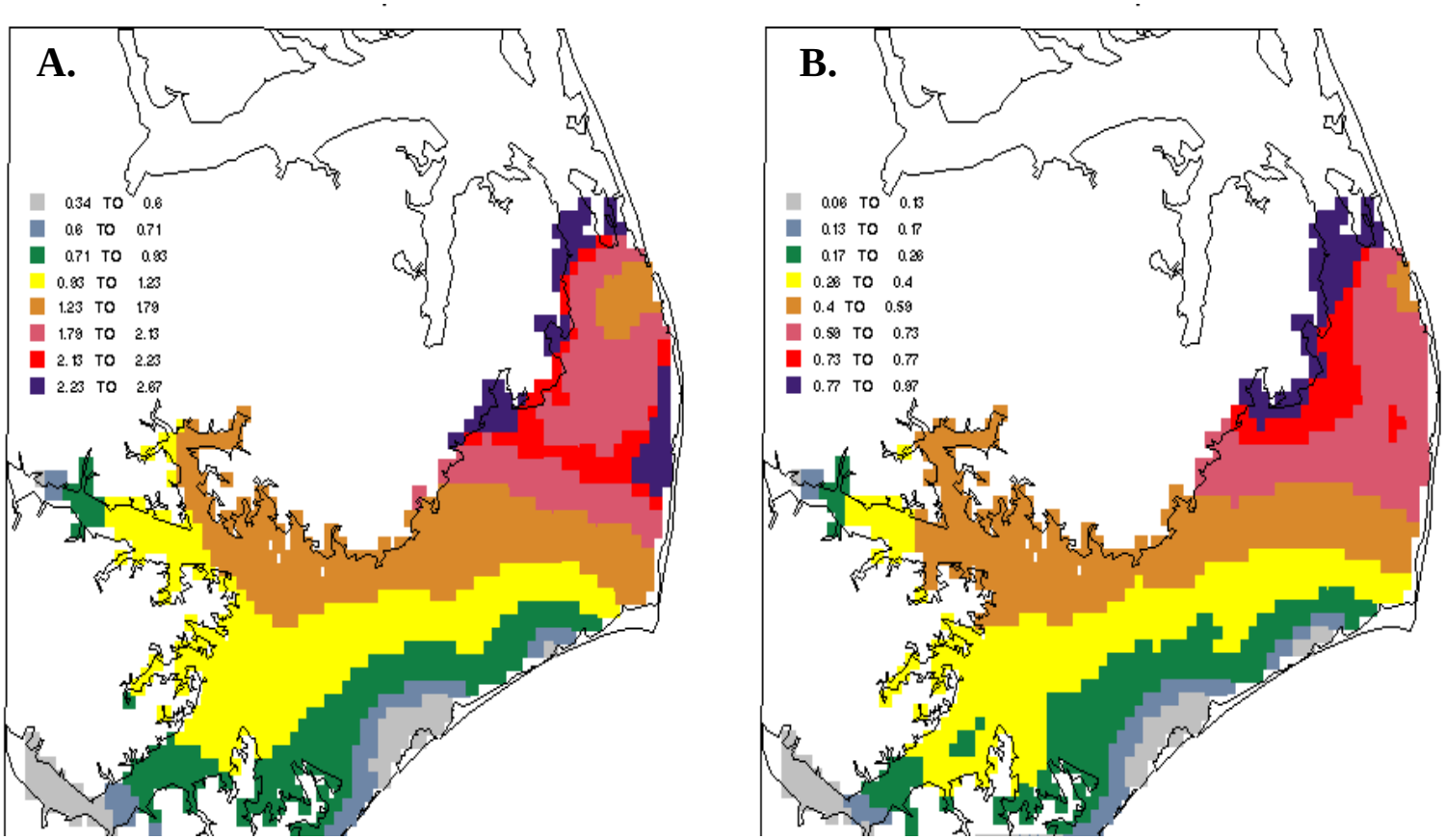

Figure 12. Map images of predicted $\overline{SSB_{at}}$ as generated from the best-fitting aggregation model for A: June 1992 and B: June 2003 where legend quantiles are time-period specific.

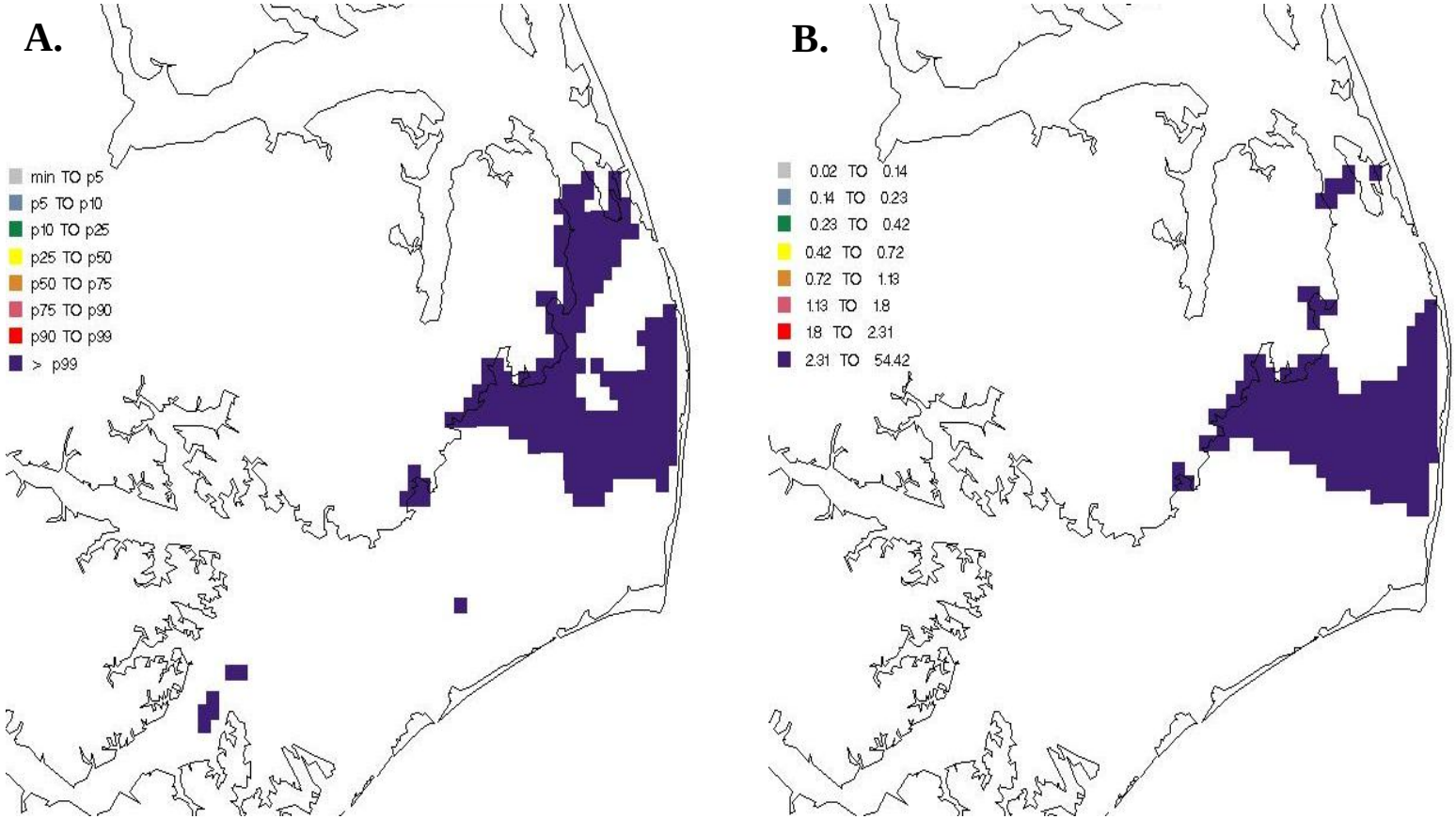

Figure 13. Summary maps of $\overline{SSB_{at}}$ predictions across all June time periods.

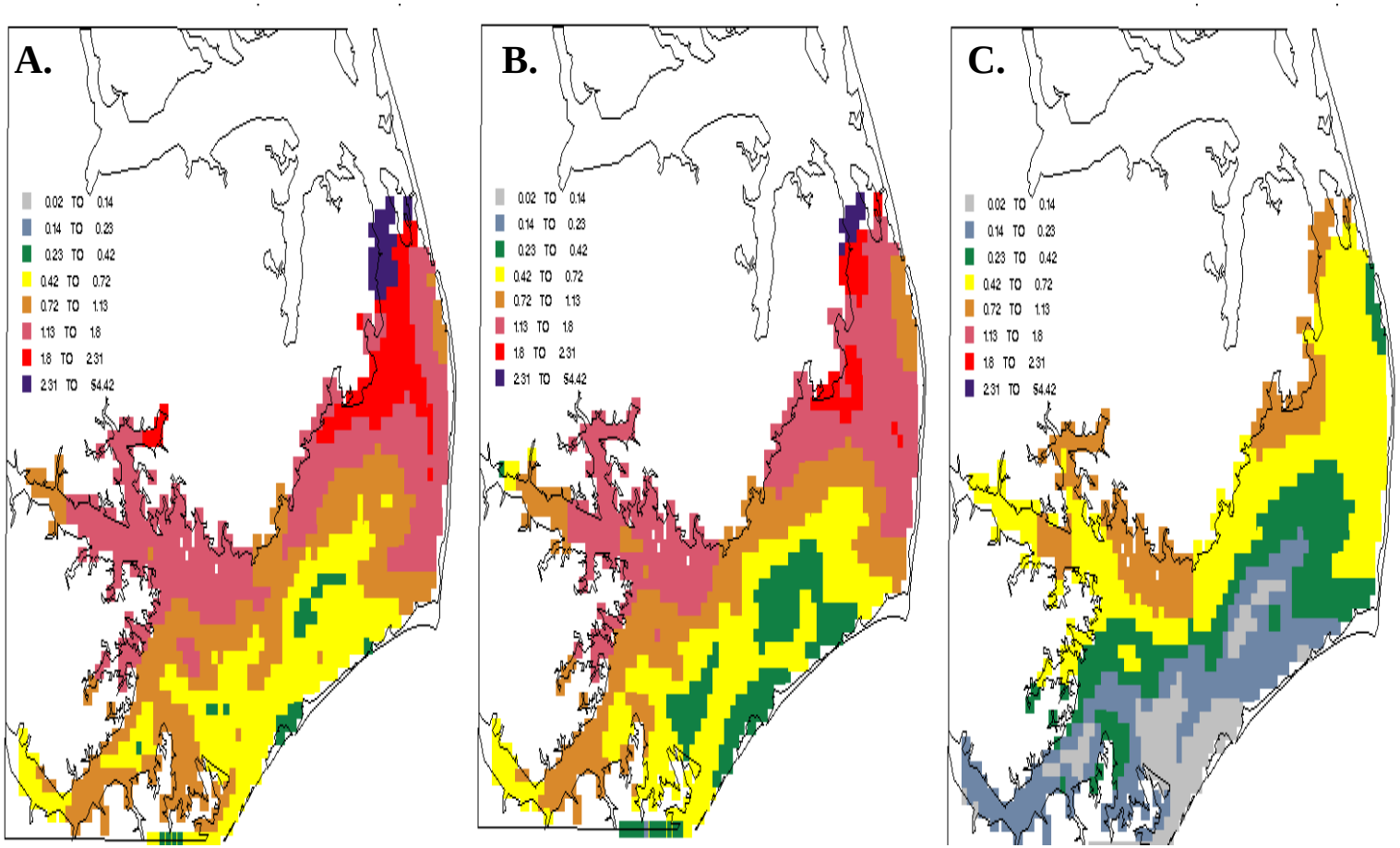

Figure 14. Map images of predicted $\overline{SSB_{at}}$ as generated from the best-fitting aggregation model for A: September 1998, B: September 1999, and C: September 2000 where legend quantiles are the same for all three maps.

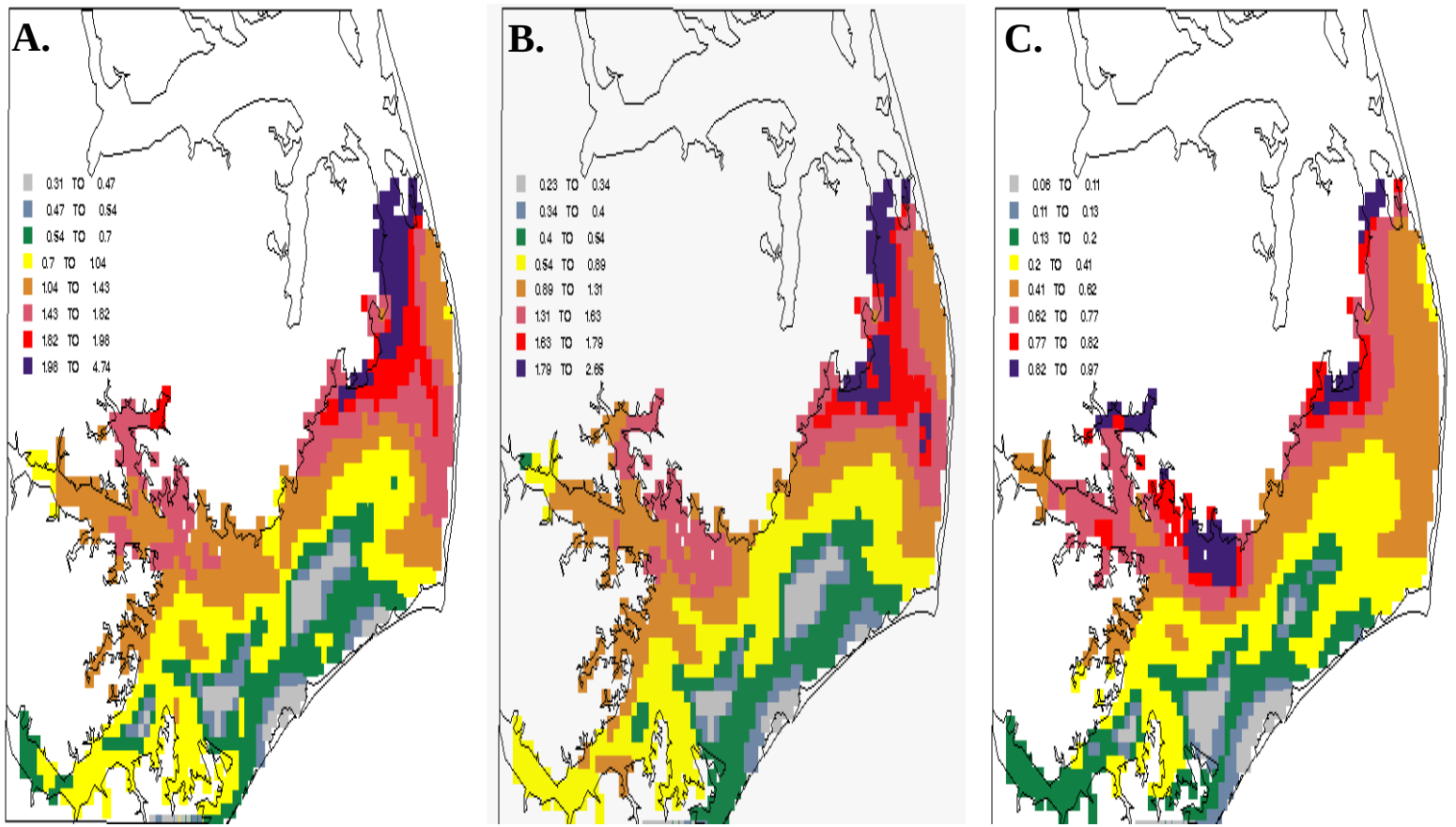

Figure 15. Map images of predicted $\overline{SSB_{at}}$ as generated from the best-fitting aggregation model for A: September 1998, B: September 1999, and C: September 2000 where legend quantiles are time-period specific.

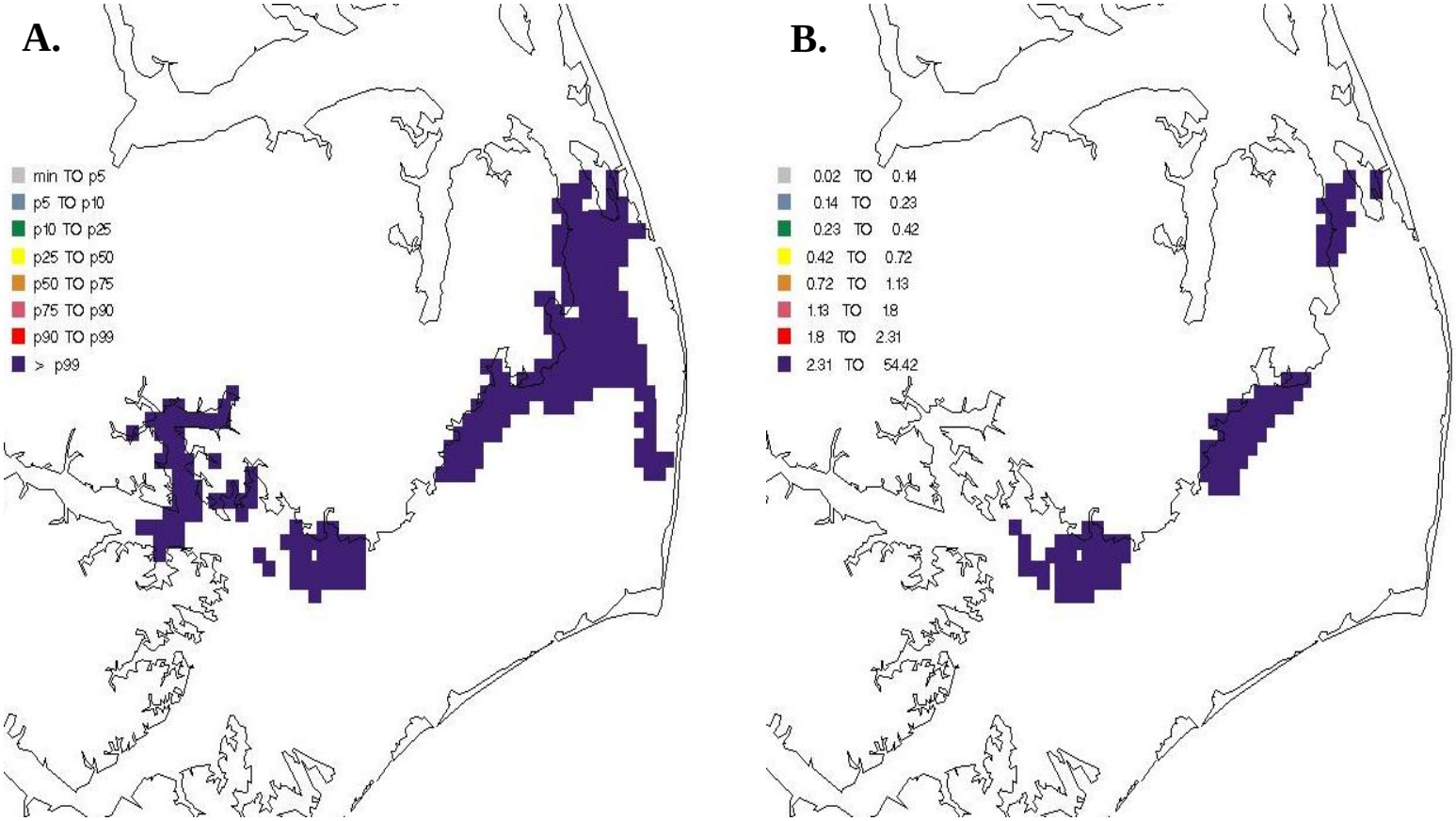

Figure 16. Summary maps of $\overline{SSB_{at}}$ predictions across all September time periods.

Appendix 1. Derivation of the probability density function for a ZIG distribution.

Consider the discrete random variable Z, which has point mass at zero. Specifically, the probability mass function for Z is given by

$$f_Z(z) \equiv P(Z = z) = \begin{cases} 1 & z = 0 \\ 0 & z \neq 0 \end{cases}.$$

The expected value of Z is given by $EZ = 0$, and the variance is $Var(Z) = 0$. We refer to Z as a degenerate random variable because it has zero variance.

Also consider the continuous random variable X, which has a Gamma distribution. The probability density function under the usual parameterization is given by

$$f_X(x) = \frac{1}{\Gamma(\alpha)\beta^{\alpha}} x^{\alpha-1} e^{-x/\beta},$$

where $x \geq 0$, $\alpha > 0$, $\beta > 0$. Then $EX = \alpha\beta$, and $Var(X) = \alpha\beta^2$. Re-parameterizing by setting $\mu = \alpha\beta$ so that $\mu > 0$, $EX = \mu$, and $Var(X) = \mu\beta$ allows representation of the expected value with a single parameter. The resulting pdf is given by

$$f_X(x) = \frac{1}{\Gamma(\mu/\beta)\beta^{\mu/\beta}} x^{\mu/\beta-1} e^{-x/\beta}.$$

Now consider the random variable Y, which is equal to Z with probability π and to X with probability $(1-\pi)$, where we take X and Z to be independent. The probability density function for Y is given by $f_Y(y) = \pi f_Z(y) + (1-\pi) f_X(y)$, or, equivalently, by

$$f_Y(y) = \begin{cases} \pi & y = 0 \\ (1-\pi)\dfrac{1}{\Gamma(\mu/\beta)\beta^{\mu/\beta}} y^{\mu/\beta-1} e^{-y/\beta} & y > 0 \end{cases}.$$

The expected value of Y is derived as follows:

$$EY = \pi \cdot 0 \cdot f_Z(0) + (1-\pi)\int_0^\infty y f_X(y)dy = (1-\pi)EX = (1-\pi)\mu .$$

The variance is similarly derived:

$$Var(Y) = \pi \cdot [0-(1-\pi)\mu]^2 f_Z(0) + (1-\pi)\int_0^\infty \left[y-(1-\pi)\mu\right]^2 f_X(y)dy$$

$$= (1-\pi)\mu \left[4\mu - 3\pi\mu + \beta\right] .$$

Appendix 2. SAS® proc NLMIXED code sample

Here we model the means of the ZI and Γ components as functions of salinity and salinity^2 (salinity2). This model as coded has a single intercept in both ZI and Γ for all time periods**.** Including *time_period*$_{it}$ changes the model to have different intercepts (a0 and b0) for each time period.

```
proc NLMIXED data = saladj_ssb maxiter = 1000 maxfunc = 5000;

parameters a0=-0.90 a1=0 a2=0 b0=0.88 b1=0 b2=0;

linppi =  a0+ a1*salinity+ a2*salinity2;
/* linppi=linear predictor for the zero inflation probability pi */

pi = 1 /(1+exp(-linppi));
/* pi = zero inflation probability and logistic function of linppi*/

oneminuspi=1-pi;
/* oneminuspi = probability of observing a non-zero value*/

linpmu = b0+ b1*salinity+ b2*salinity2;
/* linpmu=linear predictor for mu, the mean of the gamma distribution*/

mu = (linpmu)**(-1);
/*mu= inverse of linpmu*/

alpha = mu/beta;
/* since mean of Γ = alpha*beta and alpha and beta are part of the gamma
log likelihood function */

/* if/else statements build the ZIG log likelihood */
if ssb = 0 then ll = log(pi) ;

else ll =
log( (1-pi)*ssb**(alpha-1)*exp(ssb/beta)/(gamma(alpha)*beta**(alpha)));

model  ssb~ general(ll);

predict pi out=saladj_pi_preds;

predict mu out=saladj_mu_preds;

predict oneminuspi*mu out=saladj_mean_preds;

run; quit;
```